INSTITUTO
UNIVERSITÁRIO
DE LISBOA

Cost-effective ROADM architectures for SDM optical networks

André Filipe Aldeinhas Ribeiro

Master's degree in Telecommunications and Computer Engineering,

Supervisor:

PhD Luís Gonçalo Lecoq Vences e Costa Cancela, Associate Professor,

ISCTE-Instituto Universitário de Lisboa

Co-Supervisor:

PhD João Lopes Rebola, Associate Professor,

ISCTE-Instituto Universitário de Lisboa

October, 2024

TECNOLOGIAS
E ARQUITETURA

Department of Information Science and Technology

Cost-effective ROADM architectures for SDM optical networks

André Filipe Aldeinhas Ribeiro

Master's degree in Telecommunications and Computer Engineering,

Supervisor:

PhD Luís Gonçalo Lecoq Vences e Costa Cancela, Associate Professor,

ISCTE-Instituto Universitário de Lisboa

Co-Supervisor:

PhD João Lopes Rebola, Associate Professor,

ISCTE-Instituto Universitário de Lisboa

October,2024

Família

Acknowledgment

With the completion of this work, my stage of university life at Iscte-Instituto Universitário de Lisboa comes to an end, a stage that has been both challenging and rewarding, a journey full of growth, learning and countless memorable experiences that I won't forget. I would like to thank Iscte-Instituto Universitário de Lisboa, for all the experiences and moments that I was able to share between teachers and colleagues in such a unique environment that challenged me and helped me to achieve my personal goals. I would like to extend my deepest gratitude to the Instituto de Telecomunicações (IT) and Iscte – Instituto Universitário de Lisboa for providing me with the resources and support to pursue my work in such a stimulating environment. My sincere thanks go to Professors Luís Cancela and João Rebola, whose guidance, expertise, patience and support have been essential to my journey of conclusion of the dissertation .

I am deeply grateful to my family and friends, who have been my pillars of strength and who have offered me unconditional support throughout this journey and have always encouraged me to continue my efforts in the most difficult moments. Special thanks to my parents and brother for being there for me and also to Vanda Cardoso whose love, patience, and unwavering belief in me have been my constant source of motivation and joy throughout this dissertation.

Finally, I would like to make an honourable mention of my great-grandfather, whom I remember very fondly and who always had a special appreciation for me.

Resumo

Nos últimos anos, o tráfego nas redes óticas, tanto submarinas como terrestres, tem crescido exponencialmente, impulsionado pelas aplicações que necessitam de uma elevada largura de banda. Com a capacidade das fibras monomodo a atingir o seu limite, a multiplexagem por divisão espacial (SDM) surge como uma solução promissora, utilizando múltiplos canais espaciais, tais como múltiplas fibras, núcleos ou modos, para satisfazer estas exigências de capacidade.

Esta dissertação analisa arquiteturas de nós multiplexadores óticos de inserção/extração reconfiguráveis (ROADM) para redes SDM, avaliando diferentes estratégias para reduzir o custo. É estudada uma arquitetura com granularidade fracionada no espaço e no comprimento de onda, bem como uma arquitetura modular, e o seu custo é comparado com o custo de uma arquitetura SDM convencional.

Concluímos que arquiteturas modulares, em particular com comutadores seletivos no comprimento de onda (WSS), são promissoras para reduzir o custo dos ROADMs SDM, especialmente para um elevado número de direções. Observa-se uma redução de custos de cerca de 10% para um ROADM 16×16, em comparação com a arquitetura SDM convencional com *lane changes*, utilizando a estratégia *Full colorless, directionless, and contentionless* (CDC). No entanto, a arquitetura com granularidade fracionada no espaço e no comprimento de onda é sempre mais dispendiosa que a arquitetura SDM convencional sem *lane changes* e apresenta menor flexibilidade de comutação. O custo das arquiteturas modulares reduz-se ainda mais com a estratégia CDC por direção na estrutura de inserção/extração, em vez de *Full* CDC, permitindo uma redução de 52% nos custos para um ROADM 16×16.

Palavras-chave: Arquiteturas modulares e fracionadas; custo do *hardware*; estrutura de inserção/extração; multiplexador ótico de inserção/extração reconfigurável; multiplexagem por divisão no espaço; redes óticas.

Abstract

In recent years, optical networks traffic, both submarine and terrestrial, has grown exponentially, driven by bandwidth-intensive applications. With the capacity of single-mode fibers reaching its limit, space division multiplexing (SDM) emerges as a promising solution, utilizing multiple spatial channels, such as multiple fibers, cores, or modes, to meet future capacity demands.

This dissertation analyses reconfigurable optical add/drop multiplexer (ROADM) node architectures for SDM networks, evaluating strategies to reduce the cost. An architecture that has a fractional granularity in both space and wavelength dimensions, as well as, a modular architecture, are studied and its cost is compared with the cost of a common core-wise switching architecture.

We have concluded that modular architectures, in particular with wavelength selective switches (WSS) modules, offer a promising approach to reduce the cost in SDM ROADMs, in particular when the number of directions increases. A cost reduction of about 10% is achieved for a 16×16 ROADM comparing to the common core-wise switching architecture with lane changes considering Full colorless, directionless, and contentionless (CDC) strategy. We show that the fractional space-wavelength architecture is always more expensive than the core-wise switching architecture without lane changes and has also less switching flexibility. The cost of modular architectures can be further reduced by the CDC per direction strategy in the add /drop structure, instead of a Full CDC strategy. A 52% cost reduction is achieved for a 16×16 ROADM.

Keywords: Add/Drop structure; hardware cost; modular and fractional architectures; optical networks; reconfigurable optical add/drop multiplexer; space-division multiplexing.

Contents

List of Figures

List of Tables

List of Acronyms

A/D: Add/Drop

B&S: Broadcast and Select

CD: Colorless and Directionless

CDC: Colorless, Directionless and Contentionless

DC: Delivery-and-Coupling

EDFA: Erbium-Doped Fiber Amplifier

JS WSS: Joint Switch Wavelength Selective Switch

MB: Multi-Band

MCF: Multi-Core Fiber

MCS: Multicast Switch

MF: Multiple Fibers

M/J: Main/Junction

OXC: Optical Cross-Connect

PLI: Physical Layer Impairment

R&S: Route and Select

ROADM: Reconfigurable Optical Add-Drop Multiplexer

Rx: Receiver

SCF: Single-Core Fiber

SDM: Spatial-Division Multiplexing

SMF: Single-Mode Fiber

SPOC: Spatial and Planar Optical Circuit

Tx: Transmitter

WDM: Wavelength Division Multiplexing

WSS: Wavelength Selective Switch

List of Symbols

α	Cost of the M-array $1 \times B$ JS WSS
$\alpha'_{wo_{lc}}$	Cost of the $1 \times [(D-1)+1]\ WSS$
α'_{w_lc}	Cost of the $1 \times [(D-1 \times\ M+1\ )]\ WSS$
β	Cost of the 1×2 WSS
δ	Cost of the $N_b \times N_b$ DC Space Switch
θ	Cost of the $(D \cdot M) \times (D \cdot M \cdot W)\ WSS$
φ	Cost of the $D \times (D \cdot W)\ WSS$
γ	Cost of the$1 \times (B+1)$WSS
η	Relative routing capacity of the SDM-ROADM
$\eta[\rho]$	Relative routing capacity of an SDM-ROADM node with a limited number of A/D transceivers compared to an unconstrained node
λ	Wavelength
μ	Cost of the transponder
ω	Cost of the $M \times (M \cdot W)\ WSS$
σ	Spatial modes
A/D_{ratio}	Add/Drop ratio
B	Number of bands
D	Number of fibers or directions
D_S	Number of inputs of a module or subsystem
f_{intra}	Number of fibers connected to an adjacent module
G	*S*patial groups
L	Idle states
M	Number of cores or spatial channels
M_{Total}	Total number of spatial configurations across all wavelengths and spatial channels
n	Number of fibers per group
N_{Bcw}	Total number of WSSs required to build all the cascaded WSSs for the B&S conventional architecture
N_b	Groups of fibers
N_{cw}	Number of WSSs in a conventional architecture required to build a cascaded WSS

N_{Rcw}	Total number of WSSs required to build all the cascaded WSSs for the R&S conventional architecture
N_{SUB}	Number of modules or subsystems
$N_{Total\mathrm{B\&S}}$	Total number of WSSs required to build the subsystems in an interconnected architecture, for a B&S architecture
$N_{TotalR\&S}$	Total number of WSSs required to build the subsystems in an interconnected architecture, for a R&S architecture
N_W	Number of wavelengths per spatial channel and per direction
N_{WSS}	Number of WSSs needed to interconnect the subsystems
Q	Number of adds/drops
R	Switching capacity of an SDM-ROADM node with specific features
$R[\rho]$	Switching capacity of a CDC SDM-ROADM for a given number ρ of A/D transceivers
R_{total}	Switching capacity of an unconstrained SDM-ROADM node (when all possible routing and A/D states are supported)
W	Number of A/Ds per node
Y_Q	Total number of permutations for Q

CHAPTER 1

Introduction

1.1. Motivation and context

Over the last few decades, the volume of traffic carried over optical networks that span the globe, whether through undersea cables across the oceans or terrestrial networks embracing continents, has consistently grown at an exponential rate in the tens of percent range and has been efficiently satisfied using wavelength division multiplexing (WDM) and other technological solution, like coherent detection, the flexible grid and the reconfigurable optical add-drop multiplexer (ROADM) that enhance the efficient utilization of the available C-band in an optical fiber [1].

There is no indication that the trend of network traffic growth will stop any time soon, so we are approaching the day when the capacity limit of conventional single-mode fiber will be fully exploited due to new applications and services that need more and more capacity [2].

One of the leading candidates offering a significant capacity enhancement is space division multiplexing (SDM), leading to the concept of SDM optical networks for high-capacity transmission, which is a promising solution with scaling potential to meet future transmission capacity demands and switching efficiency, that is considered a long-term solution for optical networks. SDM consists in using different spatial channels to transport information, using multicore fiber (MCF), multimode fiber (MMF) or parallel fibers. Each spatial channel is used to transport a WDM signal [3]. SDM is considered, nowadays, more suitable for submarine networks, because of the large volume of data traffic these networks carry [4].

In order to analyse and study signal transmission in these SDM transmission networks, new ROADM node models need to be developed. The dimension of these ROADMs tends to be considerable large in comparison with ROADMs working in conventional networks, which brings out cost issues and implementation problems. In this dissertation, we focus our study on SDM ROADM nodes that present cost effective solutions, by exploring spatial and wavelength switching dimension schemes and A/D structures with less hardware [5-7].

1.2. Goals

This work aims to study the cost of two SDM ROADM architectures - the fractional and wavelength architecture and the modular architecture - and compare it with the common core-wise switching architecture. Therefore, the following goals are considered relevant:

1. Study conventional architectures of ROADMs nodes for SDM networks in terms of

functionality, number of hardware components and cost;

2. Analyse the functionality and cost of the fractional and wavelength architecture and of the modular SDM architecture;
3. Make a comparison study between the fractional space and wavelength and the modular SDM architectures with the common core-wise switching architecture;
4. Study different A/D structures to reduce the cost of the SDM-ROADM nodes.

1.3. Dissertation organization

This section describes how this dissertation is organized.

In **Chapter 2**, a brief review of the SDM concept and of the ROADM architectures classification is presented. Different switching strategies (space granularity, wavelength-space granularity, wavelength granularity, fractional space-full wavelength granularity) and their functionalities are analysed. For each switching strategy, a possible SDM ROADM architecture, and the required hardware used in that architecture are presented.

In **Chapter 3**, we study and analysed the switching strategy with fractional space-wavelength granularity for further comparison with the conventional core-wise switching without lane changes. We discuss the required hardware and its functionalities and perform an analysis on the hardware cost. Then, we address the internal operation and hardware used in the ROADM-subsystems modular architectures, as well as its advantages/disadvantages. Both modular and fractional architectures are compared to the conventional core-wise switching assuming different add/drop (A/D) structures and using different WSS dimensions. Next, we study solutions for further reducing the cost of the A/D structure of the modular and fractional space-wavelength architectures. Then, a brief overview of the node switching capacity is done.

In **Chapter 4**, the final conclusions of this work, and considerations for future work are presented.

1.4. Main contributions

The main contributions of this dissertation are:

- Cost comparison between the fractional SDM ROADM architecture, the modular SDM ROADM architecture and the conventional core-wise switching SDM ROADM architecture.
- Study and analysis cost effective solutions for A/D structures in SDM ROADMs, such as the CDC per direction and the CDC per spatial channel solutions.

CHAPTER 2

Literature review on ROADM-based SDM optical networks

2.1. Introduction

In this chapter, we briefly review the concept of SDM multiplexing in section 2.2. In section 2.3 the ROADMs architectures classification is explained. The different switching strategies (space granularity, wavelength-space granularity, wavelength granularity, fractional space-full wavelength granularity) and their functionalities are analysed in section 2.4. For each switching strategy, it is presented a possible SDM ROADM architecture, and the hardware used in each architecture.

2.2. ROADM-based SDM optical networks

The adoption of new SDM-supporting fibers in the optical network potentially increases the capacity per fiber by a factor of M, the number of guided spatial modes or cores. Considering that each fiber mode or core still spectrally spans the optical communication band, WDM can be applied, carrying N wavelength channels per spatial mode or core [8]. The WDM-SDM fiber capacity can be defined by a two-dimensional spatial-spectral array, with wavelengths ($\lambda 1$, …, λN) and spatial modes ($\sigma 1$,…, σM) defining its columns and rows.

Another solution for increasing the capacity of optical networks is the multi-band (MB) solution that explore other bands than the C-band [9]. This solution is considered a short-term solution since the fiber installation, mandatory for the SDM solution, is not needed in this scenario. Nevertheless, the capacity of a multiband solution can be at most 8 to 10 times the capacity of C-band systems (nowadays only C+L+S systems are being considered so a 3 times increase is achieved), whereas the capacity of SDM systems has the potential to be must larger [9].

Nowadays it is foreseen that the transmission capacity aspect of SDM transmission can be scaled to the level of 1 Pbit/s (which is equivalent an equal to 1,000 Terabits by employing uncoupled Multi-Core Fiber (MCF) directly. Each core of the uncoupled MCF has nearly identical optical properties as a single-mode fibers (SMF), thereby enabling the immediate utilization of existing digital coherent transceivers. The number of parallel cores can be increased to 32 within a cladding diameter of 250 µm, while ensuring the mechanical reliability of the MCF [9].

SDM has several applications notably in data centers that aim to improve data transmission capacity, enhance network performance, and provide more reliable communication, where it is projected that, by the year 2030, the required transmission capacity and optical node throughput will exceed 1 and 10 Pbit/s, respectively. data centers can benefit from SDM by using parallel optical links or waveguide which enables high-speed data transfer between servers and storage devices [9].

Another potential application of SDM networks in the future lies in submarine cables, where these systems face unique challenges due to the harsh underwater environment, long transmission distances, and the need for high data rates. SDM is a valuable technology for submarine cables by allowing multiple data streams to be transmitted simultaneously through different cores which helps meeting the growing demand for high-bandwidth connections between continents and supports the expansion of international internet traffic [9].

SDM can also serve as a potential solution for fronthaul networks, to increase capacity and support the demanding requirements like the high bandwidth and low latency which are essential for the successful deployment and operation of emerging technologies like 5G and future wireless communication systems [9].

SDM can also be applied to core networks, allowing them to meet the increasing demands for capacity, speed, and reliability in modern telecommunications. It supports the efficient and cost-effective transmission of diverse services and ensures that core networks can adapt to the evolving needs of the digital age [9].

The use of submarine cables and datacenters is seen as the short-term application of SDM networks. This technology is currently being used and tested in the real world, such as the successful test of a 4-core submarine fiber cable. This test, which connects Taiwan, the Philippines, Guam and California, was carried out in collaboration between Google and NEC. It marks the pioneering application of MCF technology in the submarine cable sector and has been validated for its ability to meet the stringent requirements of global telecommunications networks [10,11]. This short-term application is crucial to meet the growing demands of global connectivity and high data processing capacity requirements in data center environments. On the other hand, the use of SDM in fronthaul and core networks is considered a long-term application as the network is characterized by supporting a multitude of connections scenarios, but the SDM solution will be also crucial in these networks due to the continuous need to increase capacity, reduce latency, improve reliability, support new technologies in telecommunications networks [9].

Nowadays optical networks employ WSSs at network nodes to perform the switching and are exclusively based on SMF interfaces [9]. A conventional WSS accepts a single fiber carrying WDM traffic and switches each wavelength channel to one of the possible output fiber ports, i.e., a $1 \times D$ WSS (D is the number of fibers or directions) is needed, whereas a WSS for a SDM node must have a much larger dimension with $D \times M$ outputs (M is the number of cores or spatial channels) [9]. Several solutions have been proposed in the literature for using smaller WSS dimensions, namely exploring switching architectures with modular structures, and exploring switching architectures that sacrifice the switching flexibility so that the WSSs dimension is reduced [9]. Besides the dimension issue these large WSSs, also introduce significant challenges in terms of complexity, resources cost and physical impairments which are a challenge especially over long distances.

2.3. Classification of ROADM architectures and A/D structures according with their hardware and functionalities

The most commonly used ROADM architectures today are the broadcast and select (B&S) and the route and select (R&S) which are represented, respectively, in Figure 2.1 a) and b). In a B&S architecture, represented in Figure 2.1 a), the input wavelength channels coming in on each degree are broadcasted to the egress side of every other ROADM degree including the A/D structure. Usually, optical splitters are used on the ROADM input and WSSs on the output in this type of architecture. In R&S-type architectures, represented in Figure 2.1 b), wavelength channels are selected on the ingress WSS and sent to a specific destination. In this case these architectures use WSS both in input and output stages. The absence of a splitter and the independence of loss from the number of WSS ports contribute to their increased scalability.

The A/D structures presented in these architectures are classified according with their functionalities. In Figure 2.1 a) it is shown a colorless and directionless (CD) ROADM A/D structure. This structure has contention since it is not possible to drop the same nominal wavelength channel from different directions in the same A/D structure, as there is a common link between the two WSSs in the drop structure. Presently, there are already commercially available programable $M \times N$ WSSs allowing for greater scalability in exchange for a higher cost [1]. Therefore, the solution presented in Figure 2.1 a) is no longer considered practical in present ROADMs architectures. In Figure 2.1 b), it is shown a colorless, directionless and contentionless (CDC) ROADM A/D structure. In this architecture, it is possible to extract any wavelength channel (colorless) from any direction (directionless) without contention from channels with the same wavelength from different directions that are extracted to the same A/D structure (contentionless). Usually, this structure is built with multicast switches (MCSs) or $M \times N$ WSSs [9].

Currently, CD and CDC applications encompass the rerouting of wavelengths in response to failures or proactive avoidance of future service degradation. CDC can offer advantages over CD in networks with higher loads and at nodes with significant quantities of A/D channels. Despite the fact that CDC structures, in general, provide greater flexibility in comparison to CD, this implies that the associated cost increases, as illustrated in the Figure 2.2 [1].

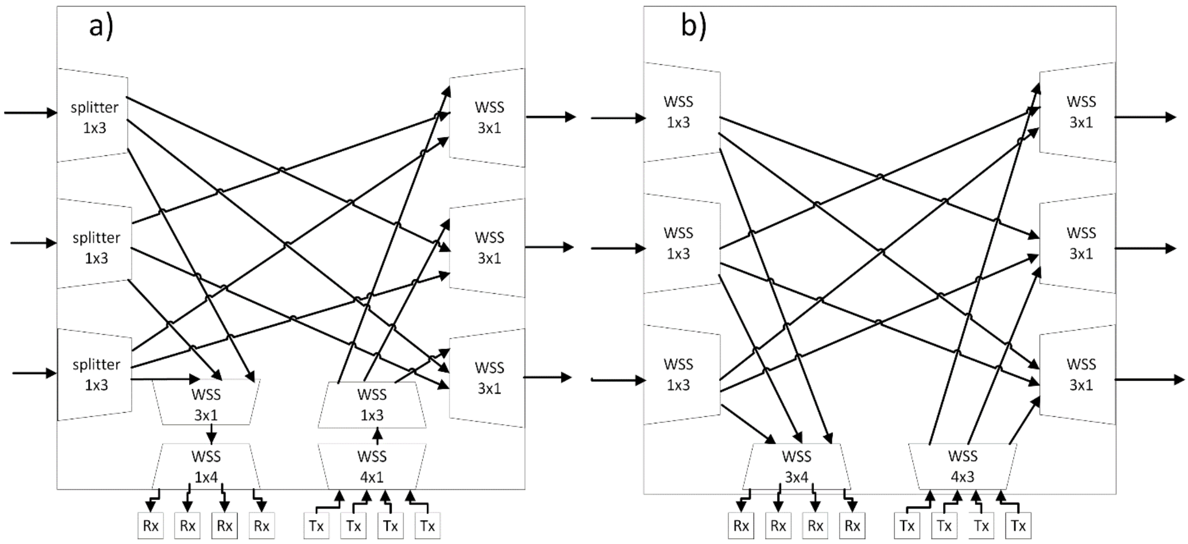

Figure 2.1 - a) Broadcast and select ROADM architecture with a CD A/D structure. b) Route and select ROADM architecture with a CDC A/D structure [12].

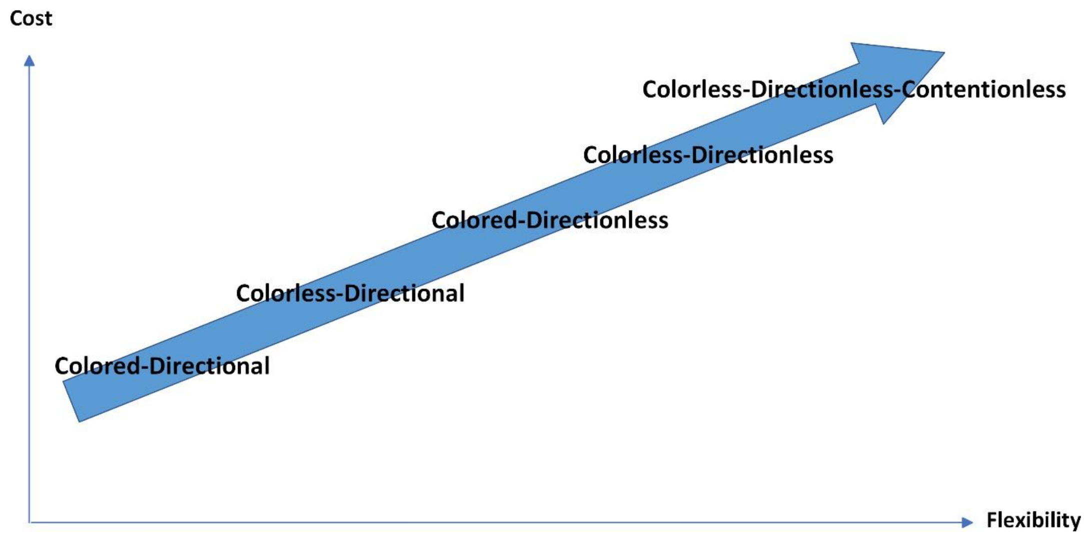

Figure 2.2 - Comparison of ROADM A/D flexibility and cost [12].

Typically, B&S ROADMs exhibit a lower number of directions compared to R&S ROADMs due to the challenge of managing splitting losses in ROADMs with more than 4 directions (as a rule 1×9 WSS are commonly used for B&S ROADMs on the output stage. This means that the difference in performance between B&S and R&S is insignificant when using a 1×9 or smaller WSS. However, when using a larger WSS, such as 1×20 or larger, R&S exhibits a performance superiority. Additionally, CD ROADMs are commonly employed in core networks with fewer nodes and a reduced demand for flexibility. Conversely, CDC ROADMs find typical usage in metro networks characterized by a substantial number of nodes and a greater requirement for flexibility [1].

2.4. SDM switching strategies

In SDM-based optical networks, characterized by *M* spatial channels and *N* wavelength channels per spatial channel, switching can be done in two dimensions, space and wavelength, leading to four switching strategies: space granularity, wavelength-space granularity, wavelength granularity, fractional space- full wavelength granularity [9].

In the space granularity strategy, represented in Figure 2.3 a), the switching is done between spatial channels. This operation can be classified, as spatial switching and can be performed with or without lane changes. Spatial switching without lane changes means that the spatial channel in one direction is switched to another direction, but always to the same spatial channel, e.g., spatial channel 1 on the south direction is switched to spatial channel 1 on the north direction. Spatial switching with lane changes means that the spatial channel in one direction is switched to another direction but it can be switched to a different spatial channel, e.g., spatial channel 1 on the south direction is switched to spatial channel 2 on the north direction.

In the space-wavelength granularity strategy, represented in Figure 2.3 b), the switching is done between wavelength channels and in any spatial channels, e.g., wavelength λ_1 in spatial channel 1 in the south direction, is switched to wavelength λ_3 in spatial channel 4 on the north direction. This strategy can also be implemented with or without lane changes. The space-wavelength granularity strategy will lead to a more flexible switching architecture, but at the cost of more complexity.

In the wavelength granularity strategy, represented in Figure 2.3 c), the switching is done between groups of the same wavelength channels, i.e., all wavelength channels λ_1, on the south direction (of all spatial channels), are switched together to the north direction. A joint switch (JS) WSS is used to perform this operation [9].

In the fractional space-full wavelength granularity strategy, represented in Figure 2.3 d), the switching is done between groups of the same wavelength channels, but in this strategy these groups are previously defined, i.e. wavelength channels λ_1 of group 1 in the south direction, are all switched together to group 1 of the north direction, and wavelength channels λ_1 of group 2 on the south direction, are all switched together to group 2 on the east direction.

In the fractional space-wavelength granularity strategy, represented in Figure 2.3 e), the switching is done between groups of spatial channels and wavelength channels. In this strategy the groups are previously defined, i.e., σ_1 and σ_2 are grouped together with λ_1 and λ_2 to form a group.

In the following sections we analyse with more detail the spatial, spatial-wavelength, wavelength granularity, fractional space-full wavelength granularity and fractional space- wavelength granularity strategies.

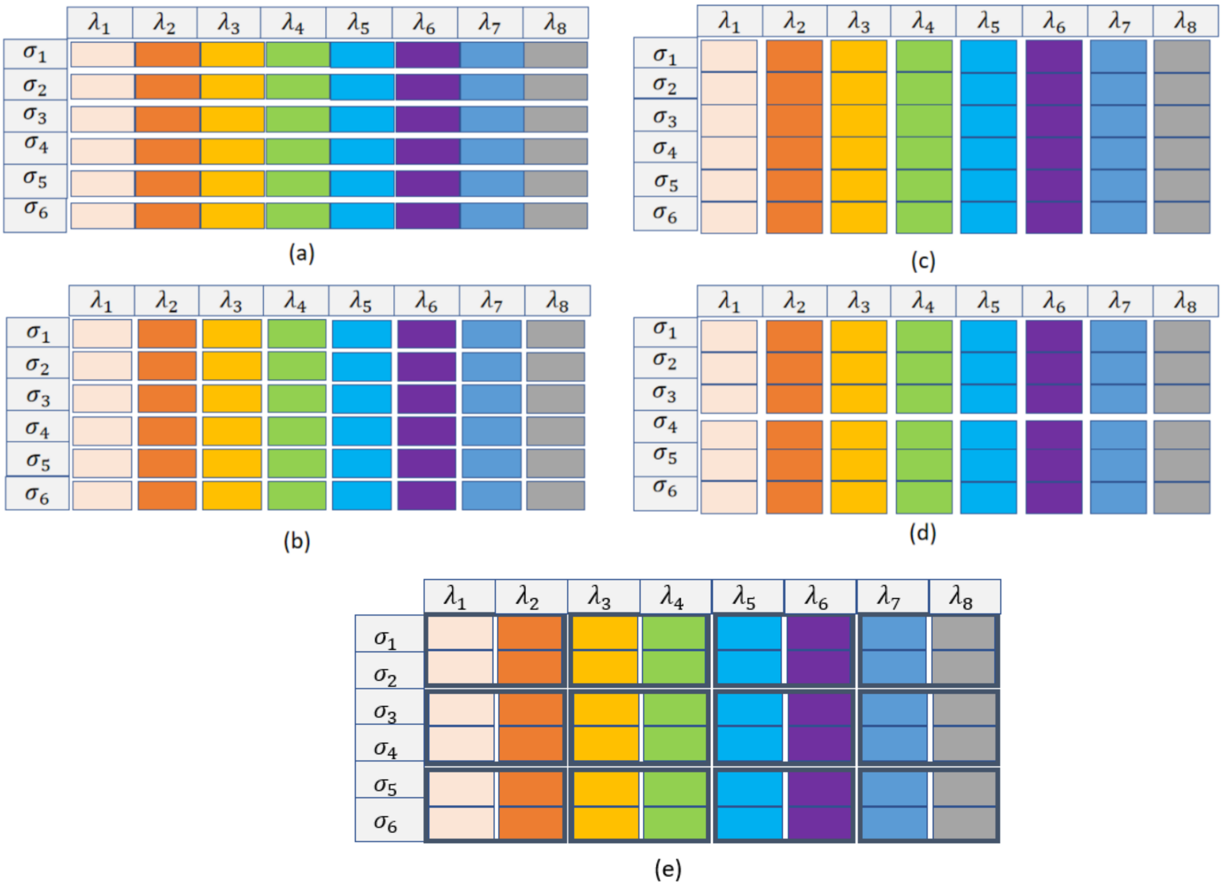

Figure 2.3 - The strategies for SDM switching are delineated by bold "white" lines that establish the switching granularity of each strategy. a) spatial granularity switching strategy, b) spatial-wavelength granularity switching strategy, c) wavelength granularity, d) fractional space-full wavelength granularity strategy and e) the fractional space-wavelength granularity strategy [9]

2.4.1. Spatial granularity architecture

In this approach, it is necessary to utilize switches to route the complete communication band of each separated spatial channel to its intended destination. This routing process can be implemented with or without the use of lane changes. The spatial ROADM architecture is usually called a fiber- level switching or independent switching ROADM [13].

In the scenario where spatial lane changes are not utilized, the routing of data from an ingress spatial channel (core or mode) is accomplished by transmitting the data on the same spatial channel in the egress fiber [7,9]. Switching without lane changes can be achieved by utilizing a collection of small optical cross-connects (OXCs), with one OXC assigned to each spatial channel. The input/output port count of each individual OXC, dedicated to a particular spatial channel, must be no less than the number of directions, *D*, which means that at least *M* $(D+1)\times(D+1)$ OXCs are required. Therefore, in order to accomplish switching without lane changes, *M* of such OXCs are required [9].

Lane changes support means that the spatial channel in one direction can be switched to another direction, and another spatial channel. In this scenario, it is recommended to utilize a single large OXC to handle all the node traffic. In this scenario, the port count of the OXC is $(D \cdot M) \times (D \cdot M)$ [9]. One significant drawback of an architecture based on a single large OXC is the event of this OXC failure. To mitigate this risk, a second OXC can be implemented in parallel as a protective measure.

However, this solution increases cost, space requirements, and fiber-routing complexity. In contrast, when utilizing a bank of smaller OXCs without lane changes, a failure of a single switch would only impact $1/M$ of the node traffic [9].

In Figure 2.4, it is represented a SDM ROADM-based architecture with spatial granularity without lane changes, considering 2 directions (*D*=2), 4 spatial channels (*M*=4), 80 wavelengths per spatial channel (N_W=80) and an A/D ratio of 20%. The spatial channels are represented in different colours: blue, red, black and yellow. To build this architecture $4\ 3 \times 3$ OXC are used. Each OXC is responsible for routing the spatial channels of a particular colour, and each OXC has also an input/output stage for the ROADM A/D structure [9].

The drop structure represented in Figure 2.4 consists of $4\ 1 \times 17$ WSSs, where each 1×17 WSS is responsible for extracting 20% of the 80 wavelengths in a particular spatial channel (i.e., core) plus an additional output, that goes to the switching architecture, with wavelength signals that continue on the optical domain and were not dropped. In this drop structure, it is possible to extract any wavelength (colorless) on any of the 17 ports of each 1x17 WSS and to drop one spatial channel of a given colour of any of the ROADM directions (directionless) however its limitation is that it can only extract signals from one spatial channel at a time hence the A/D structure is only CD [9]. The add structure is similar to the drop structure using $4\ 17 \times 1$ WSSs instead as can be observed in Figure 2.4.

In Figure, 2.5 it is represented a SDM ROADM-based architecture with spatial granularity with lane changes, considering 2 directions (*D*=2) and four spatial channels (*M*=4), 80 wavelengths per spatial channel (N_W=80) and an A/D ratio of 20%. The spatial channels are represented in different colours: red, blue, black and yellow. This architecture has a single 12×12 OXC. This OXC is responsible for routing any spatial channel to any of the ROADM directions and also has 4 input/output for assessing the ROADM A/D structure, which has the same structure of the one used in Figure 2.4, for the architecture without lane changes.

This type of switching architecture could be potentially used in core networks where spatial granularity is sufficient to obtain the required routing flexibility [1].

In this approach, the utilization of space-wavelength granularity provides the finest level of switching granularity. However, the implementation complexity associated with this approach is considerably higher compared to the spatial granularity architecture [9].

Access to space-wavelength granularity is attained by initially demultiplexing the signal spatially. This is then followed by a WSS dedicated on each spatial channel, which facilitates the routing of the signal to other output ROADM directions [9].

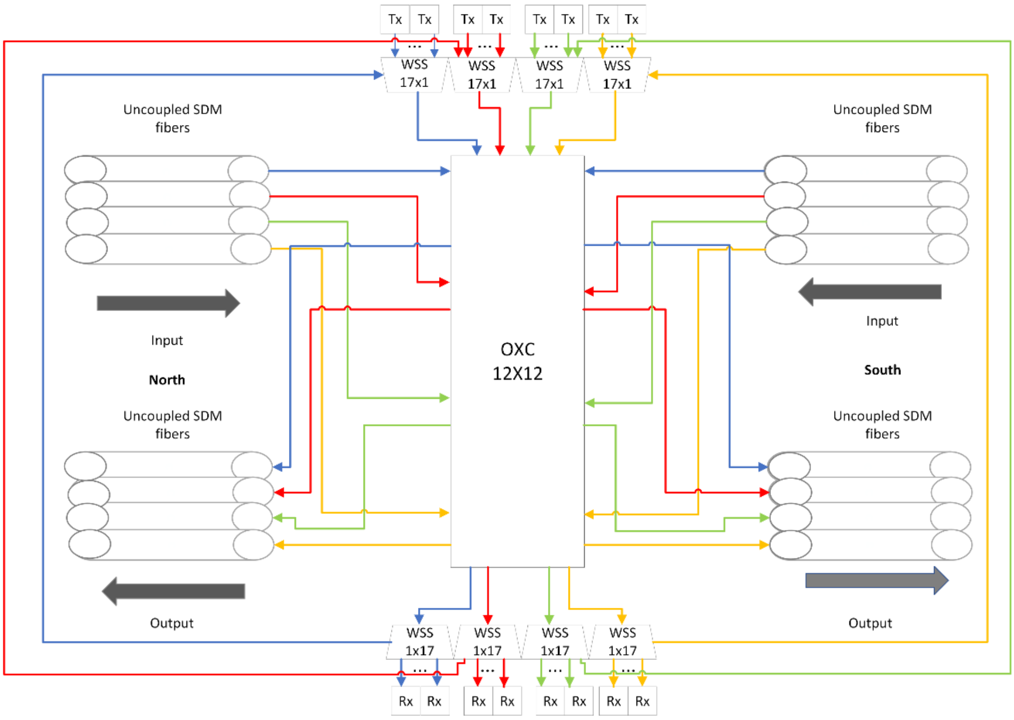

Figure 2.4 - Spatial granularity architecture without lane changes (Rx- receivers Tx-transmitters) with two directions (D=2) and four spatial channels (M=4) , with 80 wavelengths per channel and a 20% A/D ratio.

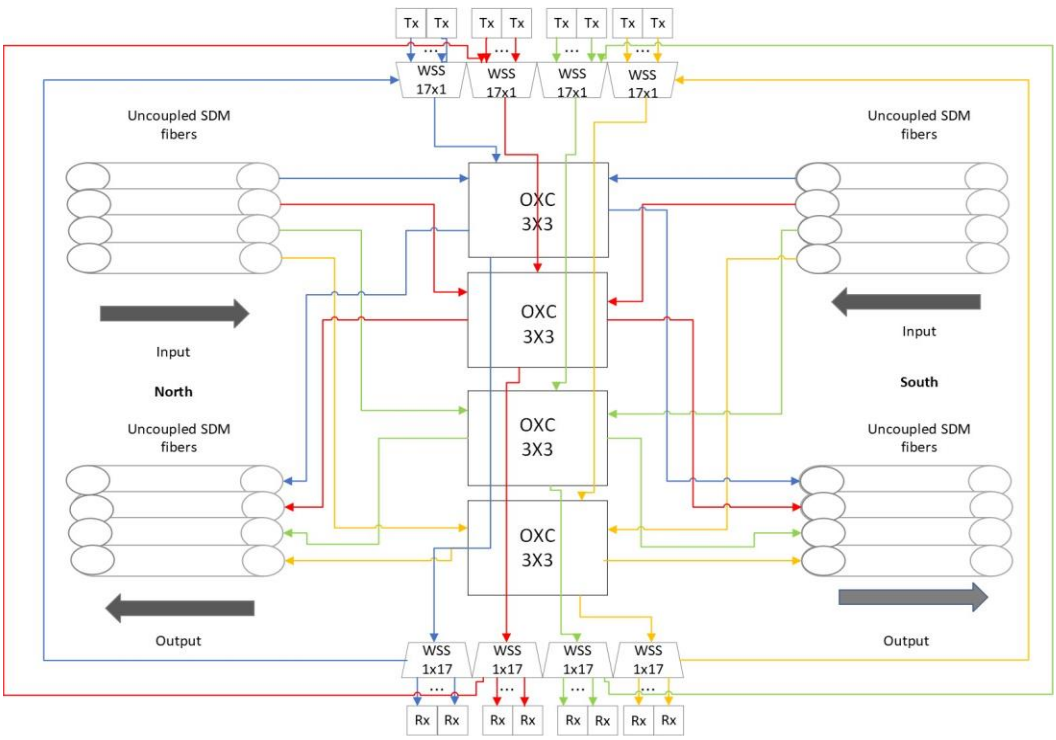

Figure 2.5 - Spatial granularity architecture with lane changes with two directions (D=2) and four spatial channels (M=4) , with 80 wavelengths per channel and a 20% A/D ratio.

2.4.2. Spatial-wavelength granularity architecture

This architecture can be also implemented with or without lane changes as the spatial architecture in subsection 2.4.1. In Figure 2.6 it is represented, a SDM R&S ROADM-based architecture with spatial-wavelength granularity without lane changes, considering 2 directions (*D*=2) and 4 spatial channels (*M*=4), with the spatial channels differentiated by colours: blue, red, yellow, black. This architecture can be called core-wise switching architecture [13]. In this approach, the elimination of inter-core switching within an MCF aims to prevent a rise in WSS port count. This architecture is composed by $16\ 1 \times 2$ WSSs. For a generic spatial-wavelength granularity architecture without lane changes with *D* directions and *M* spatial channels $2 \cdot M \cdot D\ \ 1 \times (D-1)+1$ WSSs are needed, assuming one output to the drop structure (+1). In Figure 2.7, a SDM R&S ROADM-based architecture with spatial-wavelength granularity with lane changes, considering 2 directions (*D*=2) and 4 spatial channels (*M*=4) is represented. This architecture is composed by $16\ 1 \times 5$ WSSs. For a generic spatial-wavelength granularity architecture with lane changes with *D* directions and *M* spatial channels $2 \cdot M \cdot D\ \ 1 \times (D-1) \cdot M+1$ WSSs are needed, assuming one output to the drop structure (+1) [8].

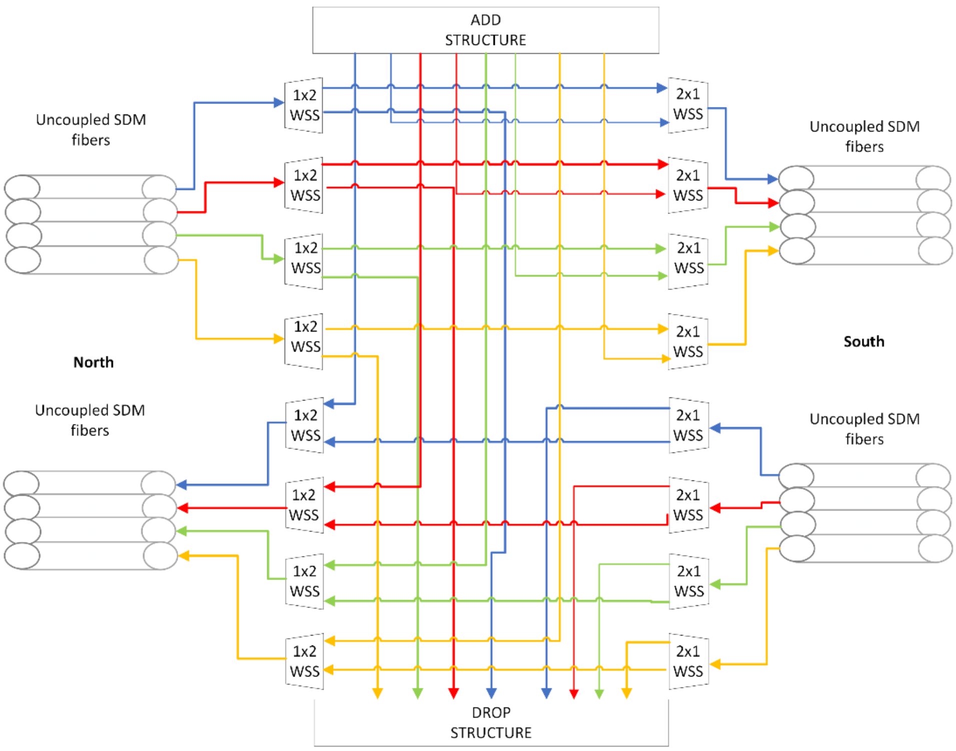

Figure 2.6 - Spatial wavelength granularity architecture without lane changes with two directions (D=2) and four spatial channels (M=4)

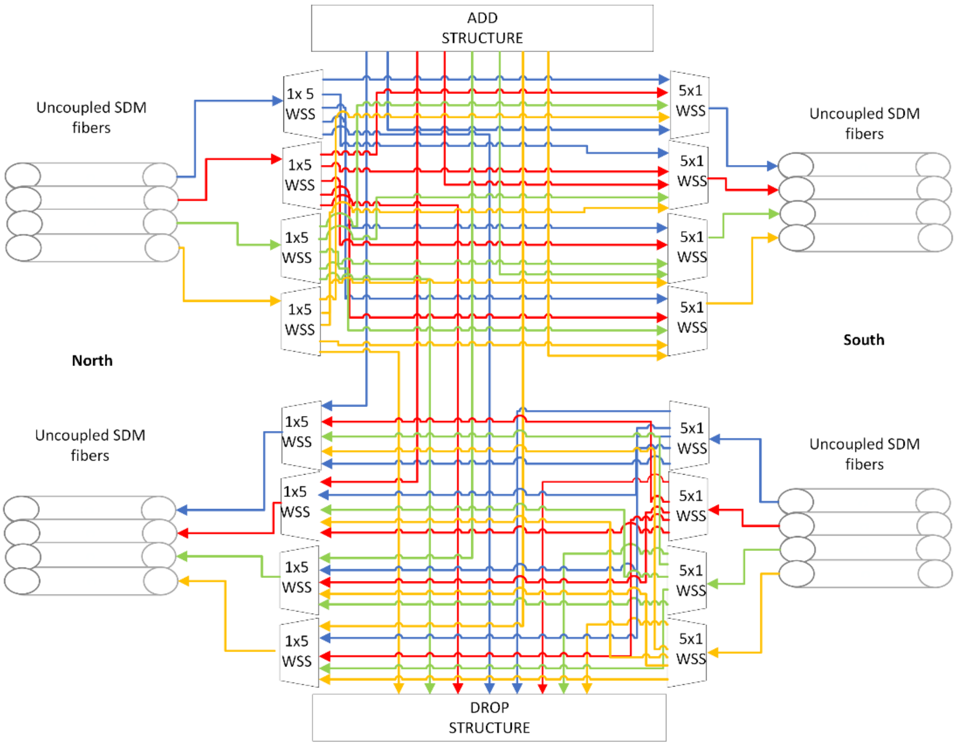

Figure 2.7 - Spatial wavelength granularity architecture with lane changes with two directions (D=2) and four spatial channels (M=4)

The A/D structure for the ROADM architectures presented in Figures 2.6 and 2.7 can be implemented with four different strategies [7].

The first strategy, represented in Figure 2.8 a), considers a single WSS that serves all directions and spatial channels. This WSS has $D \times M$ inputs, where D is the number of directions and M the number of spatial channels in each direction, and $D \times M \times W$ outputs that depend on the A/D ratio considered (with $W = N_W \times A/D_{ratio}$, where N_W is the number of wavelength channels considered in each core or spatial channel) . This A/D structure provides the ROADM with CDC capability but has the disadvantage of using WSSs with large dimensions [7].

The second strategy is represented in Figure 2.8 b) and considers $D \times (D \cdot W)$ WSS per spatial channel with D inputs and $D \cdot W$ outputs with a total of M WSSs per A/D structure, so it only has CDC capability per spatial channel. This strategy has less flexibility than the previously referred, but it has the potential of using WSSs with a smaller dimension and commercially available. Moreover, such strategy is advantageous in gradual SDM deployment over existing networks since the network operator can add one spatial channel at a time when it needs more capacity [7].

The third strategy is represented in Figure 2.8 c) and considers a $M \times (M \cdot W)$ WSS per direction, with a total of D WSSs per A/D structure with M inputs and $M \times W$ outputs, so it only has CDC capability per direction. This A/D structure is CDC only within in each direction. Once again, this strategy has a lower flexibility than the first one previously referred but has the potential of using WSSs with a smaller dimension and commercially available. This strategy may be used for a greenfield SDM network deployment, where more nodes can be added to the network topology as the network grows [7].

The fourth strategy considers a CDC A/D structure for one specific direction. In this strategy, the transmitter-receivers are directly connected to the input/output WSSs and are thus bound to a given spatial degree and nodal direction, being this strategy known as pure directional SDM-ROADM [7].

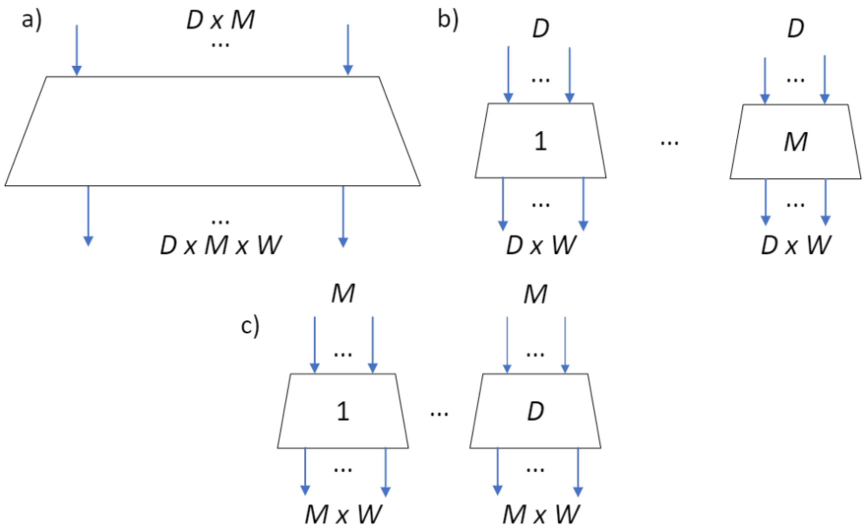

Figure 2.8 - a) A/D structure with Full CDC capability with a single M×N WSS with DxM inputs and N outputs, b) A/D structure with CDC capability per spatial channel, c) A/D structure with CDC capability per direction.

Table 2.1 - Dimensions of the WSSs associated with each strategy considering for various values of D and M for the drop structure

Strategy	*D* = 2			*D* = 4			*D=16*		
	M = 4	*M* = 7	*M* = 12	*M* = 4	*M* = 7	*M* = 12	*M* = 4	*M* = 7	*M* = 12
Full CDC	8 x 128 WSS	14 x 224 WSS	24 x 384 WSS	16 x 256 WSS	28 x 448 WSS	48 x 768 WSS	64 x 1024 WSS	112 x 1792 WSS	192 x 3072 WSS
CDC per spatial Channel	4 WSSs 2 x 32	7 WSSs 2 x 32	12 WSSs 2 x 32	4 WSSs 4 x 64	7 WSSs 4 x 64	12 WSSs 4 x 64	4 WSSs 16 x 256	7 WSSs 16 x 256	12 WSSs 16 x 256
CDC per Direction	2 WSSs 4 x 64	2 WSSs 7 x 112	2 WSSs 12 x 192	4 WSSs 4 x 64	4 WSSs 7 x 112	4 WSSs 12 x 192	16 WSSs 4 x 64	16 WSSs 7 x 112	16 WSSs 12 x 192

Table 2.1 shows the dimensions of the WSSs in the drop structure associated with each strategy mentioned above, considering various values of *D* and *M* and assuming an A/D ratio of 20% and N_W=80 wavelengths per spatial channel .

From Table 2.1 it is possible to notice that for each strategy the dimension associated with each

WSS increases with *D* and *M*. In particular, in the first strategy, the dimensions of the WSS increase with *D* and *M*, where a higher value of these parameters leads to a larger WSS dimension. However, in the second and third strategies WSSs have smaller dimensions. Specifically, for the second strategy, the dimension of the WSSs is kept constant regardless of the value of *M* for a given *D*, while the number of WSSs in parallel increases with *M*. For the third strategy, it can be observed that the dimension of the WSSs remains the same for a fixed *M* regardless of *D*. Considering a maximum WSS dimension of 35, and a future increase to 60 in the next years [12] it can be easily concluded that the majority of the WSSs presented in Table 2.1 are not commercially available at this moment and it will be very hard to become available in the next years.

Assuming the reference case of *D*=2 and *M*=4, the first strategy considered above for implementing the A/D structure should be built using a single 8×128 WSS where the number of outputs is calculated with the expression $D \times M \times W$ $(2 \times 4 \times 80 \times 0.2 = 128)$. For the second strategy presented, we need 4 2×32 WSS in parallel where the number of outputs of each WSS $D \times W$ $(2 \times 80 \times 0.2 = 32)$. For the third strategy we need to use 2 4×64 WSS in parallel where the number of outputs of each WSS is $M \times W$ $(4 \times 80 \times 0.2 = 64)$.

From this reference case (*D*=2 and *M*=4) it is observed that in all strategies, except the second strategy, the WSSs are not commercially available. A possible solution to address this situation for the first strategy is to use smaller WSSs in parallel, e.g., 8 (8×16) WSS in parallel. The 8×16 WSS can be replaced by 8×16 MCS for a more cost-effective solution. In both these solutions the ROADM input WSS should have 8 more outputs intended to the drop structure. On the other side the ROADM output WSS should have 8 more inputs. For example, considering the ROADM of Figure 2.6 the value of outputs should be 9, since 8 are for the A/D structure and one to the other direction.

Architectures based on spatial and wavelength switching granularity could be potentially used in metro networks since these networks require greater routing flexibility [12].

2.4.3. Wavelength granularity architecture

In this scenario, all spatial channels are routed as a whole per wavelength channel. This functionality can be provided by a single WSS modified to support joint switching over all SDM channels on a wavelength basis by employing spatial diversity [1]. This ROADM architecture is usually named a spatially jointed switching ROADM [13].

Contrary to space granularity, which forfeited access to the spectral domain, wavelength granularity sacrifices the spatial domain to simplify the switching hardware. Implementations rely on modified WSSs in support of joint switching of all *M* spatial channels on a wavelength basis [8,14].

Unlike conventional WSS designs, where fiber ports are dispersed and imaged to the same positions at the switching plane, as shown in Figure 2.9 a), the joint-switching WSS allows for simultaneous redirection of multiple incident beams, resulting in the same beam-steering shift for all beams. If the input/output fibers of the WSS are arranged in a regularly spaced array, the steering of a set of inputs is reimaged onto different sets of outputs [8]. Figure 2.9 b) illustrates a JS WSS, which accommodates 3 spatial channels and 2 wavelength channels per spatial channel. The spatial channels are depicted in black, while the wavelength channels are represented in blue and red. The steering mirror is divided into sections [8,15], and each spatial channel is directed to a distinct section. As a result, each section of the steering mirror introduces a unique steering angle, causing wavelength channels with the same index (e.g., λ1) from all spatial channels to align in the same direction. This alignment forms a spatial channel group in that specific direction.

In Figure 2.10 it is represented a R&S SDM ROADM-based architecture with wavelength granularity, considering 2 directions (*D*=2), 4 spatial channels (*M*=4), 80 wavelength channels (N_W=80), A/D ratio of 20% and with each spatial channel group (with channels with the same wavelength) represented by a single colour at the input/output of the JS WSSs. This architecture has two, $4 \times (1 \times 2)$ input JS WSSs, and two, $4 \times (2 \times 1)$ output JS WSSs. The JS WSSs are responsible for directing a spatial channel group which combines multiple individual wavelengths or subcarriers into a single high-capacity transmission channel with a specific wavelength to either an output direction or to the drop structure. The output JS WSS receives the spatial channel group from other directions or from the add structure.

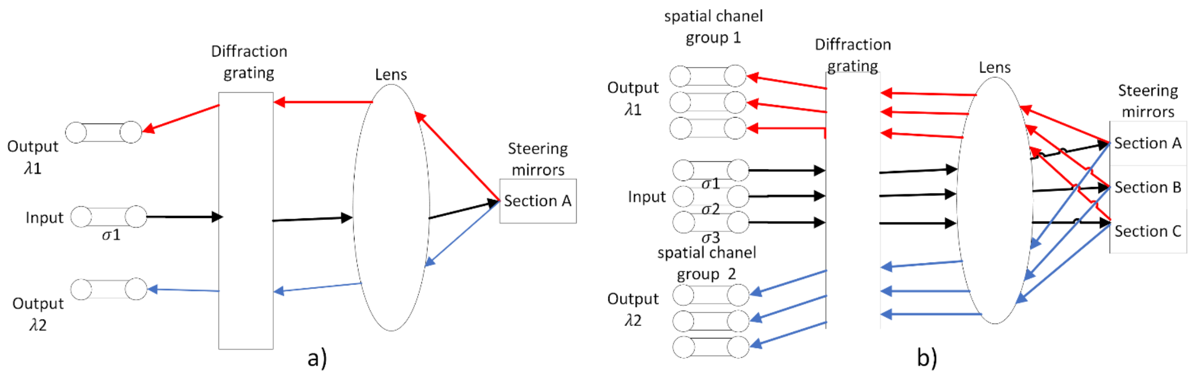

Figure 2.9 - a) Conventional 1×2 WSS with 2 wavelength channels b) Joint switch 1×2 WSS with 3 spatial channels [1]

In Figure 2.11, it is represented a CDC A/D structure for a SDM ROADM-based architecture with wavelength granularity. This A/D structure is responsible to extract/add a spatial channel group, using JS WSSs. The drop structure is comprised of a single $4 \times (1 \times 16)$ JS WSS, featuring 64 output links directed towards receivers, as well as 4 input links originating from an input JS WSS. Similarly, the add structure consists of a single $4 \times (16 \times 1)$ JS WSS, with 64 input links coming from transmitters and 4 output links directed towards an output JS WSS.

While Figures 2.10 and 2.11 depict a wavelength granularity solution for uncoupled fibers, this approach is also applicable to coupled SDM fibers [1]. Regarding Figure 2.10, it is necessary to replace each group of 4 conventional receivers units dedicated to a spatial channel group with a SDM receiver that can decouple the 4 spatial channels forming the spatial channel group [8].

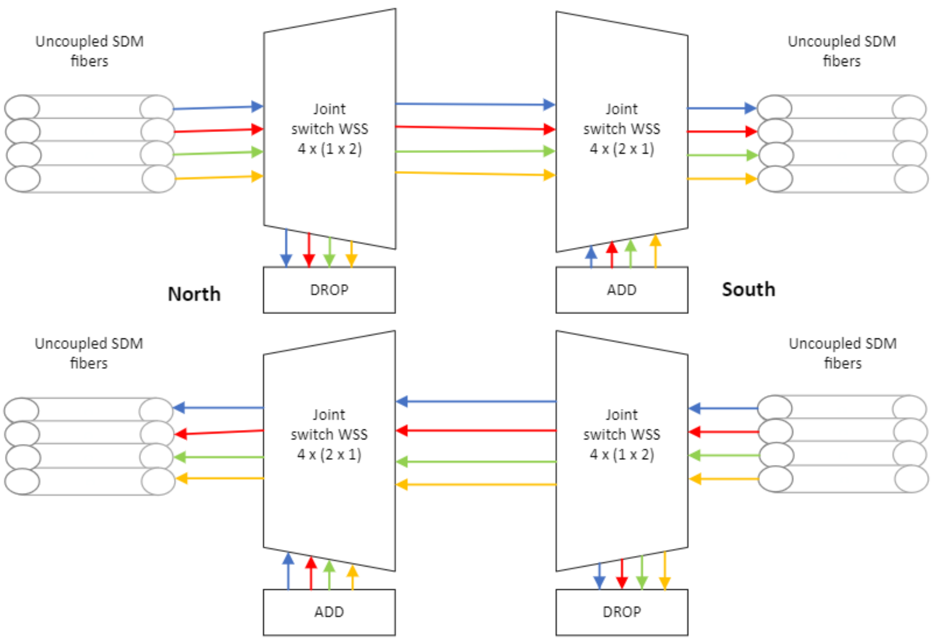

Figure 2.10 - Wavelength granularity ROADM architecture

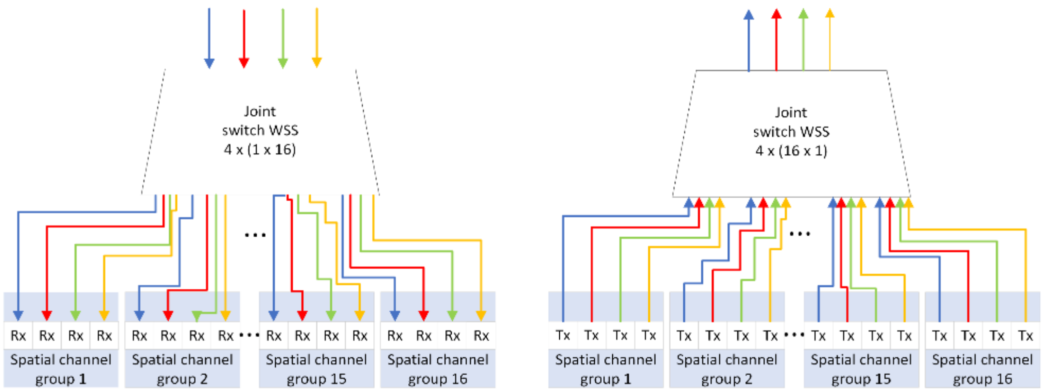

Figure 2.11 - CDC A/D structure for the wavelength granularity architecture

2.4.4. Fractional space-full wavelength granularity architecture

In this scenario, instead of existing only one spatial group per wavelength as in the wavelength granularity scenario, several spatial groups of the same wavelength can be formed. This is useful in high-capacity optical networks, such as those used in data centers or communication backbones, where flexibility and efficiency in the use of resources are essential [8,14]

Figure 2.12 illustrates a routing scenario involving an SDM ROADM-based architecture operating at fractional space-full wavelength granularity and with no lane changes. It considers two directions (D=2), four spatial channels (M=4), and two spatial groups (G=2). The spatial channels groups are differentiated by colour, namely blue, red, yellow, and green. The first spatial group comprises the spatial channels represented by the red and blue colours, while the second spatial group consists of the spatial channels represented by the yellow and black colours. This architectural configuration includes two $2\ (1 \times 2)$ input JS WSSs and two $2\ (2 \times 1)$ output JS WSSs. On one hand, the input WSS serves the dual purpose of routing all wavelength channels within a common spatial group to an output WSS in the opposite direction, which is also part of the same spatial group. Additionally, the input WSS must have two output links connected to the drop structure. On the other hand, the output WSS is tasked with receiving and grouping wavelength channels originating from the input WSS that belong to the same spatial group or from the add structure.

Figure 2.13 illustrates an SDM ROADM-based architecture featuring fractional space-full wavelength granularity with lane changes. This configuration assumes values of D=2, M=4, and G=2. Within this architecture, there are two sets of $2\ (1 \times 3)$ input JS WSSs and two sets of $2\ (3 \times 1)$ output JS WSSs. To accommodate a CDC A/D structure for fractional space-full wavelength granularity, it must be capable of independently extracting or adding each spatial channel group. Since there are two spatial channel groups in this scenario, two JS WSSs are necessary per A/D structure [8].

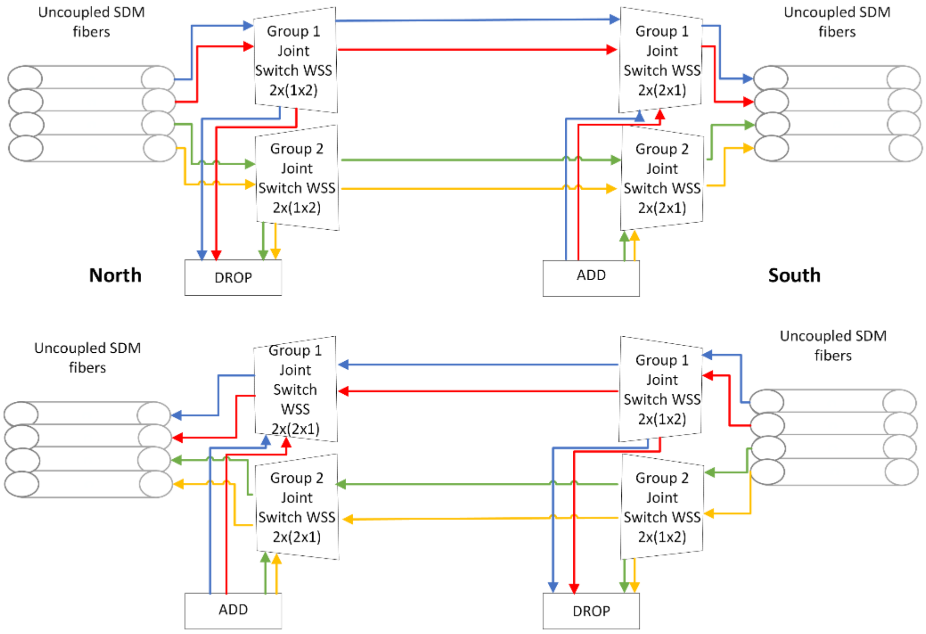

Figure 2.12 - Architecture with fraction space-full wavelength granularity without lane changes, considering 2 directions, 4 spatial channels and two groups.

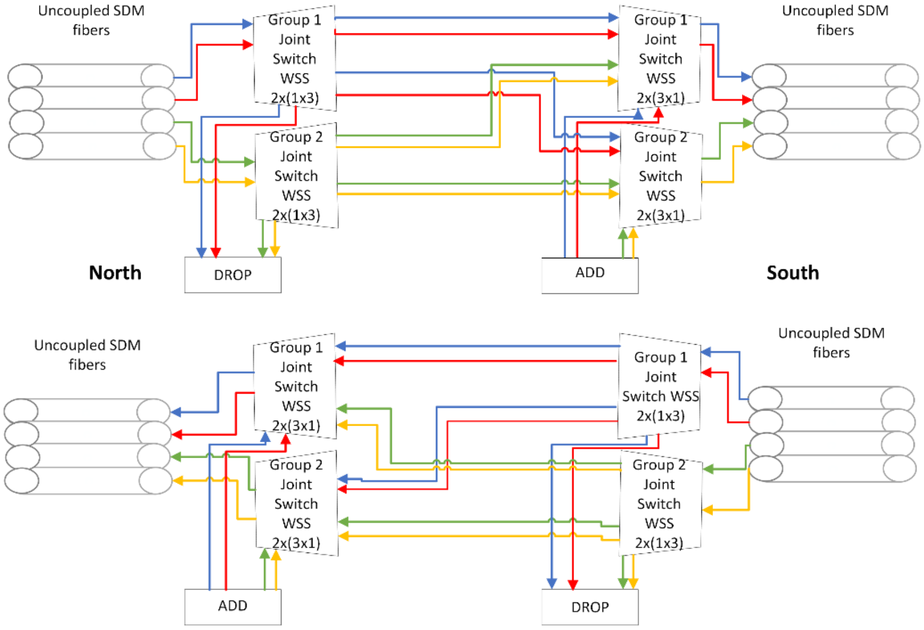

Figure 2.13 - Architecture with fractional space-full wavelength granularity with lane changes, considering 2 directions, 4 spatial channels and two groups.

The drop structure, represented in Figure 2.14 a), comprises two $2\ (1 \times 16)$ JS WSSs equipped with 32 output links leading to conventional optical receivers, and it has 2 input links connected to an input JS WSS. Likewise, the add structure, represented in Figure 2.14 b), consists of two $2\ (16 \times 1)$ JS WSSs with 32 input links from transmitters and 2 output links directed towards an output JS WSS.

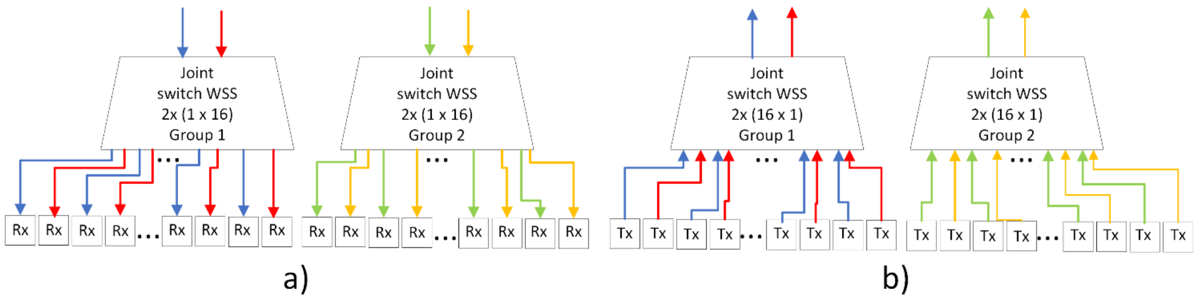

Figure 2.14 - CDC A/D structures for fraction space-full wavelength granularity architecture.

2.5. Conclusions

In this chapter, a comprehensive review of SDM-based ROADM architectures is performed, their switching strategies are analysed, and practical applications are presented.

ROADM architectures have been categorised into two main ones: B&S and R&S noting that the main difference between them lies in the way the optical signals are routed and processed.

The A/D structures in ROADMs were also discussed, focusing on their functionalities (colorless, directionless and contentionless).

The potential applications of SDM were discussed, including data centres, submarine cables, fronthaul networks for 5G and core networks.

Different switching architectures were discussed as space granularity, wavelength-space granularity, wavelength granularity, fractional space- full wavelength granularity, as well as their limitations. In summary, the spatial granularity architecture where the switching is done between spatial channels provides significant flexibility and resilience benefits, particularly with lane changes, it also introduces complexities and higher costs, especially when ensuring redundancy. Additionally, without lane changes, the architecture offers simpler, more localized failure management but at the cost of reduced routing flexibility. In the space-wavelength granularity where, the switching is done between wavelength channels and in any spatial channels approach offers the finest level of switching granularity, providing greater routing flexibility which is particularly beneficial for metro networks. However, this advantage comes at the cost of significantly increased implementation complexity compared to simpler spatial granularity architectures. The wavelength granularity architecture where, all spatial channels are routed as a whole per wavelength channel presents advantages, such as simplified hardware and the ability to redirect multiple incident beams simultaneously, which enhances efficiency and flexibility in managing high-capacity transmission channels. However, this comes with disadvantages, including the sacrifice of spatial domain granularity and the need for complex SDM receivers to handle decoupling of spatial channels, which could complicate the system design and implementation. Finally, the fractional space-full wavelength granularity architecture where, several spatial groups of the same wavelength can be formed allows for more dynamic and granular routing options, potentially improving overall network performance and adaptability. However, the routing mechanisms required to manage the multiple spatial groups can lead to potential challenges in ensuring consistent performance and reliability across the network.

CHAPTER 3

Strategies for cost reduction in SDM ROADM nodes

3.1. Introduction

In this chapter, we begin by studying the fractional space-wavelength granularity switching strategy, which will later be compared to core-wise switching without lane changes, as explained in section 3.2. Additionally, we discuss the hardware used and its functionalities. Finally, an analysis is conducted on the hardware cost and switching capacity of the SDM ROADM architecture.

Next we address the advantages/disadvantages as well and the internal operation/hardware used for B&S or R&S in the ROADM-subsystems modular architectures presented in [16] in section 3.3. Next a study will be carried out considering the modular architectures with $D_S \times D_S$ R&S as modules which will be compared to core-wise switching with lane changes explained in chapter 3.3.1 assuming different A/D structures using either 1×9 WSSs or 1×4 WSS whereas in chapter 3.3.2, $N \times N$ WSSs directly in the subsystems are considered where an initial cost comparison is made with a modular architecture with $D_S \times D_S$ R&S as modules.

In section 3.4 we study solutions for further reducing the cost of modular and fractional space-wavelength architectures, such as using alternative A/D structures (CDC per spatial channel or CDC per direction).

Section 3.5 provides a brief overview of how SPOC technology can address the challenges of reducing space inside the large dimension SDM optical nodes by integrating multiple optical components into compact modules.

Additionally, an analysis of the switching capacity of the node is conducted in section 3.6.

3.2. Fractional space-wavelength granularity architecture

In this scenario, groups involving spatial channels with more than one wavelength are possible, as represented in Figure 2.3 e). For example, spatial channel 1 involving λ_1 can be joined with spatial channel 2 involving λ_2 resulting in a spatial channel group involving λ_1 and λ_2.

A switching architecture with fractional space and wavelength granularity is proposed in [5] and is represented in Figure 3.1, considering four directions (D =4), with one fiber per direction with four spatial channels or cores (*M*= 4), two fibers per group (*n*=2), two groups of fibers (N_b=2), so that $D = n \times N_b$, two bands (*B*=2) and 80 wavelengths per fiber (N_W=80). The two bands (*B*) are differentiated by the blue and red coloured arrows. Generally, this architecture configuration includes $N_b \cdot n$ sets of $1 \times M$ fan-outs, $N_b \cdot M \cdot n$ 1×2 WSSs, $N_b \cdot n$ *M*-array $1 \times B$ JS WSSs, $B \cdot M \cdot n$ $N_b \times N_b$ delivery-and-coupling (DC) space switches, $N_b \cdot M \cdot n$ $(B+1) \times 1$ WSSs, and $N_b \cdot n$ sets of $M \times 1$ fan-ins. The

$N_b \times N_b$ DC space switch consists of N_b $1 \times N_b$ optical switches and N_b $N_b \times 1$ optical couplers [5]. So, the total dimension of the ROADM architecture is given by $N_b \cdot M \cdot n \times N_b \cdot M \cdot n$. In particular when $M = 4, n = 2, N_b = 2$, a 16x16 ROADM is obtained.

The ROADM operation, represented in Figure 3.1, consists of four steps. Initially, the fan-out component present at the input stage of the architecture separates the optical signals from the various cores of the MCF for switching. The optical paths coming from the fan-out are sent into two paths: either towards the drop section or the express section using a 1×2 WSS. Subsequently, optical paths originating from MCFs are grouped together into *B* flexible bands using $M - array$ $1 \times B$ JS WSS. The operation of a $1 \times B$ JS, with *B*=2, is exemplified in Figure 3.2 a) with an 8 array 1×2 WSS and in Figure 3.2 b) with an equivalent two by $4 - array$ 1×2 JS WSS configuration. As can be observed in Figure 3.2 one of the bands is composed by the yellow, green, light blue and dark blue wavelengths, whereas the other band is composed by the red, brown, dark green and black wavelengths. Following this, each flexible band is directed to a $(B + 1) \times 1$ WSS that is connected to the target core via an $N_b \times N_b$ DC space switch. Afterward, the outputs of the DC space switch and add-ports are fed into a $(B + 1) \times 1$ WSS. The fan-in component present at the output stage allows optical signals arriving at the output stage of the architecture to be coupled in the MCF.

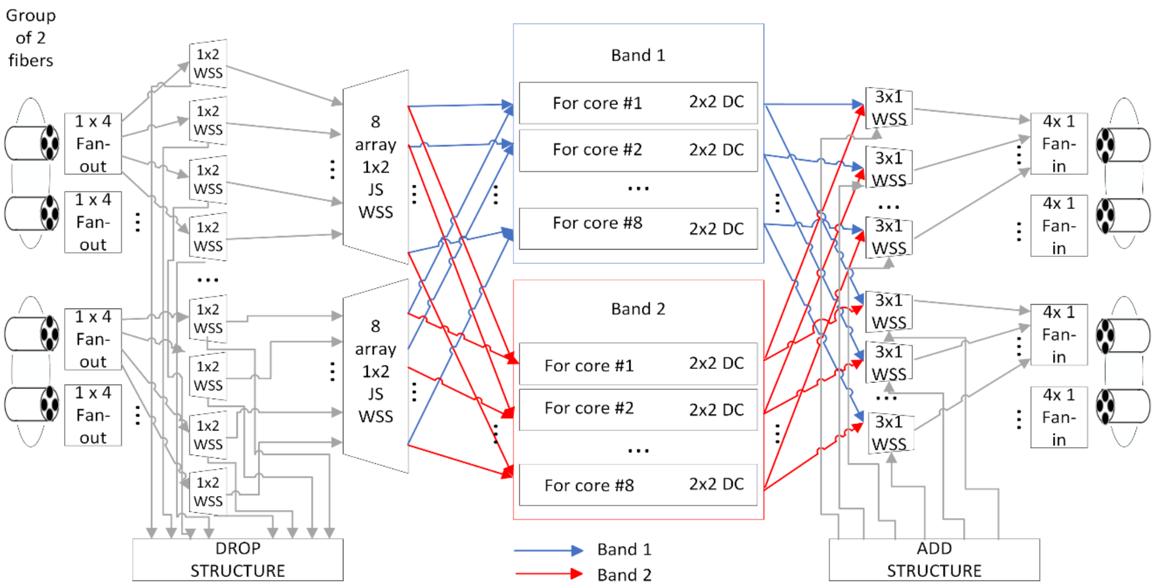

Figure 3.1 - Architecture with fractional space-wavelength granularity with four input fibers D=4, n=2, M=4, N_b=2 and B=2 and an A/D structure with 16 inputs and (16×W) outputs.

The components cost of the fractional space-wavelength granularity architecture is shown in Table 3.1. For comparison purpose, the components cost of a spatial wavelength granularity with and without lane changes (see section 2.4.2), or core-wise switching architecture with and without lane changes is also shown. Several assumptions and considerations have been made, in particular: 1) the per-port cost of the JS WSS is considered similar to conventional WSSs deployed in current single-core fiber (SCF)-based networks [5], so we have assumed in Table 3.1 that the cost of a $1 \times (4 \cdot M - 1)$ WSS, used in the core-wise switching architecture, that has $4 \cdot M$ ports has the same cost of a $M - array$ 1×3 JS WSS, used in the proposed architecture, that has also $4 \cdot M$ ports, and the cost is defined by α; 2) the cost of the DC space switch is relatively small compared to the WSS cost, since it can be manufactured cost-effectively using planar lightwave circuit technologies or silicon photonics technologies [5], so its cost can be neglected ($\delta = 0$) and 3) the cost of the fan-in and fan-out is not considered in this work [5].

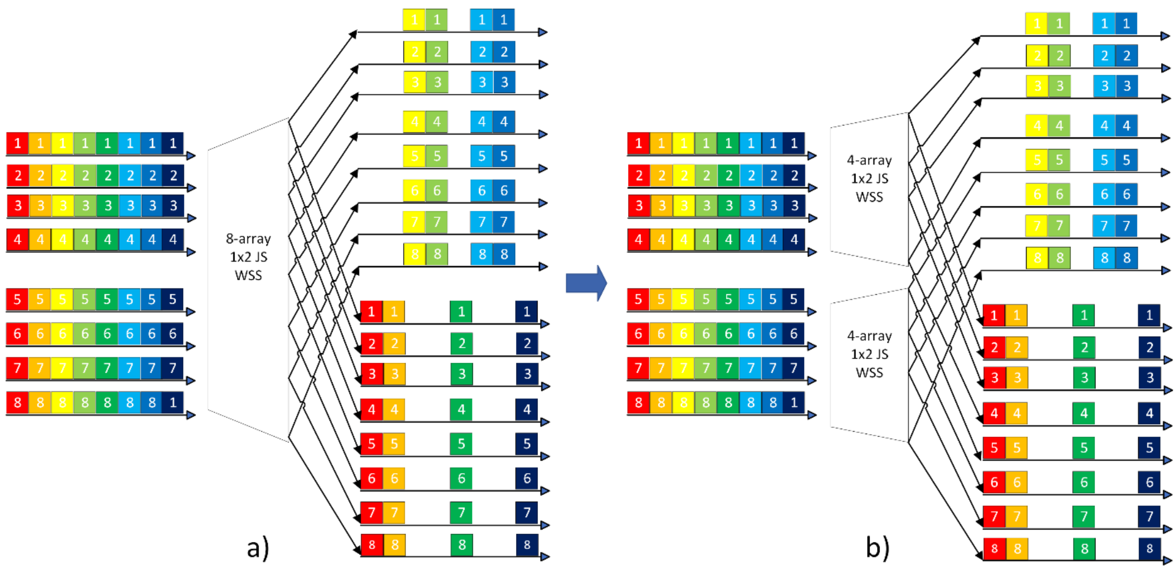

Figure 3.2 - Two alternatives for implementing the 8-array 1×2 JS WSS a) with an 8-array 1×2 JS WSS and b) with two by 4-array 1×2 JS WSS.

Analysing Table 3.1, we can conclude that the express structure cost of the fractional space-wavelength granularity architecture proposed in [5], $Cost\_new$, is given by:

$$Cost\_new = \alpha \cdot N_b \cdot n + \beta \cdot M \cdot N_b \cdot n + \gamma \cdot M \cdot N_b \cdot n + \delta \cdot B \cdot M \cdot n \quad (3.1)$$

Equation (3.1) is obtained through the sum of the components present in the fractional space-wavelength granularity architecture, with α representing the JS WSS cost , which is equivalent to the cost of a $1 \times (M + M \cdot B - 1)$ WSS.

Table 3.1 - Hardware cost for the fractional space-wavelength granularity architecture proposed in [5] and for the core-wise switching architecture.

<table>
<tr><th rowspan="2">Hardware</th><th colspan="2">Core-wise switching architecture</th><th rowspan="2">Fractional space-wavelength granularity architecture proposed in [5]</th></tr>
<tr><th>Without lane changes</th><th>With lane changes</th></tr>
<tr><th>Express structure components and unitary cost</th><th colspan="3">Express structure cost components</th></tr>
<tr><td>$1 \times [(D-1)+1]\ WSS$
Cost: α'_{wo_lc}</td><td rowspan="2">$\alpha'_{wo\_lc} \cdot M \cdot D \cdot 2$</td><td rowspan="2">$\alpha'_{w\_lc} \cdot M \cdot D \cdot 2$</td><td rowspan="2"></td></tr>
<tr><td>$1 \times [(D - 1 \times\ M + 1\ )]\ WSS$
Cost: α'_{w_lc}</td></tr>
<tr><td>$1 \times 2\ WSS$
Cost: β</td><td colspan="2" rowspan="4"></td><td>$\beta \cdot M \cdot N_b \cdot n$</td></tr>
<tr><td>$M - array\ (1 \times B)\ JS\ WSS$
Cost: α</td><td>$\alpha \cdot N_b \cdot n$</td></tr>
<tr><td>$1 \times (B+1)\ WSS$
Cost: γ</td><td>$\gamma \cdot M \cdot N_b \cdot n$</td></tr>
<tr><td>$N_b \times N_b$
DC Space Switch
Cost: δ</td><td>$\delta \cdot B \cdot M \cdot n$</td></tr>
<tr><th>Total cost of the express structure</th><td>$\alpha'_{wo\_lc} \cdot M \cdot D \cdot 2$</td><td>$\alpha'_{w\_lc} \cdot M \cdot D \cdot 2$</td><td>$\alpha \cdot N_b \cdot n +$
$\beta \cdot M \cdot N_b \cdot n +$
$\gamma \cdot M \cdot N_b \cdot n +$
$\delta \cdot B \cdot M \cdot n$</td></tr>
<tr><th>A/D structure components</th><th colspan="3">A/D structure cost components</th></tr>
<tr><td>$(D \cdot M) \times (D \cdot M \cdot W)\ WSS$
Figure 2.8 a) Cost: θ</td><td colspan="3">$\theta \cdot 2$</td></tr>
<tr><td>$D \times (D \cdot W)\ WSS$
Figure 2.8 b) Cost: φ</td><td colspan="3">$\varphi \cdot M \cdot 2$</td></tr>
<tr><td>$M \times (M \cdot W)\ WSS$
Figure 2.8 c) Cost: ω</td><td colspan="3">$\omega \cdot D \cdot 2$</td></tr>
<tr><td>Transponder
Cost: μ</td><td colspan="3">$\mu \cdot (D \cdot M \cdot W)$</td></tr>
</table>

Furthermore, it can also be concluded that the cost of express structure of the core-wise switching architecture without and with lane changes, $Cost\_cw$, is given by:

$$Cost_{cw} = \alpha'_i \cdot M \cdot D \cdot 2 \qquad (3.2)$$

where $i = wo\_lc$ refers to the core-wise without lane changes and $i = w\_lc$ refers to the core-wise with lane changes. Equation (3.2) is obtained by multiplying the number of $1 \times D$ or $1 \times (D-1) \times M + 1$ WSSs in both the input and output stages of the ROADM by its cost, α'_{wo_lc} or α'_{w_lc} respectively. The number of $1 \times D$ or $1 \times (D-1) \times M + 1$ WSSs in each stage is equal to $M \times D$ (or $M \times N_b \times n$). The multiplication by two in eq. (3.2) is due to the R&S architecture type, which means that it has WSSs at the input and output stages.

A SDM ROADM architecture switching capacity is defined in space (spatial) and in frequency (wavelength). A ROADM architecture with full switching capacity in space means that any specific core in any of the input fibers can be routed to any core in any of the output fibers. Meanwhile, full switching capacity in frequency means that any specific wavelength (or channel) in any of the input core fibers can be directed to any corresponding core in any of the output fibers. For instance, λ_1 on channel σ_1 of input fiber 1 can be routed to channel σ_1 of any of the output fibers. The core-wise switching architecture without lane changes has total switching capacity in the frequency, but in space it doesn't allow core switching, whereas the core-wise switching architecture with lane changes has total switching capacity in frequency and in space. The fractional space- wavelength granularity architecture is more flexible when the number of fibers per group, *n*, is lower, while when *n* is higher the switching capacity of the architecture decreases. For example , for *n*=1 (N_b=*D*) the fractional space-wavelength granularity architecture allows the same switching capacity in space than the core-wise switching architecture with or without lane changes, but in the frequency, it depends on the value of *B*. If *B*=N_W and *n=1,* the fractional space-wavelength granularity architecture has the switching capacity of the core wise without lane changes, however if *B*=N_W and *n*=*D* the switching capacity in space is reduced to just 1 fiber at the output. Note that in this scenario the dimension of the space switches is 1×1 because N_b=1.

For example, for a 16×16 architecture with *D*=4 and *M*=4 (and *B*=2), if you use one fiber per group, *n*=1, and four fiber groups, N_b=4, you can place the signal from the input core 1 (i.e. the 2 bands) in core 1 on the 4 output fibers. However, if we assume *n*=2 (N_b=2), the core 1 signal is only routed to the core 1 of 2 of the output fibers and for the case of *n*=4 (N_b=1), the signal from core 1 is only routed to core 1 of just one of the output fibers. We can therefore conclude that the fractional space-wavelength granularity architecture will never have the switching capacity of the core-wise switching architecture with lane changes, so the comparison of the fractional space-wavelength granularity architecture must be made with the core-wise switching architecture without lane changes.

The relative cost between the express structure of the fractional space-wavelength granularity architecture proposed in [5] and the express structure of the core-wise switching ROADM without lane changes is given by:

$$Cost\_rel\_\alpha'_{wo\_lc} = \frac{\alpha}{2 \cdot M \cdot \alpha'_{wo\_lc}} + \frac{\beta + \gamma}{2 \cdot \alpha'_{wo\_lc}} + \frac{B \cdot \delta}{\alpha'_{wo\_lc} \cdot N_b \cdot 2} \tag{3.3}$$

In the following analysis, we have considered that the last term in eq. (3.3) can be neglected, as δ is negligible [5]. So, by analysing eq. (3.3), it can be concluded that the fractional space-wavelength granularity architecture proposed in [5] is more cost effective when the number of cores is large and when the 1×2 WSSs and $1 \times (B+1)$ WSSs have a lower cost than the $1 \times D$ WSS (i.e. $\beta + \gamma < 2\alpha'_{wo\_lc}$), as will be analysed next in Figures 3.5 and 3.6.

The architectures cost presented in Table 3.1 can be quantified having in mind the relative cost of C-band components, using the EDFA cost as a reference, presented in Table 3.2. It is assumed also that the M-array $1 \times B$ JS WSS has a cost equivalent to the cost of a $1 \times M\,(1+B) - 1$ WSS both represented by α for the fractional space-wavelength granularity architecture. The 1×9 WSS cost and 1×20 WSS cost were taken from [17] and the other WSS costs referred in Table 3.2 are calculated in a proportional way having in mind the 1×9 WSS and 1×20 WSS cost.

Table 3.2 - Relative cost of C band components using the EDFA cost as a reference.

Component	Relative cost
EDFA	1
WSS 1x2	1.25
WSS 1×4	2.5
WSS 1×9	5
WSS 1×20	7.5
WSS 1x40	12
WSS 1x80	25.25
WSS 9x18	20
WSS 16x24	30
WSS 9x9	14
WSS 4x4	6
100 Gbit/s transponder	36

It should be noted that for WSSs with more than 40 ports cascading is used. For example, to build a 1×80 WSS, we use a 1×2 WSS in cascade with two 1×40 WSSs in parallel as it is represented in Figure 3.3 [18].

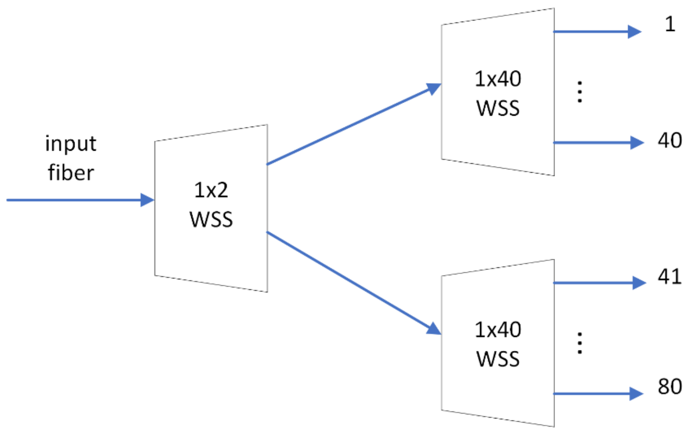

Figure 3.3 - Example of a 1 × 80 WSS using two WSSs stages in cascade.

Another issue that was considered in this cost analysis is related with the dimension of the $M \times N$ WSSs in the A/D structures. As the WSSs in the A/D structures considered (Figure 2.8 a) are larger than the commercially available WSSs, e.g. 9×18 WSS presented in Table 3.2 (the 9×18 WSS cost was taken from [17]), these larger WSSs have to be built with these smaller dimensions WSSs, as shown in [19]. For example, to build a 16×256 WSS , to be used in the drop structure of Figure 3.1, with 16×24 WSSs (note that the 16×24 WSS cost is derived from the cost of the 9×18 WSS in a proportional way regarding the number of ports), we need 11 (16×24) WSSs. As a consequence, the ROADM input WSSs will have to provide more 12 outputs, 11 for the drop structure and one for the express structure, and the ROADM output WSSs will have to $11 + B$ inputs, 11 coming from the add structure and B inputs from the express structure. For the particular case of the architecture proposed in [5] and represented in Figure 3.1 with *D*=4, *M*=4 and *B*=2, we have considered an A/D structure composed by 11 (16×24) WSSs (drop structure) and 11 (24×16) (add structure) plus an express structure composed by 16 (1×12) WSSs at the ROADM inputs and 16 (13×1) WSSs at the ROADM output as shown in Figure 3.4. It is important to note that the cost of the transponders was not taken into account in the analysis carried out because the cost associated with the transponders is quite high in comparison with the cost of the express and A/D structure of the architectures in question and all the architectures studied require the same number of transponders.

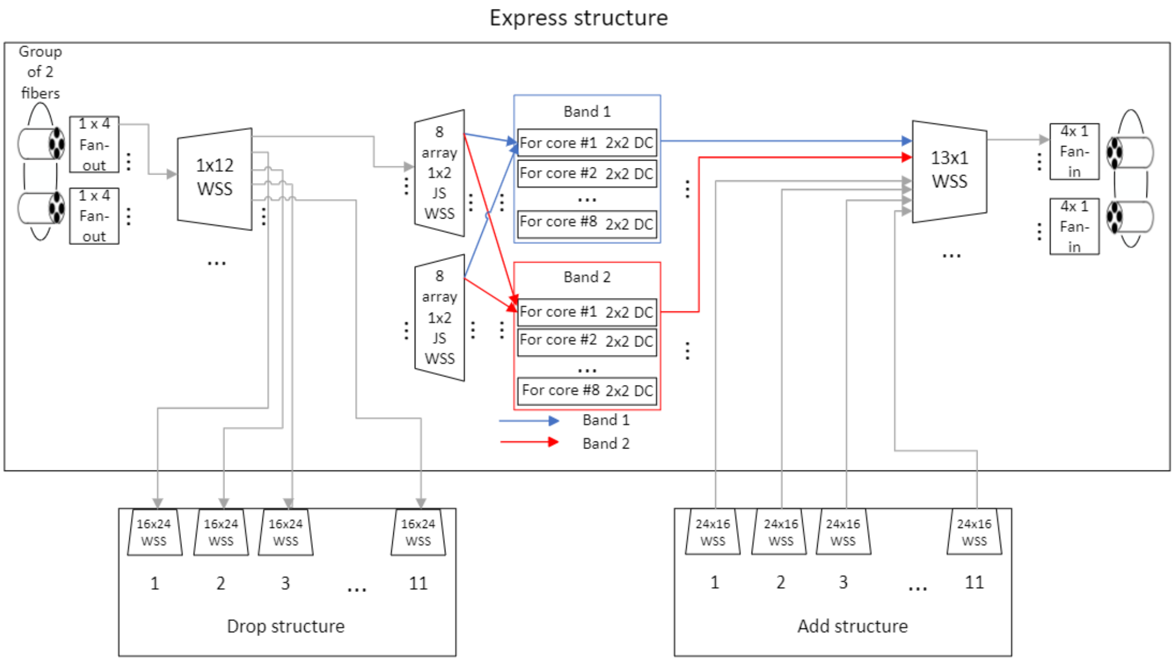

Figure 3.4 - A/D structure example and its connections to the express structure considering D=4, M=4 and B=2.

In Figure 3.5, the relative cost, given by eq. (3.3), between the express structure of the fractional space-wavelength granularity architecture proposed in [5] and the express structure of the core-wise switching ROADM is represented as a function of the number of cores (*M)* considering *D*=4, *B*=1,3,4,6 and 10 and β=1.25. The γ, α and α'_{wo_lc} values (assuming a single $M \times N$ WSS in the A/D structure) are presented in Table 3.3.

Table 3.3 - γ, α and α'_{wo_lc} values considered for B=1,3,4,6,10 as a function of M considering a single MxN WSS in the A/D structure.

	B=1		B=3		B=4		B=6		B=10		
M	γ	α	γ	α	γ	α	Γ	α	γ	α	α'_{wo_lc}
1	1.25	1.25	2.5	2.5	5	2.5	5	5	7.5	7.5	5
2	1.25	2.5	2.5	5	5	5	5	7.5	7.5	12	5
3	1.25	5	2.5	7.5	5	7.5	5	7.5	7.5	12	5
4	1.25	5	2.5	7.5	5	7.5	5	12	7.5	25.25	5
5	1.25	5	2.5	7.5	5	12	5	12	7.5	25.25	5
6	1.25	7.5	2.5	12	5	12	5	25.25	7.5	25.25	5
7	1.25	7.5	2.5	12	5	12	5	25.25	7.5	25.25	5
8	1.25	7.5	2.5	12	5	12	5	25.25	7.5	38.5	5
9	1.25	7.5	2.5	12	5	25.25	5	25.25	7.5	38.5	5
10	1.25	7.5	2.5	12	5	25.25	5	25.25	7.5	38.5	5

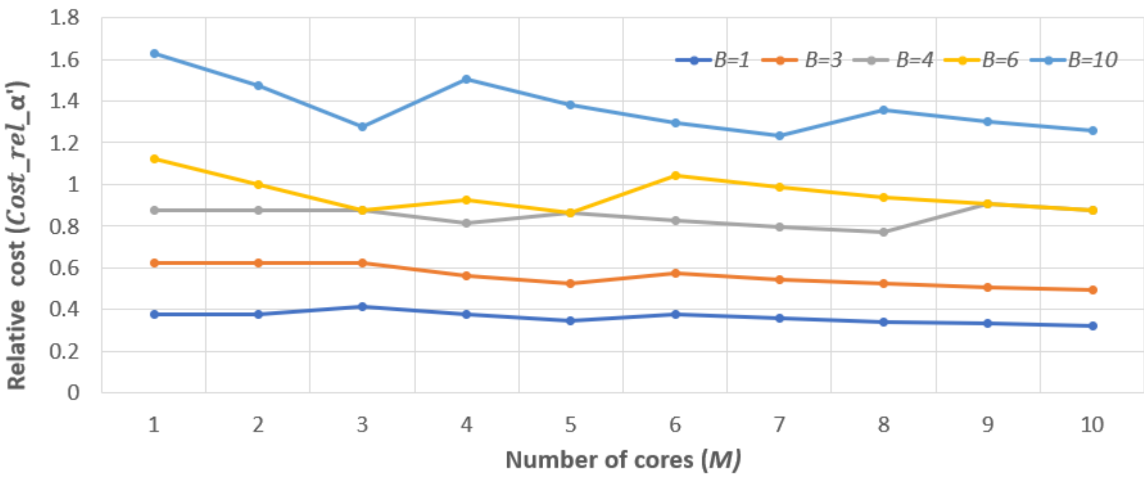

Figure 3.5 - Relative cost between the express structure of the fractional-space wavelength granularity architecture proposed in [5] and the express structure of the core-wise switching ROADM as a function of the number of cores M considering D=4, B=1,3,4 and β=1.25

From Figure 3.5, it can be seen that as the number of cores ,*M,* increases, the relative cost stays practically constant for all values of *B* considered. Nevertheless, it is observed that as *B* increases, the relative cost becomes less constant. Figure 3.5 shows that the fractional space-wavelength granularity architecture is less expensive than the core-wise switching architecture, for *B*<6. For *B* greater than 6, there is no significant cost advantage in using the fractional space-wavelength granularity architecture. For *B*=10 (light blue line), the relative cost is the highest with α =7.5 and γ=7.5 (see Table 3.3) since the term $\beta + \gamma$ is higher than the term $2 \cdot \alpha'$ and it is more advantageous to use the core-wise switching architecture. The most significant differences in the relative cost for *B*=6 and *B*=10 are found between: 1) *M*=1 and *M*=3 as the parameter α increases from 5 to 7.5 and from 7.5 to 12 for *B*=6 and *B*=10, respectively (as shown in Table 3.3); 2) *M*=3 and *M*=4 as α increases for *B*=10 from 12 to 25.25 for *B*=10 due to the cost of a 1×80 WSS (Table 3.3) and 3) *M*=4 and *M*=7. For *B*=1, *B*=3 and *B*=4*,* the parameter α does not increase in a significant way, and as a consequence the slope of the curves is almost constant and independent of *M*. Although for *B*=1, it can be observed that the express structure of the fractional space-wavelength granularity architecture has the lower relative cost, it is the solution with the lower switching capacity, while for *B*=10 it has the higher relative cost with the highest switching capacity. In this case, it is more advantageous to use the core-wise switching architecture.

In Figure 3.6, the relative cost given by eq. (3.3) is represented as a function of the number of cores M , for the particular case of $\alpha = \alpha'$. This scenario is the one considered in [5] and represents the situation where the cost of the input and output WSSs of the core-wise switching architecture is dependent of the JS WSS cost that depends on the number of bands *B*. It can be observed that different results are obtained in comparison with the results obtained in Figure 3.5.

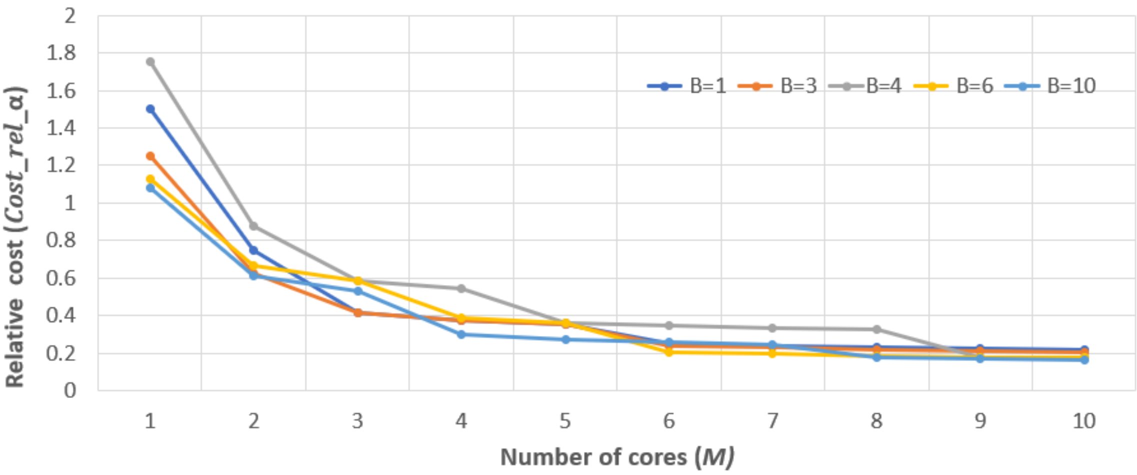

Figure 3.6 - Relative cost between the express structure of the fractional-space wavelength granularity architecture proposed in [5] and the express structure of the core-wise switching ROADM considering α=α′ as a function of the number of cores M considering D=4, B=1,3,4,6,10 and β=1.25

From Figure 3.6, it can be seen that as the number of cores ,*M,* increases, the relative cost rapidly decreases, until *M*=5, and for a number of cores higher than 5 ,the relative cost stays practically the same for all the values of *B* considered and below 0.4. It can be observed that the fractional space-wavelength granularity architecture can be about 5 times less expensive than the core-wise switching architecture, for $M > 8$ and *B*=1,3,6 and 10. However, Figure 3.5, that shows a more general case ($\alpha \neq \alpha'$), contradicts this conclusion, by showing that the increase of the number of cores does not contribute to the reduction of the relative cost between the two architectures. The relative cost is constant as a function of *M* and depends on the value of *B* considered with the core-wise switching architecture being more expensive for *B*<5 and less expensive for *B*>5 which shows that the situation in [5] is a very particular situation, and as shown in Table 3.3, there are only six cases with $\alpha = \alpha'$, e.g. *M*=2 and *B*=3 and *M*=1 and *B*=6.

Next, a cost analysis of the fractional space-wavelength granularity architecture proposed in [5] as a function of the number of bands *B*, and the number of cores is done. The following results were normalized in relation to the fractional space-wavelength granularity architecture with *D*=4, *M*=4 and *B*=3 (because in [5] it is concluded that using three wave bands results in good routing performance) with the A/D structure presented in Figure 2.8 a). For this particular case, we have considered α=7.5 since the 4-array (1×3) JS WSS has 16 ports , the same number of ports as a 1×15 WSS and its cost is considered 7.5 (Table 3.2), the cost of a 1×20 WSS is γ=2.5 , since the cost of a 1×4 WSS is considered to be half the cost of a 1×9 WSS, β= 1.25 (the cost of a 1×2 WSS) following the same reasoning as before, and the space switch cost is considered negligible, i.e. δ=0. The express structure and the A/D structure cost of the fractional space-wavelength granularity architecture is, respectively, 90 and 660 giving a total cost of 750.

In Figure 3.7, the normalized cost of the fractional space-wavelength granularity architecture proposed in [5] is represented as a function of the number of bands *B* considering *D*=4, and *M*=4, 7. The A/D structure considered is represented in Figure 2.8 a).

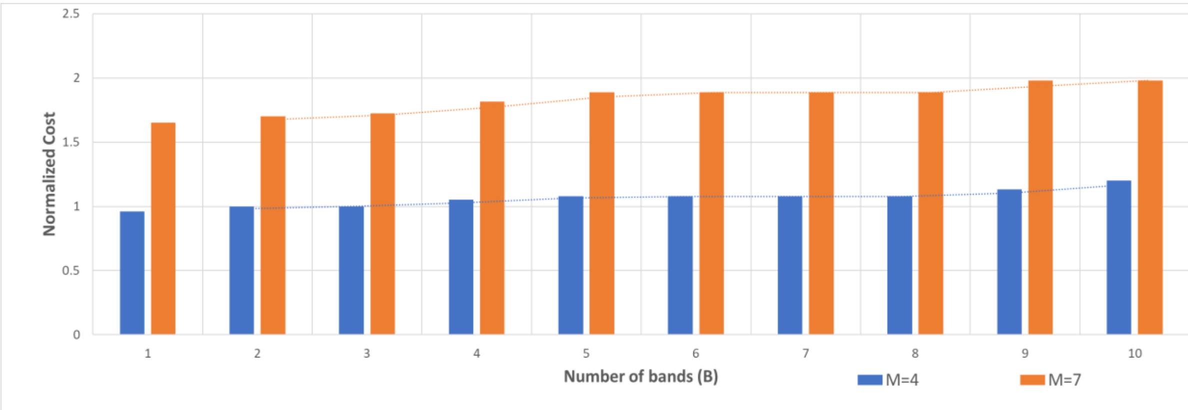

Figure 3.7 - Normalized cost of the fractional-space wavelength granularity architecture proposed in [5] as a function of the number of bands B considering D=4, and M=4,7.

From Figure 3.7, it can be seen that as the number of bands (*B*) increases, the normalized cost also increases, from 0.96 for *B*=1 to 1.20 for B=10 for *M*=4 represented by the blue bar. For the case *M*=7 represented by the orange bar the normalized cost also increases, in this scenario, from 1.65 for *B*=1 to 1.98 for *B*=10. The increase in the normalized cost values for both scenarios between *B*=1 and *B*=2 is due to the γ value ,associated with the output WSS, being doubled in this case to 2.5 and due to α increase from 5 to 7.5 , between *B*=4 and *B*=5 , is due to α increases from 7.5 to 12 with *M*=4 and from

12 to 25.25 with *M*=7, between *B*=8 and *B*=9 , is due to γ increase from 5 to 7.5 and between *B*=9 and *B*=10 with *M*=4 is due to α increase from 12 to 25.25 (see Table 3.3).

In Figure 3.8, the normalized cost of the fractional space-wavelength granularity architecture proposed in [5] is again represented as a function of the number of bands *B* , but considering *D*=8, and *M*=4, 7.

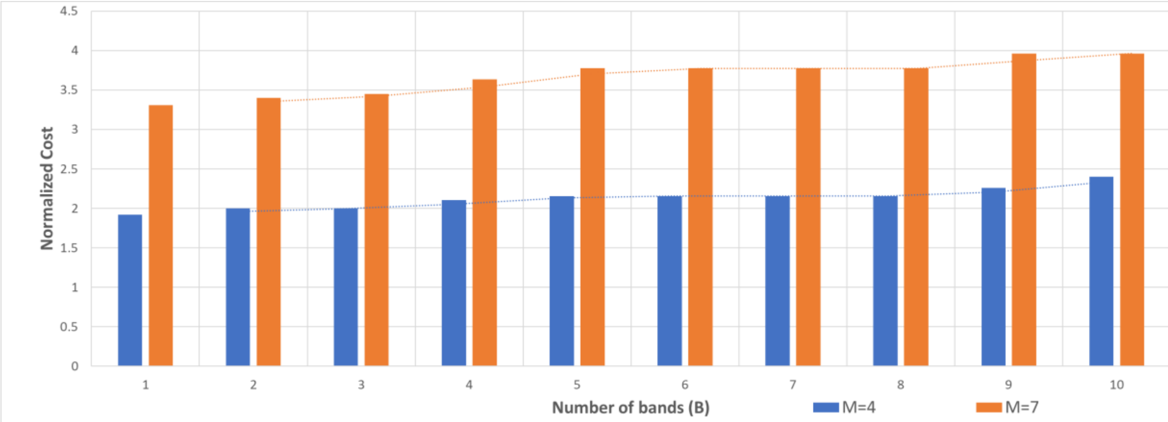

Figure 3.8 - Normalized cost of the fractional space-wavelength granularity architecture proposed in [5] as a function of the number of bands B considering D=8, and M=4,7.

From Figure 3.8, it can be seen that as the number of bands (*B)* increases, the normalized cost also increases, as in Figure 3.7, from 1.92 (*B*=1) to 2.40 (*B*=10) for *M*=4 (blue bar). For the case *M*=7 represented by the orange bar the normalized cost also increases, in this scenario, from 3.30 from *B*=1 to 3.92 for *B*=10. It can be concluded after analysing the scenarios with *D*=4 and *D*=8 that as the number of directions increases and also the number of cores, greater will be the cost associated with the architecture - the scenario with 8 directions (*D*=8) almost doubles (1.8 times) the cost in comparison with the 4 directions scenario (*D*=4) for all values of *B*.

In Figure 3.9, the normalized cost of the fractional space-wavelength granularity architecture proposed in [5] is represented as a function of the number of cores *M* architecture considering *D*=4,8 and *B*=3. The A/D structure considered is represented in Figure 2.8 a). considering *D*=4,8 and *B*=3. The A/D structure considered is represented in Figure 2.8 a).

From Figure 3.9, it can be seen that as the number of *cores (M)* increases, the normalized cost also increases, from 0.27 for *M*=1 to 2.93 for *M*=12 for *D*=4 represented by the blue bar. For *D*=8 represented by the orange bar the normalized cost also increases, in this scenario, from 0.54 for *M*=1 to 5.86 for *M*=12. The cost increase between *M*=1 and *M*=2 is due to the α parameter, associated with the output WSS, being doubled in this case to 5, between *M*=2 and *M*=3 , is due to the α parameter increase from 5 to 7.5, between *M*=5 and *M*=6 , due to the γ value has increased from 7.5 to 12 and between *M*=10 and *M*=11 , is due to the α parameter increase from 12 to 25.25 (see Table 3.3). It can be concluded that, for both *D*=4 and *D*=8 as the number of cores increases, greater will be the normalized cost associated with the fractional space-wavelength architecture noting that the scenario with 8 directions (*D*=8) almost doubles the cost in comparison with the 4 directions scenario (*D*=4) for all values of *M*.

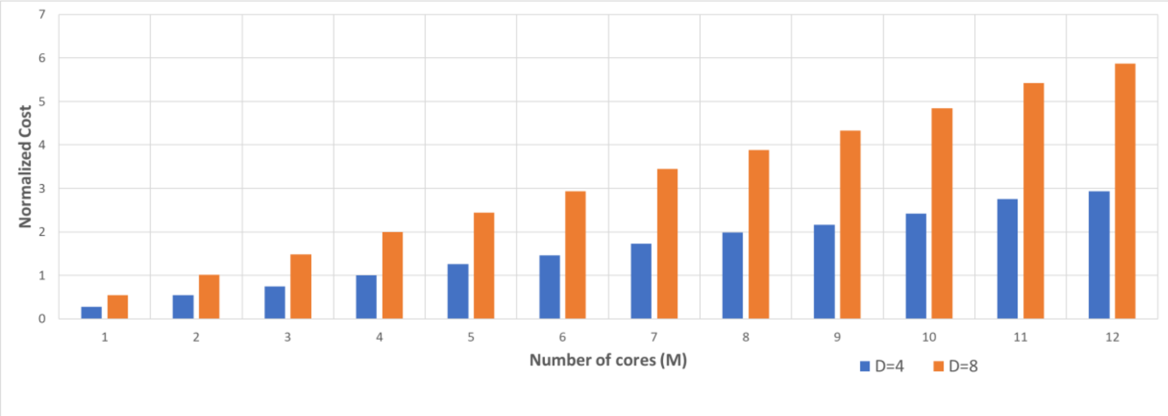

Figure 3.9 - Normalized cost of the fractional space-wavelength granularity architecture proposed in [5] as a function of the number of cores M considering D=4,8 and B=3

In Figure 3.10, the normalized cost of the fractional space-wavelength architecture proposed in [5] is represented again as a function of the number of bands *B* considering *D*=4, and *M*=4, 7, but the normalization is to the core-wise switching architecture with *D*= 4 and *M*=4 instead. The express structure cost is 240, whereas the A/D structure cost is 660, giving a total cost of 900. The A/D structure considered is represented in Figure 2.8 a).

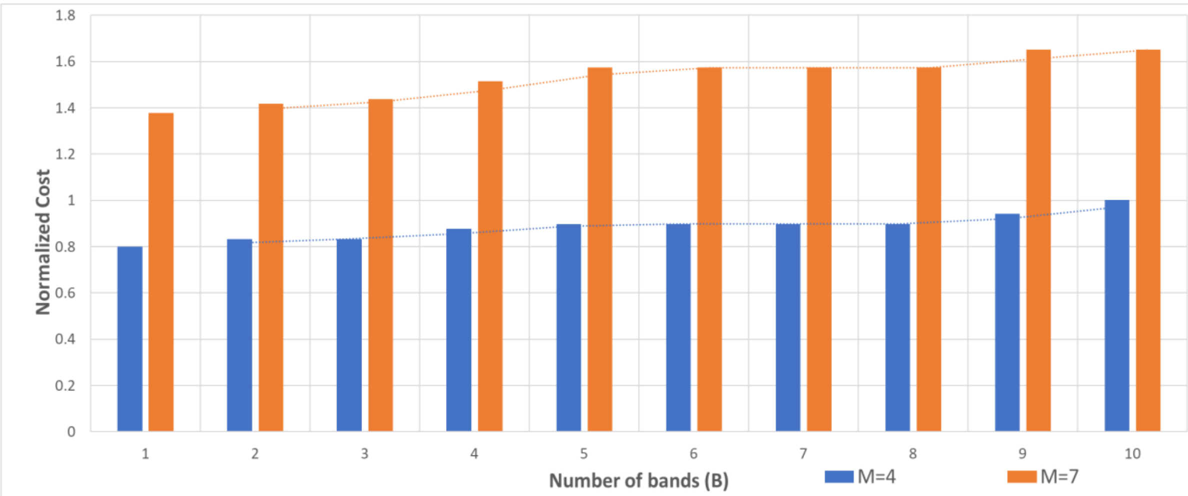

Figure 3.10 - Normalized cost of the fractional space-wavelength granularity architecture proposed in [5] as a function of the number of bands B considering D=4, and M=4, 7

From Figure 3.10, it can be seen that as the number of bands, *B,* increases, the normalized cost also increases, from 0.8 for *B*=1 to 1 for *B*=10 for the particular case of *M*=4 represented by the blue bar. For the case *M*=7 represented by the orange bar the normalized cost also increases, in this scenario, from 1.37 *B*=1 to 1.65 for *B*=10.

In Figure 3.11, likewise Figure 2.22, the normalized cost of the fractional space-wavelength architecture proposed in [5] is again represented as a function of the number of bands *B*, but considering *D*=8, and *M*=4, 7.

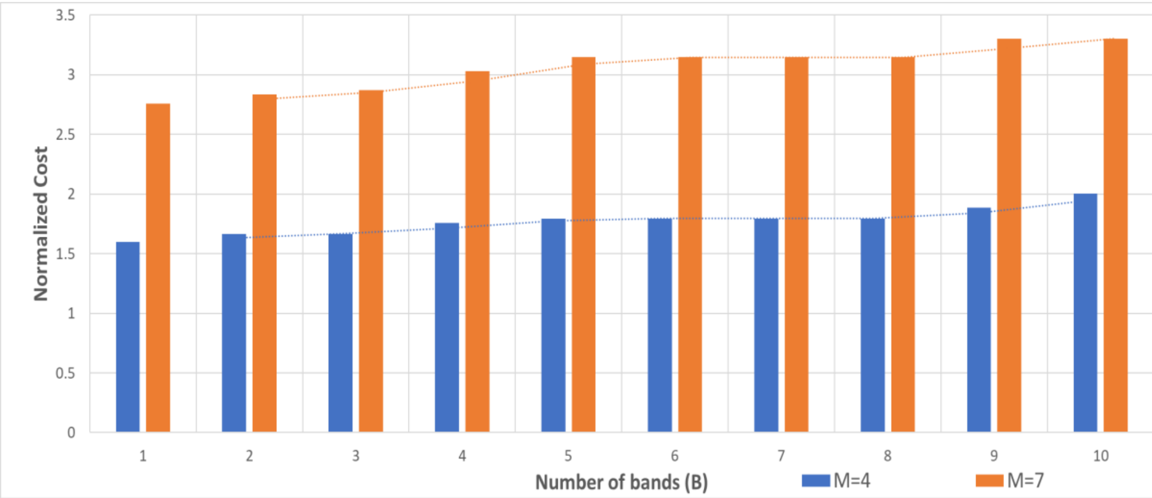

Figure 3.11 - Normalized cost of the fractional space-wavelength granularity architecture proposed in [5] as a function of the number of bands B considering D=8, and M=4, 7

From Figure 3.11, it can be seen that as the number of bands, *B,* increases, the normalized cost also increases, as in Figure 3.9, from 1.6 (*B*=1) to 2 (*B*=10) for *M*=4 (blue bar). For the case *M*=7 represented by the orange bar the normalized cost also increases, in this scenario, from 2.75 for *B*=1 to 3.30 for *B*=10. Table 3.4 shows the number of hardware components required by the fractional-space wavelength and core-wise switching without lane changes (see Figure 2.6) architectures, for several ROADM dimensions, from 4×4 to 64×64 (the ROADM dimension is given by $(N_b \cdot M \cdot n \times N_b \cdot M \cdot n)$ assuming a single $M \times N$ WSS for the A/D structure with an A/D ratio of 20% and *B*=3. Note that the DC space switches, fan-in and fan-out components costs have been neglected in this analysis. For example, the 8x8 ROADM based on the fractional space-wavelength architecture with *D*=4 and *M*=2 needs $8\, WSS\ (1 \times 2)$ + $4\ \ 2-array\, 1 \times 3\, JS\, WSS$ + $8\, WSS\ (4 \times 1)$ in the express structure and a 8×128 WSS in the A/D structure (Figure 2.8a). For the core-wise switching architecture 8×8 scenario, $8\, WSS\ (1 \times 5)$ and $8\, WSS\ (5 \times 1)$ are needed (4 outputs/inputs for the express structure and 1 for the A/D structure), respectively, for the R&S stage of the ROADM, whereas the A/D structure used is the same as for the fractional space-wavelength architecture assuming a single $M \times N$ WSS.

Table 3.4 - Number and dimension of the components used for the fractional-space wavelength [5] and core-wise switching architecture without lane changes for a given ROADM as a function of the number of cores M considering D=4, B=3 and single M×N WSS in the A/D structure with an A/D ratio of 20%

ROADM Dimension	Fractional space-wavelength Architecture *B*=3	Core-wise switching architecture	
	Express components	A/D components	Express components
8x8 (D=4; M=2; N_b=2; n=2)	8 WSS 1x2+4 2-array 1x3 JS WSS+ 8 WSS 4x1	8x128 WSS + 128x1 WSS Transponders: 128	8 1x5 WSS + 8 5x1 WSS
16x16 (D=4; M=4 ;N_b=2; n=2)	16 WSS 1x2+4 4-array 1x3 JS WSS+ 16 WSS 4x1	16x256 WSS + 256x16 WSS Transponders: 256	16 1x5 WSS + 16 5x1 WSS
24x24 (D=4; M=6; N_b=2; n=2)	24 WSS 1x2+4 6-array 1x3 JS WSS+ 24 WSS 4x1	24x384 WSS + 384x24 WSS Transponders: 384	24 1x5 WSS + 24 5x1 WSS
32x32 (D=4; M=8: N_b=2; n=2)	32 WSS 1x2+4 8-array 1x3 JS WSS+ 32 WSS 4x1	32x512 WSS + 512x32 WSS Transponders: 512	32 1x5 WSS + 32 5x1 WSS
40x40 (D=4; M=10; N_b=2; n=2)	40 WSS 1x2+4 10-array 1x3 JS WSS+ 40 WSS 4x1	40x640 WSS + 640x40 WSS Transponders: 640	40 1x5 WSS + 40 5x1 WSS
48x48 (D=4; M=12; N_b=2; n=2)	48 WSS 1x2+4 12-array 1x3 JS WSS+ 48 WSS 4x1	48x768 WSS + 768x48 WSS Transponders: 768	48 1x5 WSS + 48 5x1 WSS
56x56 (D=4; M=14; N_b=2; n=2)	56 WSS 1x2+4 14-array 1x3 JS WSS+ 56 WSS 4x1	56x896 WSS + 896x56 WSS Transponders: 896	56 1x5 WSS + 56 5x1 WSS
64x64 (D=4; M=16; N_b=2; n=2)	64 WSS 1x2+4 16-array 1x3JS WSS+ 64 WSS 4x1	64x1024 WSS + 1024x64 WSS Transponders: 1024	64 1x5 WSS + 64 5x1 WSS

The cost of the fractional-space wavelength architecture and core-wise switching without lanechanges architectures is represented in Figure 3.12 as a function of the ROADM dimension (the number of cores (M) is increased, considering that the number of directions, is kept constant, D=4) assuming a single $M \times N$ WSS for the A/D structure. The costs in Figure 3.12 are obtained considering the hardware equipment shown in Table 3.4 and the corresponding costs shown in Table 3.2.

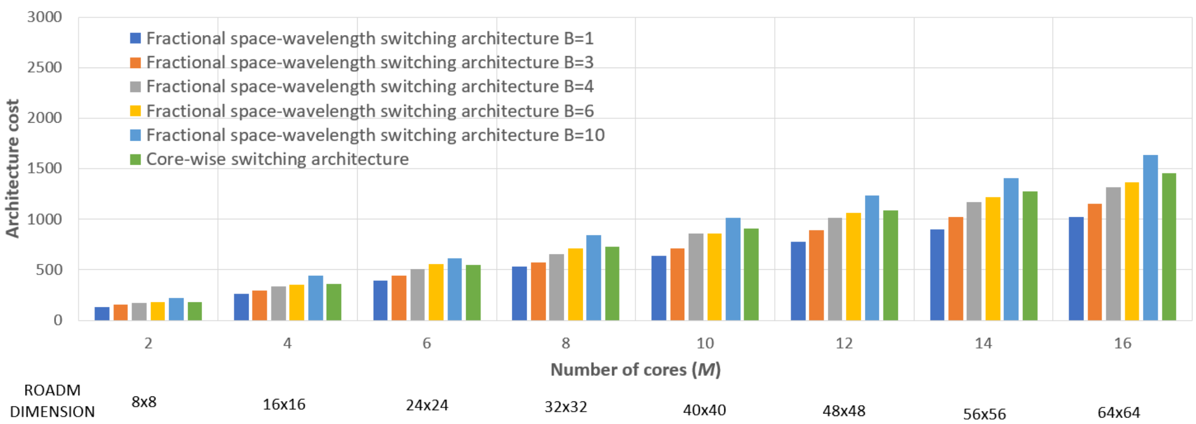

Figure 3.12 - Cost of the fractional space-wavelength granularity architecture proposed in [5] and the core-wise switching ROADM without lane changes as a function of the ROADM dimension considering D=4 and B=1,3,4,6,10 assuming a single MxN WSS in the A/D structure and an A/D ratio of 20%

From Figure 3.12, it can be seen that as the size of the ROADM increases, the cost associated with the architectures also increase for any number of bands considered. Figure 3.12 also shows that the core-wise switching architecture has a higher cost than fractional space-wavelength architecture for every value of *B* considered except for *B*=10. This behaviour happens due to input and output WSS dimension in the core-wise switching architecture increase with *D* and *M*, whereas the fractional space-wavelength architecture always considers a 1×2 WSS at the input stage and a $(B+1) \times 1$ WSS at the output, since the A/D structure has no influence as it is the same in both architectures.

Table 3.5 shows the number of hardware components required by the fractional-space wavelength and core-wise switching without lane changes architectures, for several ROADM dimensions, from 4×4 to 64×64, for *B*=3, but assuming a bank of WSSs in parallel in the A/D structure with an A/D ratio of 20%. Again, the DC space switches, fan-in and fan-out components costs have been neglected in this analysis. To increase the ROADM dimensions, the number of cores is kept constant, *M*=4, and the number of directions is increased.

Table 3.5 - Number and dimension of the components used for the fractional-space wavelength [5] and core-wise switching without lane changes architectures for a given ROADM dimension as a function of the number of directions D considering M=4, B=3 and assuming a bank of WSSs in parallel in the A/D structure with an A/D ratio of 20%

ROADM Dimension	Fractional space-wavelength Architecture B=3	Core-wise switching architecture	
	Express components	A/D components	Express components
8x8 (D=2; M=4; N_b=2; n=1)	8 WSS 1x7+2 4-array 1x3 JS WSS+ 8 WSS 9x1	6 WSS 16x24 + 6 WSS 24x16 Transponders: 128	8 1x8 WSS + 8 8x1 WSS
16x16 (D=4; M=4 ;N_b=2; n=2)	16 WSS 1x12+4 4-array 1x3 JS WSS+ 16 WSS 14x1	11 WSS 16x24 + 11 WSS 24x16 Transponders: 256	16 1x15 WSS + 16 15x1 WSS
24x24 (D=6; M=4; N_b=3; n=2)	24 WSS 1x17+6 4-array 1x3 JS WSS+ 24 WSS 19x1	16 WSS 16x24 + 16 WSS 24x16 Transponders: 384	24 1x22 WSS + 22x1 WSS
32x32 (D=8; M=4: N_b=4; n=2)	32 WSS 1x23+8 4-array 1x3 JS WSS+ 32 WSS 25x1	22 WSS 16x24 + 22 WSS 24x16 Transponders: 512	32 1x30 WSS + 32 30x1 WSS
40x40 (D=10; M=4; N_b=5; n=2)	40 WSS 1x28+10 4-array 1x3 JS WSS+ 40 WSS 30x1	27 WSS 16x24 + 27 WSS 24x16 Transponders: 640	40 1x37 WSS + 40 37x1 WSS
48x48 (D=12; M=4; N_b=6; n=2)	48 WSS 1x33+12 4-array 1x3 JS WSS+ 48 WSS 35x1	32 WSS 16x24 + 32 WSS 24x16 Transponders: 768	48 1x44 WSS + 48 44x1 WSS
56x56 (D=14; M=4; N_b=7; n=2)	56 WSS 1x39+14 4-array 1x3 JS WSS+ 56 WSS 41x1	32 WSS 16x24 + 32 WSS 24x16 Transponders: 896	56 1x46 WSS + 56 46x1 WSS
64x64 (D=16; M=4; N_b=8; n=2)	64 WSS 1x44+16 4-array 1x3 JS WSS+ 64 WSS 46x1	32 WSS 16x24 + 32 WSS 24x16 Transponders: 1024	64 1x48 WSS + 64 48x1 WSS

For example, the 8×8 ROADM based on the fractional space-wavelength architecture with *D*=4 and M=2 needs $8\ WSSs\ (1 \times 7)\ +\ 2\ \ 4 - array\ 1 \times 3\ JS\ WSSs\ +\ 8\ WSSs\ (9 \times 1)$ in the express structure and $6\ WSSs\ (16 \times 24)$ for the drop structure and $6\ WSSs\ (24 \times 16)$ for the add structure. The A/D structure of Figure 2.8 a) is assumed with 20% A/D ratio like in Table 3.4. For the core-wise architecture scenario, $8\ WSSs\ (1 \times 8)$ and $8\ WSSs\ (8 \times 1)$ are needed (2 for the directions and 6 for the A/D structure), respectively, for the R&S stage of the ROADM whereas the A/D structure used is the same as the one used by the fractional space-wavelength architecture. Finally, it can be concluded that the biggest difference between Table 3.5 and Table 3.4 is the size of the input and output WSSs in the express structure for both architectures, since the scenario in Table 3.5 requires more outputs for the drop structure and more inputs from the add structure, which makes the size of the WSS of the express structure larger than the scenario with a single WSS in A/D structure.

In Figure 3.13, the cost of the fractional-space wavelength architecture and core-wise switching without lane changes architectures is represented as a function of the ROADM dimension (the number of cores (M) is increased and considering that the number of directions, is kept constant, D=4) considering in the A/D structure WSSs in parallel with an A/D ratio of 20% . The hardware components required are the same as Table 3.5 except the size of the D M-array $1 \times B$ JS WSSs in the express structure of the fractional-space wavelength architecture, where we exchange the value of D for M and vice versa.

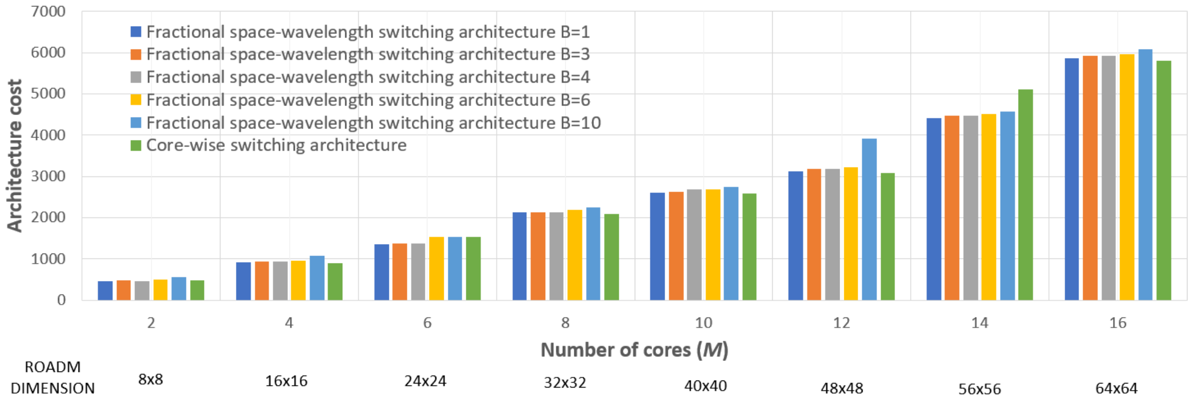

Figure 3.13 - Cost of the fractional space-wavelength granularity architecture proposed in [5] and the core-wise switching ROADM without lane changes as a function of the ROADM dimension considering D=4 and B=1,3,4,6,10 and assuming a bank of WSSs in parallel in the A/D structure and an A/D ratio of 20%

From Figure 3.13 , when considering the same number of cores, the cost of the fractional space wavelength architecture increases only slightly with B. It is possible to observe that only for M=12, there is a significant cost difference for the fractional space-wavelength architecture when changing B=6 to B=10. This is because, in the scenario with M=12 and B=10, the size of the JS WSS increases from 1×80 with M=10 to a 1×160 JS WSS costing α=50.5 and also the output WSS increases its size from a 1×40 WSS to a 1×80 WSS costing α=25.25, for the express structure, resulting in a considerable cost increase. From Figure 3.13, it is also possible to observe that the only scenario in which the core-wise switching architecture without lane changes is more expensive is for M=14. This is due to the fact that in the express structure of the core-wise switching architecture, is considered a 1×80 WSS (α=25.25) for the input and output WSSs. In the fractional space wavelength architecture, the express structure considers a 1×40 WSS (α =12) at the input, a 1×160 JS WSS (α =50.5), and finally, a 1×80 WSS (α =25.25) at the output. In summary, the cost comparison between considering a single WSS (Figure 3.12) or a bank of WSSs in parallel (Figure 3.13) in the A/D structure is quite different for all given ROADM dimensions. As an example, for B=10 and 64×64 ROADM dimension the scenario with a single WSS costs 1636 whereas the scenario with a bank of WSSs costs 6072.

In Figure 3.14, the costs of the fractional-space wavelength and core-wise switching without lane changes architectures are represented as a function of the ROADM dimension (the number of fibers (D) is increased, considering that the number of cores is kept constant, M=4), considering WSSs in parallel in the A/D structure with an A/D ratio of 20% and the hardware components presented in Table 3.5.

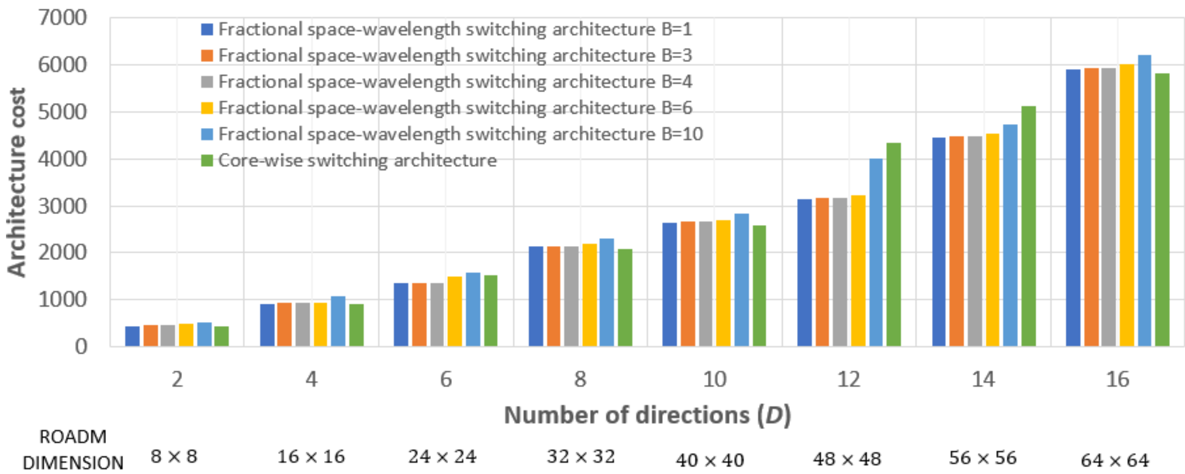

Figure 3.14 - Cost of the fractional space-wavelength architecture proposed in [5] and the core-wise switching ROADM without lane changes as a function of the ROADM dimension considering M=4 and B=1,3,4,6,10 and assuming a bank of WSSs in parallel in the A/D structure and an A/D ratio of 20%

From Figure 3.14 , it is possible to analyse that for the same number of directions, the fractional space wavelength architecture cost slightly increases with B, noting that increases less than in Figure 2.26. Only for D=12, there is a significant cost difference for the fractional space-wavelength architecture between B=6 and B=10. For D=12 and B=10, the JS WSS and the output WSS in the express structure are both costing α=25.25, leading to a considerable cost increase. The core-wise switching architecture becomes only more costly for D=12 and D=14. This happens because, in these cases, the input and output WSSs in the express structure of the core-wise switching architecture costs α=25.25. This difference in cost of the express structures of each architecture leads to the higher cost of the core-wise switching architecture. Otherwise, the fractional space-wavelength architecture is always more expensive than the core-wise switching architecture. Comparing Figures 3.14 and 3.13, it can be concluded that for both *D* (Figure 3.14) and *M* (Figure 3.13), the associated relative cost is very similar for all ROADM dimensions considered due to the fact that the values that are always changing for each scenario are the number of JS WSS components, which depends on *D*, or the size of the JS WSS *M*-array, which depends on *M*. This means that when *D* increases, *M* decreases and vice versa, so the cost remains approximately the same.

It can also be observed that for *D*=12 and *D*=14 the fractional space wavelength architecture with *B*=10 is less expensive than the core-wise switching architecture, which contradicts the scenario in Figure 3.13 for *M*=12. This happens because in the variation of *M*, the input and output WSSs in the express structure of the core-wise switching architecture costs α=12 and for the variation of *D* α=25.25. Furthermore, in the fractional space wavelength architecture with *B*=10 in the variation of *M*, fewer WSSs are considered at the input and output stages even though they have the same dimensions as in the variation of *D*. However, is considered 1×160 JS WSS costing α=50.5 for the variation of *M* and a 1×80 WSS (α =25.25) for the variation of *D*. Finally, it can be concluded from Figures 3.14 and 3.13 that when varying *M* or *D*, the relative cost is practically the same for both scenarios. The most advantageous architecture for a given value of B compared to core-wise switching architecture in general is the fractional space-wavelength architecture with *B*=3 conclusion since the solution with *B*=10 could not be considered due to having a higher relative cost compared to the core-wise switching architecture. The solution with *B*=6 was discarded since its relative cost is quite similar to that of the core wise in several scenarios, which also led to the dismissal of the solution with *B*=4. Finally, the solution with *B*=1 was disregarded because despite having the lowest relative cost it is the solution that presents the least switching capacity.

In Figure 3.15, the cost of the fractional-space wavelength and core-wise switching without lane changes architectures is represented as a function of the ROADM dimension (the number of fibers, *D*, is increased, considering that the number of cores is kept constant, *M*=4) neglecting the cost of the A/D structure (the respective HW components are indicated in Table 3.5).

When comparing Figures 3.15 and 3.14, it is possible to conclude that regardless of whether the A/D structure is considered or not, the architecture cost behaviour is very similar since the WSS dimensions are the same for both scenarios. The only difference is that the relative cost is higher when the A/D structure is included (Figure 3.14). For example, in the case of a 64×64 ROADM for the fractional space-wavelength architecture for *B*=10, we have 6216 versus 3636.

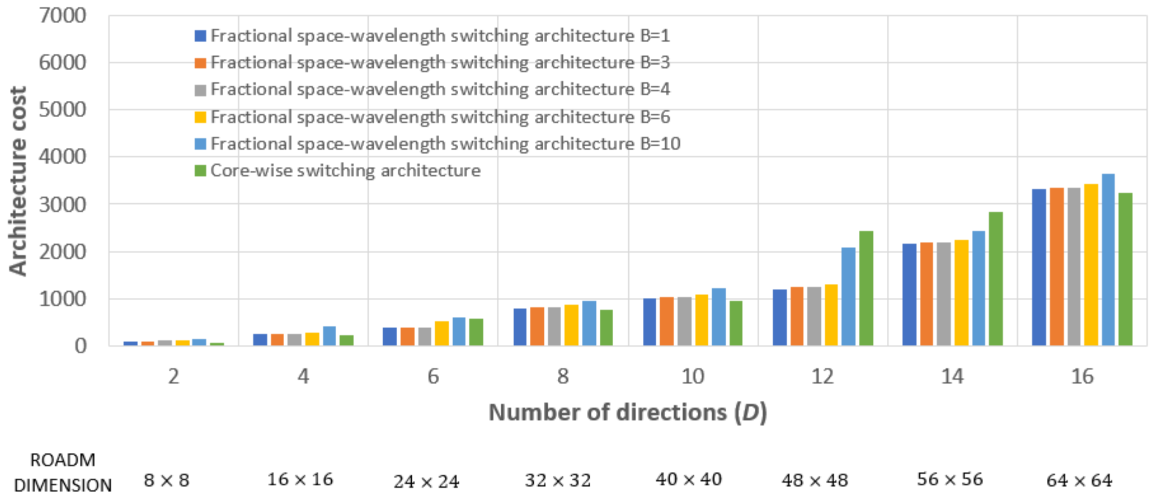

Figure 3.15 - Cost of the fractional space-wavelength granularity architecture proposed in [5] and the core-wise switching ROADM without lane changes as a function of the ROADM dimension considering M=4 and B=1,3,4,6,10 neglecting the cost of the A/D structure

After analysing the core-wise switching architecture without lane changes and the fractional space-wavelength architecture with and without a bank of WSSs in parallel in the A/D structure, it is possible to conclude that the value of B=3 is the value that ensures a more cost-effective scenario, and at the same time keeping a reasonable switching capacity in comparison with the core-wise switching architecture.

It is also possible to conclude that, the fractional space-wavelength architecture employing a single WSS in the A/D structure shows limited cost advantages and lacks the switching capacity compared to the core-wise switching architecture without lane changes. It also turns out that the fractional space-wavelength architecture with a bank of WSSs in the A/D (Figure 3.13) is almost always more expensive than the core-wise switching architecture without lane changes, which means the short cost advantage seen with a single WSS in the A/D disappears (Figure 3.12).

3.3. Ring and linear type ROADM-subsystems modular architectures

A modular architecture is built by interconnecting several ROADM-subsystems employing cost-effective low-degree WSSs. These WSSs are connected using a restricted number of fibers within each node called intranode fibers. The subsystems may be interconnected either in a ring configuration (Figure 3.16(a)) or in a linear configuration (Figure 3.16(b)) [1,6,16,20]. These ROADM-subsystems modular architectures, also called interconnected ROADM-subsystems have been proposed in [6] with the aim of reducing the number and size requirements of WSSs for the deployment of larger-scale ROADMs. However, if a wavelength must travel across multiple subsystems within the interconnected architecture, the number of WSSs it encounters increases. This increase can result in enhanced Physical

Layer Impairments (PLIs), such as in-band crosstalk and distortion caused by optical filtering, in contrast to traditional ROADM architectures [20] where at most two WSSs are crossed as in a R&S architecture.

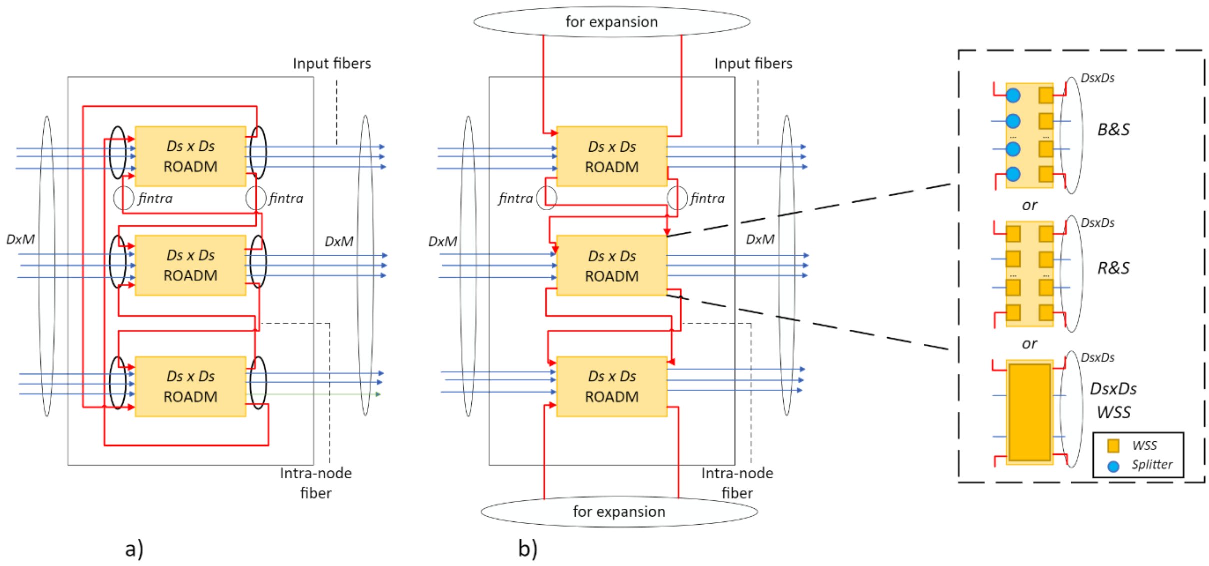

Figure 3.16 - Interconnected ROADM-subsystems node architecture [6] with a) Ring Type modular architecture and b) Linear Type Modular Architecture

3.3.1. Ring/linear type modular architectures with $D_S \times D_S$ R&S modules

The ROADM subsystems can be built with a traditional ROADM architecture, either it is a B&S or a R&S, the scenario analysed in this sub-section, or they can also be built using $D_S \times D_S$ WSSs as represented in Figure 3.16. A modular architecture has *D* input multicore fibers with *M* cores in each fiber, with a number of modules or subsystems (N_{SUB}) with dimension $D_S \times D_S$. Each module is equipped with 2 f_{intra} pairs of intra-node fibers, linking adjacent modules where f_{intra} is the number of fibers connected to an adjacent module. In the context of a linear-type architecture (as depicted in Figure 3.16(b)), there is an advantageous feature since at least one end subsystem has available intranode fibers. These fibers can be utilized to connect an extra subsystem, facilitating the node expansion process significantly, as it involves adding a subsystem and linking it to the pre-reserved intranode fibers. The difference with the ring architecture is that there is no connection between the last subsystem and the first subsystem enabling hitless expansion of the system without causing service disruption. Alternatively, introducing additional subsystems into the ring connection unavoidably leads to service disruption. There is another modular architecture proposed in [6] called the M/J type, where subsystems that accommodate incoming fibers are bridged using a junction (J) subsystem as represented in Figure 3.17. The subsystems connected with input fibers are called the main subsystems and the rest are named the junction subsystems. A limited number of input/output ports of each main subsystem is used for connection to the junction subsystems, noting that the junction subsystem size depends on the number of main subsystems and on the number of fibers used for M–J interconnection per main subsystem (represented by #s).

So, junction subsystems may have a larger dimension than main subsystems. One of the advantages of this M/J architecture is that a wavelength does only need to pass through three subsystems to get to its desired output, i.e. the signal enters in the initial subsystem, goes to the junction subsystem and is then redirected to the output module, which means less signal loss, whereas in modular ring or linear architectures the signal could cross much more than three subsystems to get to its output. However, the main disadvantage of the M/J architecture is that this architecture needs more hardware due to the existence of a junction subsystem especially when the main subsystems have a large port count .

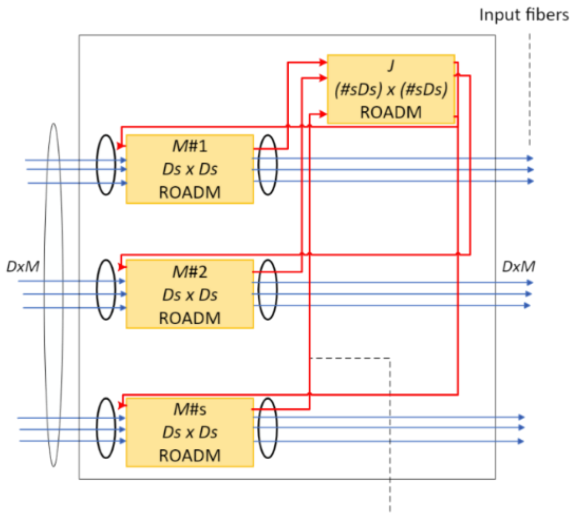

Figure 3.17 - Interconnected ROADM-subsystems node architecture [6] with M/J modular architecture

A 16×16 interconnected ring ROADM subsystem architecture is represented in Figure 3.18 with four directions (*D*=4), four spatial channels or cores (*M*=4), D_S=9, N_{SUB}=3 and f_{intra}=1. Each subsystem has D_S $1 \times D_S$ input WSSs and D_S $D_S \times 1$ output WSSs so, there is a total of $N_{SUB} \times D_S$ $1 \times D_S$ WSSs at the input stage and $N_{SUB} \times D_S$ $D_S \times 1$ WSSs at the output stage, with 4 WSSs in each module being responsible for the connections between adjacent ROADM subsystems. Additionally, this architecture also includes D $1 \times M$ fan-outs, $D \cdot M$ 1×2 WSSs that either connect to the drop structure or to the express structure, $D \cdot M$ 2×1 WSSs which either connect to the add structure or to the express structure, and D $M \times 1$ fan-ins. The A/D structure considered consists of a single $D \times M$ WSS. The ROADM represented in Figure 3.18 works as follows. The fan-out component has the same function as in Figure 3.1. The optical paths coming from the fan-out are sent into two paths: either towards the drop section or towards the express section using a 1×2 WSS. Subsequently, optical paths originating from MCFs are directed into input WSSs in the N_{SUB} ROADM subsystems. Following this, each output

WSS from a N_{SUB} ROADM subsystem is directed to a 2×1 WSS that is connected to the fan-in component present at the output stage which allows optical signals arriving at the output of the architecture to be coupled into the MCF. In the Appendix A (Figure A.1), an 8×8 (*D*=4 and *M*=2) R&S interconnected ROADM ring and linear architectures can be found using 1×9 WSSs and 1×4 WSSs assuming a single $M \times N$ WSS in the A/D structure and an A/D ratio of 20%.

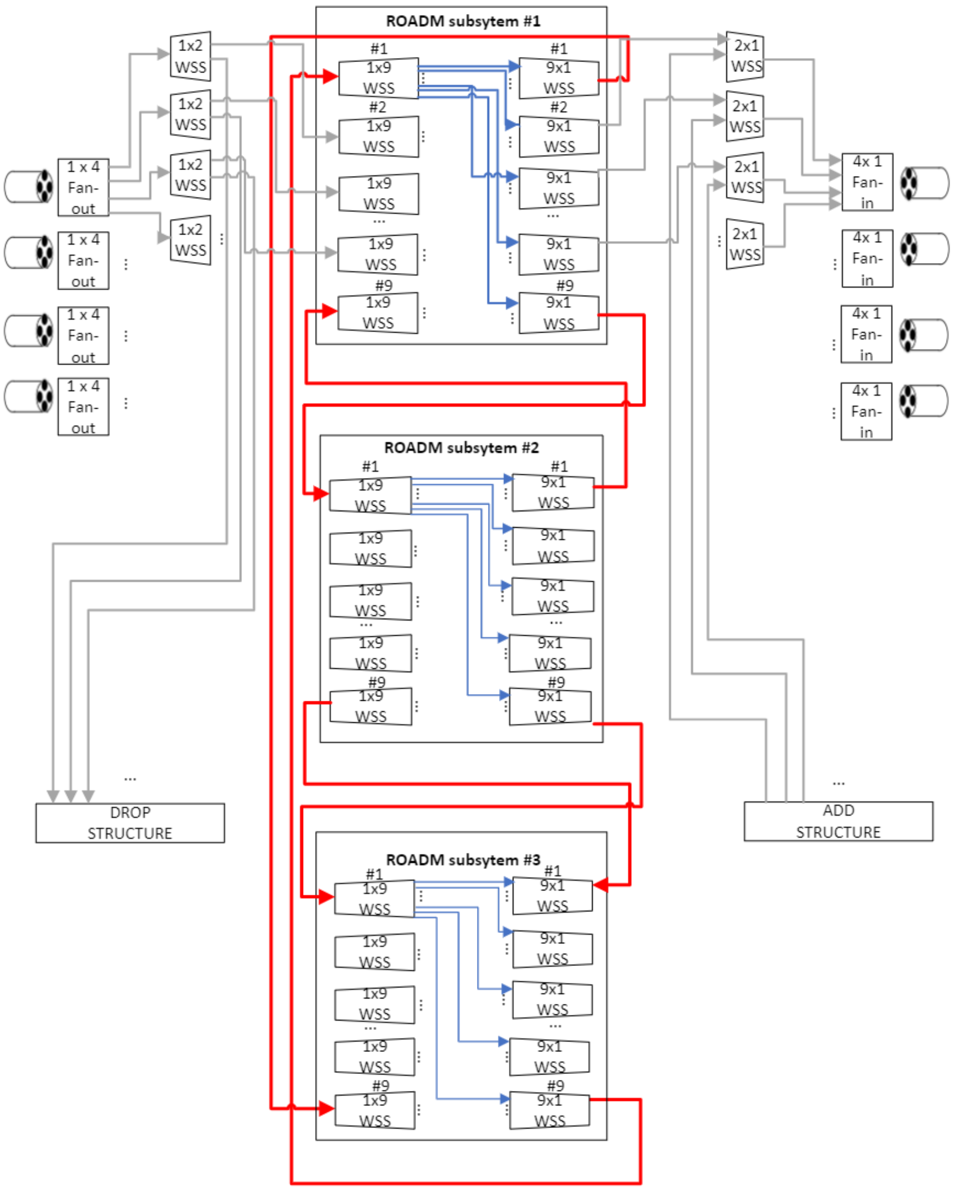

Figure 3.18 - 16x16 R&S interconnected ring modular architecture ROADM with 3 modules using 1x9 WSS considering D=4, M=4 and assuming a single MxN WSS in the A/D structure and an A/D ratio of 20%

Generically, the total number of subsystems, N_{SUB}, in an interconnected architecture node with dimension $D \cdot M \times D \cdot M$ is given by [20]:

$$N_{SUB} = \left\lceil \frac{D \times M}{D_S - 2f_{intra}} \right\rceil \quad (3.4)$$

To build a $D \cdot M \times D \cdot M$ B&S ROADM, the number of WSSs needed to interconnect the subsystems together, N_{WSS} , is given by:

$$N_{WSS} = 2f_{intra} \cdot N_{SUB} \quad (3.5)$$

Therefore, the total number of WSSs required to build the subsystems in an interconnected architecture is given by:

$$N_{Total\mathrm{B\&S}} = D \times M + N_{WSS}, \text{ for a B\&S architecture} \quad (3.6)$$

$$N_{Total\mathrm{R\&S}} = 2\ (D \times M + N_{WSS}), \text{ for a R\&S architecture} \quad (3.7)$$

It should be noted that these equations do not consider the WSSs for the input and output stages, i.e. $D \times M$ 1×2 WSSs and $D \times M$ 2×1 WSSs respectively.

The number of WSSs in a conventional architecture (like the core-wise switching architecture studied in section 3.1), N_{cw}, required to build a cascaded WSS, can be calculated using the following expression, where $D \times M$ is the ROADM size and D_L is the size of each WSS:

$$N_{cw} = \left\lceil \frac{D \times M}{D_L} \right\rceil \quad (3.8)$$

Note that this equation will lead to the same number of WSSs as the one considered in eq. (3.2), when considering a single $M \times N$ WSS in the A/D structure.

The total number of WSS required to build all the cascaded WSSs for the two conventional architectures, is given by:

$$N_{Bcw} = D \times M \times N_{cw}, \text{ for a B\&S architecture} \quad (3.9)$$

$$N_{Rcw} = 2(D \times M) \times N_{cw}, \text{ for a R\&S architecture} \quad (3.10)$$

In the following the modular architectures will be compared with the core-wise switching architecture with lane changes, because they have the same switching capacity, in both space and frequency.

As an example, suppose that we have a 64×64 ROADM with four directions (D =4), with one fiber per direction with sixteen spatial channels or cores (M=16). Consider a maximum WSS dimension of D_L= 40, 1×9 WSSs in the subsystems, i.e., D_S= 9 and f_{intra}= 1. Using Eqs. (3.4)-(3.6),(3.8) and (3.9) for a B&S architecture, the conventional node (core-wise switching architecture with lane changes) requires $64\ 1 \times 49$ WSSs (so N_{cw}=2 since the size of the 1×49 WSS exceeds the 1×40 dimension, so cascading is necessary with $128\ 1 \times 40$ WSSs), while the ring/linear modular architecture, needs $84\ 1 \times 9$ WSSs (with N_{SUB}=10). Likewise, in a R&S architecture, with the conventional architectures, $64\ 1 \times 49$ WSSs and $64\ 49 \times 1$ (so N_{cw}=2 and is necessary $128\ 1 \times 40$ and $128\ 40 \times 1$ WSSs) are required, while the ring/linear modular architecture requires $84\ 1 \times 9$ WSSs and $84\ 9 \times 1$ WSSs, giving a total of 168 WSSs. If we consider a 64×64 ROADM with 64 directions (D =64), with one fiber per direction with one channel or spatial core (M=1), the size of the WSSs in the conventional architectures will increase to 1×64, however, the number of WSSs compared to D=4 is the same for the conventional architecture for either B&S or R&S because the number of components and the WSS dimension depend on both D and M.

It can be concluded that for B&S or R&S architectures with a large or low number of directions, the conventional architecture's express structure is more expensive than modular architectures due to the increased size and cost of its WSS. For example, in the last case analysed we have $168\ 1 \times 9$ WSSs for ring/linear and $128\ 1 \times 49$ WSSs or $256\ 1 \times 40$ WSSs for core-wise switching with lane changes, which shows that the conventional architecture is more expensive since it has more WSSs and larger WSSs. However, the cost of modular architectures is further increased with the cost of the input and output stages WSSs represented in Figure 3.18.

Next, a study will be carried out considering the modular architectures with $D_S \times D_S$ R&S as modules (the following Tables only show the number and dimensions of the components of the ring architecture as the linear architecture has the same number of components) and the core-wise switching architecture for an A/D structure with a single $M \times N$ WSS or a bank of WSSs in parallel in order to assess the relative cost using either 1×9 WSSs or 1×4 WSSs inside the modules of the modular architectures.

Table 3.6 shows the minimum number of hardware components required obtained using eq. (3.8) (highlighted in red) and the actually used by the ring modular architecture (highlighted in black), for the ROADM dimensions from 4×4 to 128×128. It also shows the percentage of hardware used comparing the number of hardware components actually used with the number of components required assuming a single $M \times N$ WSSs in the A/D structure with an A/D ratio of 20% with Full CDC compatibility (see Figure 2.8 a)). To increase the ROADM dimensions, the number of directions is kept constant, *D*=4, and the number of cores is increased. For example, an 8×8 ROADM with *D*=4 and *M*=2 needs N_{SUB}=2 and 18 $WSSs$ 1×9 + 18 $WSSs$ 9×1 in each subsystem plus 8 $WSSs$ 1×2 at the input stage and 8 $WSSs$ 2×1 in the input/output stage. From Table 3.6, for the 16×16 ROADM scenario, the number of WSSs required is 16, in the input and output stages and is the same compared to the equivalent scenario for the fractional space-wavelength architecture and core-wise switching architecture in Table 3.4. However, the dimensions of the WSSs considered in each architecture are different as shown in Table 3.7.

Table 3.6 - Number and dimension of the components used for the Ring modular architecture for a given ROADM dimension considering 1x9 WSSs in the express structure ROADM as a function of the ROADM dimension considering D=4 and assuming a single M×N WSS in the A/D structure

ROADM Dimension	Number of ROADM subsystems N_{SUB}	Express components	% Used	A/D components
8x8 (*D*=4; *M*=2)	2	8 WSS 1x2+ 18 WSS 1x9+ 18 WSS 9x1 + 8 WSS 2x1 8 WSS 1x2+ 12 WSS 1x9+ 12 WSS 9x1 + 8 WSS 2x1	67	1 WSS 8x128 + 1 WSS 128x8 Transponders: 128
16x16 (*D*=4; *M*=4)	3	16 WSS 1x2 + 27 WSS 1x9+ 27 WSS 9x1+ 16 WSS 2x1 16 WSS 1x2 + 22 WSS 1x9+ 22 WSS 9x1+ 16 WSS 2x1	82	1 WSS 16x256 + 1 WSS 256x16 Transponders: 256
24x24 (*D*=4; *M*=6)	4	24 WSS 1x2 + 36 WSS 1x9+ 36 WSS 9x1+ 24 WSS 2x1 24 WSS 1x2 + 32 WSS 1x9+ 32 WSS 9x1+ 24 WSS 2x1	89	1 WSS 24x384 + 1 WSS 384x24 Transponders: 384
32x32 (*D*=4; *M*=8)	5	32 WSS 1x2+ 45 WSS 1x9+ 45 WSS 9x1+ 32 WSS 2x1 32 WSS 1x2+ 42 WSS 1x9+ 42 WSS 9x1+ 32 WSS 2x1	93	1 WSS 32x512 + 1 WSS 512x32 Transponders: 512
40x40 (*D*=4; *M*=10)	6	40 WSS 1x2+ 54 WSS 1x9+ 54 WSS 9x1+ 40 WSS 2x1 40 WSS 1x2+ 52 WSS 1x9+ 52 WSS 9x1+ 40 WSS 2x1	97	1 WSS 40x640 + 1 WSS 640x4 Transponders: 640
48x48 (*D*=4; *M*=12)	7	48 WSS 1x2+ 63 WSS 1x9+ 63 WSS 9x1+ 48 WSS 2x1 48 WSS 1x2+ 62 WSS 1x9+ 62 WSS 9x1+ 48 WSS 2x1	99	1 WSS 48x76 + 1 WSS 768x48 Transponders: 768
56x56 (*D*=4; *M*=14)	8	56 WSS 1x2+ 72 WSS 1x9+ 72 WSS 9x1+ 56 WSS 2x1 56 WSS 1x2+ 72 WSS 1x9+ 72 WSS 9x1+ 56 WSS 2x1	100	1 WSS 56x896 + 1 WSS 896x56 Transponders: 896
64x64 (*D*=4; *M*=16)	10	64 WSS 1x2+ 90 WSS 1x9+ 90 WSS 9x1+ 64 WSS 2x1 64 WSS 1x2+ 84 WSS 1x9+ 84 WSS 9x1+ 64 WSS 2x1	94	1 WSS 64x1024 + 1 WSS 1024x64 Transponders: 1024
128x128 (*D*=4; *M*=32)	19	128 WSS 1x2+ 171 WSS 1x9+ 171 WSS 9x1+ 128 WSS 2x1 64 WSS 1x2+ 166 WSS 1x9+ 166 WSS 9x1+ 64 WSS 2x1	97	1 WSS 128x2048 + 1 WSS 2048x128 Transponders: 2048

The cost of the JS WSS considered in the fractional-space wavelength architecture for *B*=3 ($4\ \ 4 - array$ 1×3 JS WSS) is less expensive than the total cost of the WSSs present in the 3 subsystems of the modulars architecture ($27\ WSS\ 1 \times 9 +\ 27\ WSS\ 9 \times 1$) and also less expensive than the express structure $(16\ WSS\ 1 \times 5 +\ 16\ WSS\ 5 \times 1)$ of the core-wise switching architecture as presented in Table 3.7. Finally, it is possible to conclude from Table 3.6 that only above a 24×24 ROADM the percentage of utilisation is higher than 90% because as the number of cores increases, increases the number of 1×2 input WSSs available to connect to the 1×9 WSSs of each subsystem.

Table 3.7 - Number and dimension of the components used for the fractional-space wavelength [5], core-wise switching architectures and Ring modular architecture for a 16x16 ROADM dimension considering D= 4 and M=4

ROADM Dimension	Ring modular architecture	Fractional space-wavelength architecture *B*=3	Core-wise switching architecture
16x16 (*D*=4; *M*=4)	16 WSS 1x2 + 27 WSS 1x9+ 27 WSS 9x1+ 16 WSS 2x1	16 WSS 1x2+4 4-array 1x3 JS WSS+ 16 WSS 4x1	16 1x5 WSS + 16 5x1 WSS

In Figure 3.19, the cost of both modular architectures, the fractional-space wavelength architecture for *B*=3 (which was concluded in Section 3.2 as the best solution) and core-wise switching architectures is represented as a function of the ROADM dimension (the number of cores, *M*, is increased and the number of directions is kept constant, *D*=4) considering a single WSS in the A/D structure with an A/D ratio of 20% . The hardware components required are the same as in Table 3.6. The cost of the A/D structure is separated from the express structure cost.

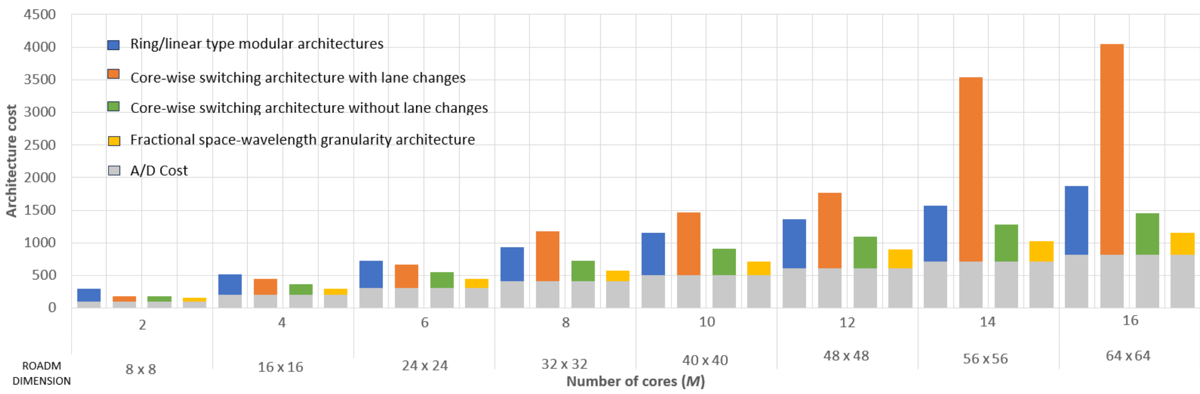

Figure 3.19 - Cost of the fractional space-wavelength granularity architecture for B=3 and the core-wise switching ROADM and both modular architectures as a function of the ROADM dimension considering D=4 assuming a single MxN WSS in the A/D structure and an A/D ratio of 20%

From Figure 3.19, it is possible to conclude that the behaviour of the architecture cost is practically independent of *M* except for core-wise switching with lane changes and the ring/linear modular architectures are always more expensive for all values of *M* considered than the two other architectures except also for the core-wise switching with lane changes because increasing the number of cores increases the size of the WSSs, leading to a much higher cost than without lane changes. For the ROADM 64×64, the core-wise switching architecture with lane changes and ring/linear modular architectures have both 64 WSSs in the input and output stage of the node, although with different dimensions: 1×49 (core-wise switching) and 1×2 (ring/linear). Although in ring/linear more hardware is still considered, in this case a total of 180 WSSs 1×9 and 1×9 that are not considered in the core-wise switching architecture with lane changes, the large size of the WSSs present in core-wise makes their total relative cost much higher as is shown in the Table 3.8. The fractional space-wavelength architecture is less expensive than the core-wise switching architecture without lane changes, because although the number of components considered is the same at the input and output stage of the node, their size is smaller (1×2 WSSs and 4×1 WSSs) with core-wise considering 1×5 WSS. The cost of the JSS WSS is not high enough to exceed the cost of the core-wise switching architecture without lane change's express structure because there is a slight reduction in switching capacity when choosing *B*=3. It is important to note that the cost of the A/D structure makes the total relative cost between modular and core-wise switching with lane changes architectures closer, since the cost of A/D for all the *M* cases considered represents more than 70% of the total cost of the architecture.

Table 3.8 - Number and dimension of the components used for the core-wise switching architecture and Ring modular architecture for a 64x64 ROADM dimension considering D= 4 and M=16

ROADM Dimension	Ring modular architecture	Core-wise switching architecture with lane changes	Fractional space-wavelength architecture *B*=3	Core-wise switching architecture without lane changes
64x64 (*D*=4; *M*=16)	64 WSS 1x2+ 90 WSS 1x9+ 90 WSS 9x1+ 64 WSS 2x1	64 1x49 WSS + 64 49x1 WSS	64 WSS 1x2+4 16-array 1x3 JS WSS+ 64 WSS 4x1	64 1x5 WSS + 64 5x1 WSS

In Figure 3.20 a)-d), the cost of modular architectures, fractional-space wavelength architecture and core-wise switching architectures is represented as a function of the ROADM dimension for a higher number of directions, from *D*=8 to *D*=64. The number of cores, *M*, is varied between 2 and 16 for each direction and a single WSS in the A/D structure with 20% A/D ratio is considered.

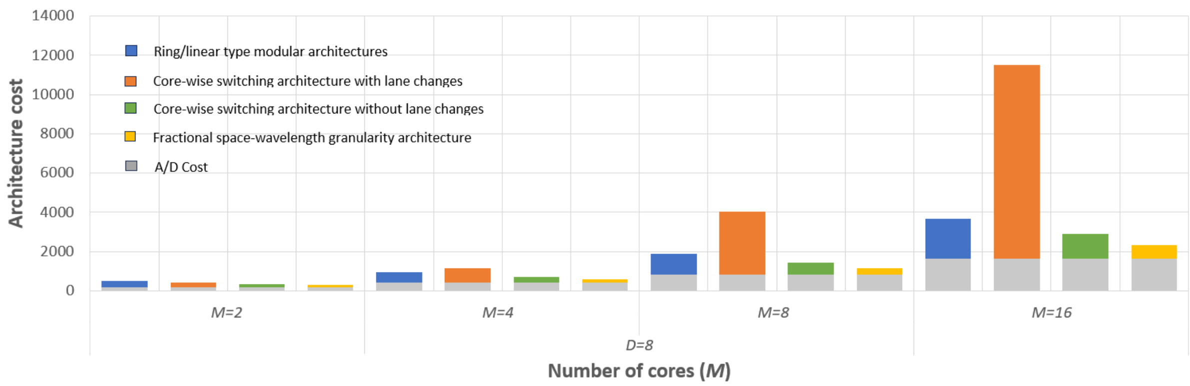

a)

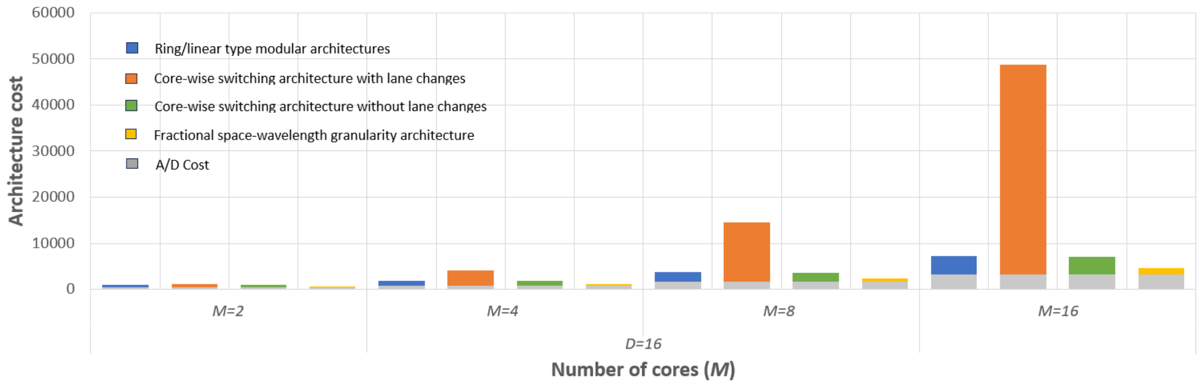

b)

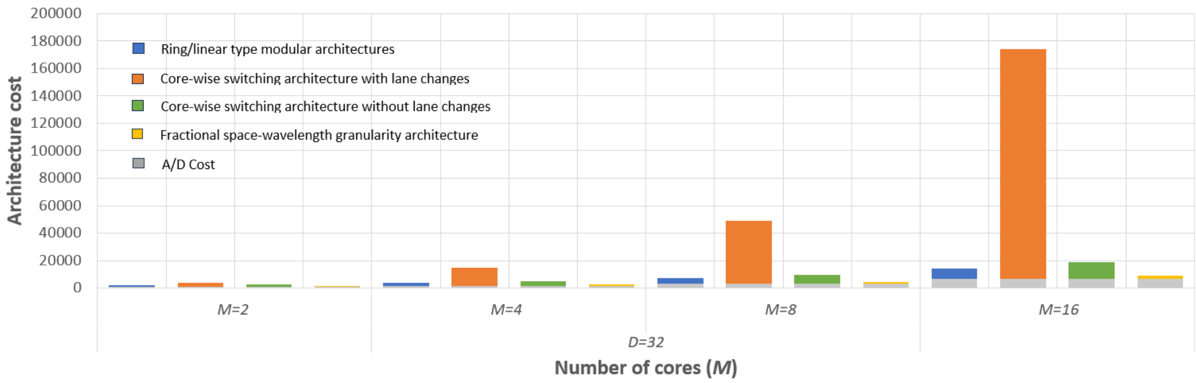

c)

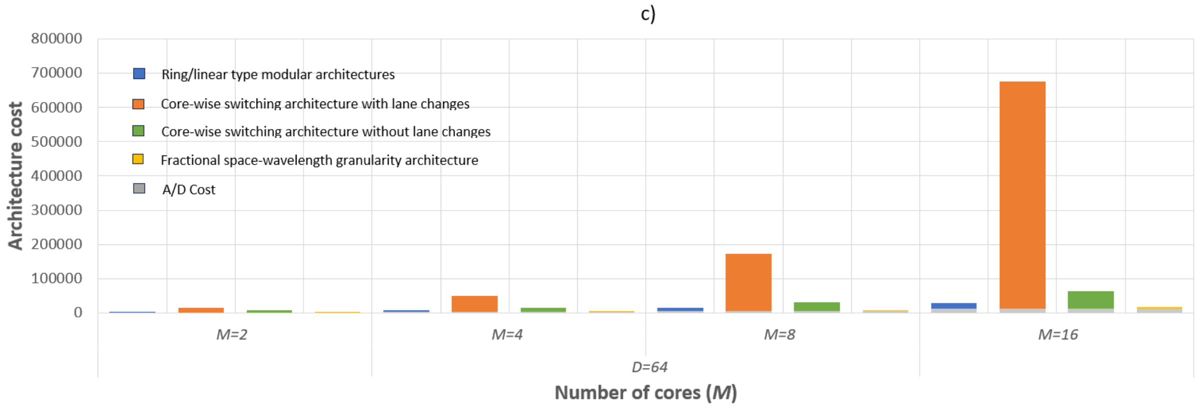

d)

Figure 3.20 - Cost of the core-wise switching ROADM, fractional-space wavelength granularity architecture for B=3 and both modular architectures as a function of the ROADM dimension considering a) D=8 ,b) D=16, c) D=32 and d) D=64 assuming a single MxN WSS in the A/D structure and an A/D ratio of 20%

From Figure 3.20, it is possible to conclude that as the number of directions increases, the relative cost of the core-wise switching architecture with lane changes in relation to the ring/linear architectures increases, achieving a significant difference for *D*=64 (Figure 3.20 d)), where the core-wise switching architecture with lane changes is more expensive independently of *M*. It is also possible to conclude that only above *D*=8 onwards, assuming an *M*=4, the core-wise switching architecture with lane changes becomes more expensive than the modular architectures noting that the core-wise becomes more expensive for higher values of *M* and for higher values of *D*. For the core-wise switching architecture without lane changes, it is possible to conclude that only above *D*=32 onwards, with *M*=2, this architecture becomes more expensive than the fractional-space wavelength architecture.

For the 1024×1024 ROADM scenario (where *D*=64 and *M*=16), both ring/linear and core-wise switching architectures with lane changes consider 1024 WSSs at the input and output stages, with different dimensions: in ring/linear, 1×2 WSSs are used (α=1.25) and in core-wise 1×1009 WSS ($1\ 1 \times 2$ WSS and $2\ 1 \times 40$ WSS) (α=324). The high value of *D* and *M* demands high size WSSs for the core-wise switching architecture with lane changes, making the architecture cost 42 times more than the modular architectures, as can be seen in the Table 3.9.

Comparing Table 3.9 for *D*=64 and *M*=16 with Table 3.8 for *D*=4 and *M*=16, it can be seen that in the modular architectures, the main difference is the number of components in the express structure, which is higher in Table 3.9. In the core-wise switching architecture without lane changes, both the number of components and their respective size increases with *D*, with a higher cost in Table 3.9 and, in the core-wise switching architecture with lane changes, the same happens, noting that the size of the WSSs of this architecture besides depending on *D*, it also depends on *M.*

Table 3.9 - Number and dimension of the components used for the core-wise switching architecture and Ring modular architecture for a given ROADM dimension considering D= 64 and M=16

ROADM Dimension	Ring modular architecture	Core-wise switching architecture with lane changes	Fractional space-wavelength architecture B=3	Core-wise switching architecture without lane changes
1024x1024 (*D*=64; *M*=16)	1024 WSS 1x2+ 1323 WSS 1x9+ 1323 WSS 9x1 + 1024 WSS 2x1	1024 1x1009 WSS + 1024 1009x1 WSS	1024 WSS 1x2+64 16-array 1x3 JS WSS+ 1024 WSS 4x1	1024 1x65 WSS + 1024 65x1 WSS

Table 3.10 shows the number of hardware components required by the ring modular architecture, for several ROADM dimensions, from 4×4 to 64×64, assuming a bank of WSSs in parallel with an A/D ratio of 20%. It should be noted that, the only difference between Table 3.6 and Table 3.10, is the dimension of the WSSs required at the input and output stages, being higher in Table 3.10 due to the number of WSS in parallel considered in the A/D structure.

Table 3.10 - Number and dimension of the components used for the Ring modular architecture for a given ROADM dimension considering 1x9 WSSs in the express structure ROADM as a function of the ROADM dimension considering D=4 and assuming a bank of WSSs in parallel in the A/D structure and an A/D ratio of 20%

ROADM Dimension	Number of ROADM subsystems N_{SUB}	Express components	% Used	A/D components
8x8 (D=4; M=2)	2	8 WSS 1x7+ 18 WSS 1x9+ 18 WSS 9x1 + 8 WSS 7x1 8 WSS 1x7+ 12 WSS 1x9+ 12 WSS 9x1 + 8 WSS 7x1	67	6 WSS 16x24 + 6 WSS 24x16 Transponders: 128
16x16 (D=4; M=4)	3	16 WSS 1x12+ 27 WSS 1x9+ 27 WSS 9x1+ 16 WSS 12x1 16 WSS 1x12+ 22 WSS 1x9+ 22 WSS 9x1+ 16 WSS 12x1	82	11 WSS 16x24 + 11 WSS 24x16 Transponders: 256
24x24 (D=4; M=6)	4	24 WSS 1x17+ 36 WSS 1x9+ 36 WSS 9x1+ 24 WSS 17x1 24 WSS 1x17+ 32 WSS 1x9+ 32 WSS 9x1+ 24 WSS 17x1	89	16 WSS 16x24 + 16 WSS 24x16 Transponders: 384
32x32 (D=4; M=8)	5	32 WSS 1x23+ 45 WSS 1x9+ 45 WSS 9x1+ 32 WSS 23x1 32 WSS 1x23+ 42 WSS 1x9+ 42 WSS 9x1+ 32 WSS 23x1	94	22 WSS 16x24+ 22 WSS 24x16 Transponders: 512
40x40 (D=4; M=10)	6	40 WSS 1x28+ 54 WSS 1x9+ 54 WSS 9x1+ 40 WSS 28x1 40 WSS 1x28+ 52 WSS 1x9+ 52 WSS 9x1+ 40 WSS 28x1	97	27 WSS 16x24 + 27 WSS 24x16 Transponders: 640
48x48 (D=4; M=12)	7	48 WSS 1x33+ 63 WSS 1x9+ 63 WSS 9x1+ 48 WSS 33x1 48 WSS 1x33+ 62 WSS 1x9+ 62 WSS 9x1+ 48 WSS 33x1	99	32 WSS 16x24 + 32 WSS 24x16 Transponders: 768
56x56 (D=4; M=14)	8	56 WSS 1x39+ 72 WSS 1x9+ 72 WSS 9x1+ 56 WSS 39x1 56 WSS 1x39+ 72 WSS 1x9+ 72 WSS 9x1+ 56 WSS 39x1	100	38 WSS 16x24+ 38 WSS 24x16 Transponders: 896
64x64 (D=4; M=16)	10	64 WSS 1x44+ 90 WSS 1x9+ 90 WSS 9x1+ 64 WSS 44x1 64 WSS 1x44+ 84 WSS 1x9+ 84 WSS 9x1+ 64 WSS 44x1	94	43 WSS 16x24 + 43 WSS 24x16 Transponders: 1024

Figure 3.21 shows the cost of the same architectures considered in Figure 3.20 as a function of the ROADM dimension, but considering in the A/D structure a bank of WSSs in parallel with an A/D ratio of 20% . The hardware components required are the same as Table 3.10.

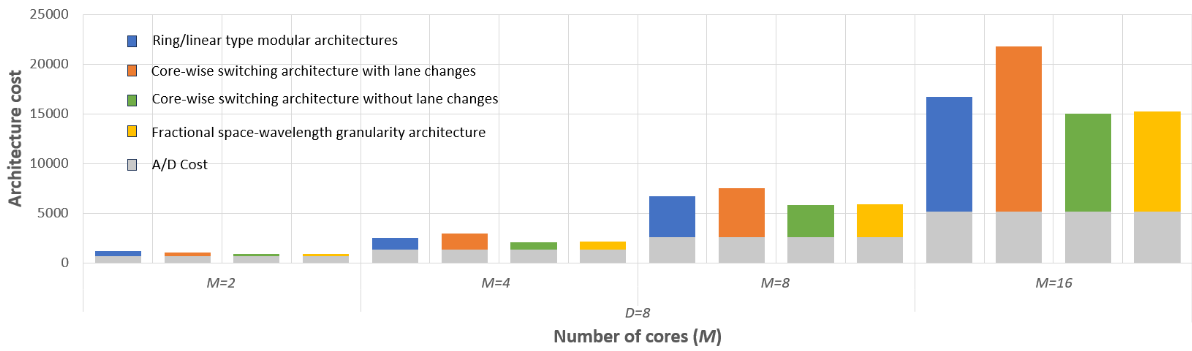

a)

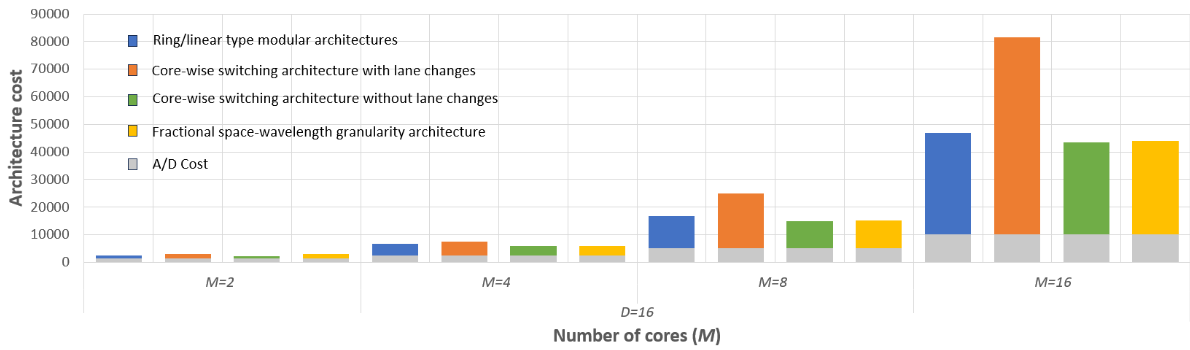

b)

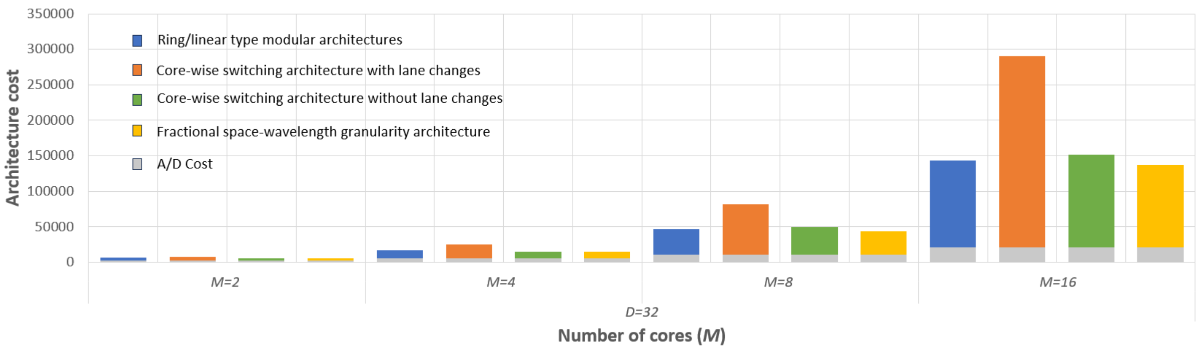

c)

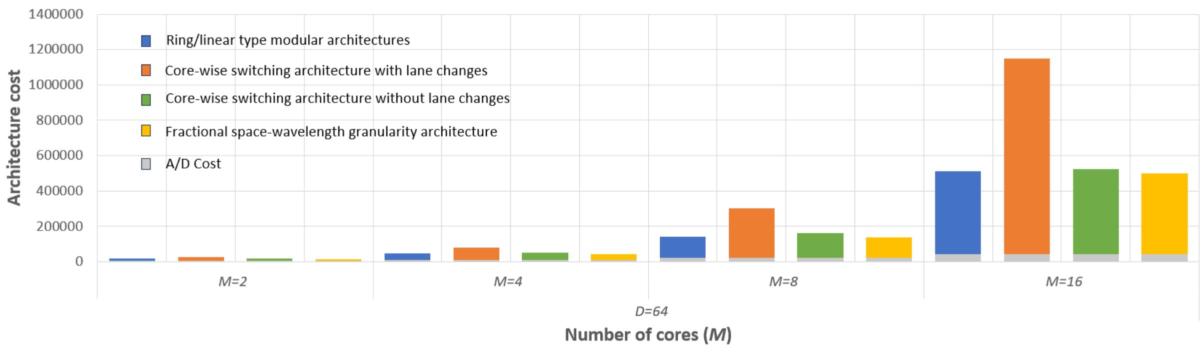

d)

Figure 3.21 - Cost of the core-wise switching ROADM, fractional-space wavelength granularity architecture for B=3 and both modular architectures as a function of the ROADM dimension considering a) D=8 ,b) D=16, c) D=32 and d) D=64 assuming a bank of WSSs in parallel in the A/D structure and an A/D ratio of 20%

From Figure 3.21, it is possible to observe that the core-wise switching architecture with lane changes is more expensive in terms of ROADM dimension compared to the modular architectures only when *D*=8 and *M*=4 onwards, as shown in Figure 3.21 a). Note that the cost associated with the architectures for a scenario with a bank of WSSs in the A/D structure is much higher than in the scenario with a single WSS, as shown in Figure 3.20. It should be noted that with a bank of WSSs, the core-wise switching with lane changes is only 2 times more expensive than modular architectures and in a scenario with a single WSS, the core-wise switching architecture is 17 times more expensive compared to modular architectures for *D*=64. For the 1024×1024 ROADM scenario where *D*=64 and *M*=16 , both ring/linear and the other three architectures consider 1024 WSSs in the input and output stages. However, considering WSSs with different dimensions as shown in Table 3.11, leads to different relative cost of the architectures.

Table 3.11 - Number and dimension of the components used for the core-wise switching architecture and Ring modular architecture for a given ROADM dimension considering D= 64 and M=16 assuming a bank of WSSs in parallel in the A/D structure

ROADM Dimension	Ring modular architecture	Core-wise switching architecture without lane changes	Fractional space-wavelength architecture B=3	Core-wise switching architecture without lane changes
1024x1024 (*D*=64; *M*=16)	1024 WSS 1x684+ 1323 WSS 1x9+ 1323 WSS 9x1 + 1024 WSS 684x1	1024 1x1691 WSS + 1024 1691x1 WSS	1024 WSS 1x684+64 16-array 1x3 JS WSS+ 1024 WSS 686x1	1024 1x747 WSS + 1024 747x1 WSS

Table 3.12 shows the number of hardware components required by the ring modular architecture, for several ROADM dimensions, from 4×4 to 64×64 , assuming a single $M \times \mathrm{N}$ WSSs in the A/D structure with an A/D ratio of 20% and 1×4 WSSs inside each subsystem. To increase the ROADM dimensions, the number of directions is kept constant, *D*=4, and the number of cores is increased.

It should be noted that, the highest difference from Table 3.6 is the number of subsystems required to build each ROADM dimension, which is much higher in the 1×4 WSSs scenario due to the smaller WSS dimension. It is also possible to conclude that the utilisation rate of the WSSs in the subsystems is 100%, which means, there are not unused WSSs in the subsystems. For an 8×8 ROADM, 4 subsystems are required, each one with 4 1×4 WSSs in the input stage, i.e., a total of 16 WSSs in the node. Since 2 WSSs in each subsystem are used for intra-system connections, only 2 WSSs remain in each subsystem that will connect to one of the 8 1×2 input WSSs. Since only 8 WSSs are available in total on the input stage and there are 8 1×2 WSSs, there are no unused WSSs.

In Figure 3.22, the cost of both modular architectures, is represented as a function of the ROADM dimension (the number of cores (*M*) is increased and the number of directions is kept constant, *D*=64, because it was concluded that modular architectures are more advantageous for high values of *D*) considering in the A/D structure, a single WSSs with an A/D ratio of 20% and two different WSSs dimensions considered in the express structure, 1×4 WSS and 1×9 WSS.

From Figure 3.22, it is possible to conclude that the solution of using 1×4 WSS in the subsystems is more advantageous in terms of cost for all values of *M* considered. This is because, when the WSS size is smaller, although a greater number of components are used in each subsystem due to the need of more subsystems, the cost of each 1×4 WSS is only 2.5, while the cost of the 1×9 WSS is 5. It is important to note that the only difference between both solutions is the size of the WSS and the number of components considered in each subsystem, since the number of WSS of the input and output stages are the same for all scenarios.

Table 3.12 - Number and dimension of the components used for the Ring modular architecture for a given ROADM dimension considering 1x4 WSSs in the express structure ROADM as a function of the ROADM dimension considering D=4 and assuming a single M×N WSS in the A/D structure

ROADM Dimension	Number of ROADM subsystems N_{SUB}	Express components	A/D components
8x8 (D=4; M=2)	4	8 WSS 1x2+ 16 WSS 1x4+ 16 WSS 4x1 + 8 WSS 2x1 8 WSS 1x2+ 16 WSS 1x4+ 16 WSS 4x1 + 8 WSS 2x1	1 WSS 8x128 + 1 WSS 128x8 Transponders: 128
16x16 (D=4; M=4)	8	16 WSS 1x2 + 32 WSS 1x4+ 32 WSS 4x1+ 16 WSS 2x1 16 WSS 1x2 + 32 WSS 1x4+ 32 WSS 4x1+ 16 WSS 2x1	1 WSS 16x256 + 1 WSS 256x16 Transponders: 256
24x24 (D=4; M=6)	12	24 WSS 1x2 + 48 WSS 1x4+ 48 WSS 4x1+ 24 WSS 2x1 24 WSS 1x2 + 48 WSS 1x4+ 48 WSS 4x1+ 24 WSS 2x1	1 WSS 24x384 + 1 WSS 384x24 Transponders: 384
32x32 (D=4; M=8)	16	32 WSS 1x2+ 64 WSS 1x4+ 64 WSS 4x1+ 32 WSS 2x1 32 WSS 1x2+ 64 WSS 1x4+ 64 WSS 4x1+ 32 WSS 2x1	1 WSS 32x512+ 1 WSS 512x32 Transponders: 512
40x40 (D=4; M=10)	20	40 WSS 1x2+ 80 WSS 1x4+ 80 WSS 4x1+ 40 WSS 2x1 40 WSS 1x2+ 80 WSS 1x4+ 80 WSS 4x1+ 40 WSS 2x1	1 WSS 40x640 + 1 WSS 640x40 Transponders: 640
48x48 (D=4; M=12)	24	48 WSS 1x2+ 96 WSS 1x4+ 96 WSS 4x1+ 48 WSS 2x1 48 WSS 1x2+ 96 WSS 1x4+ 96 WSS 4x1+ 48 WSS 2x1	1 WSS 48x768 + 1 WSS 768x48 Transponders: 768
56x56 (D=4; M=14)	28	56 WSS 1x2+ 112 WSS 1x4+ 112 WSS 4x1+ 56 WSS 2x1 56 WSS 1x2+ 112 WSS 1x4+ 112 WSS 4x1+ 56 WSS 2x1	1 WSS 56x896 + 1 WSS 896x56 Transponders: 896
64x64 (D=4; M=16)	32	64 WSS 1x2+ 128 WSS 1x4+ 128 WSS 4x1+ 64 WSS 2x1 64 WSS 1x2+ 128 WSS 1x4+ 128 WSS 4x1+ 64 WSS 2x1	1 WSS 64x1024 + 1 WSS 1024x64 Transponders: 1024

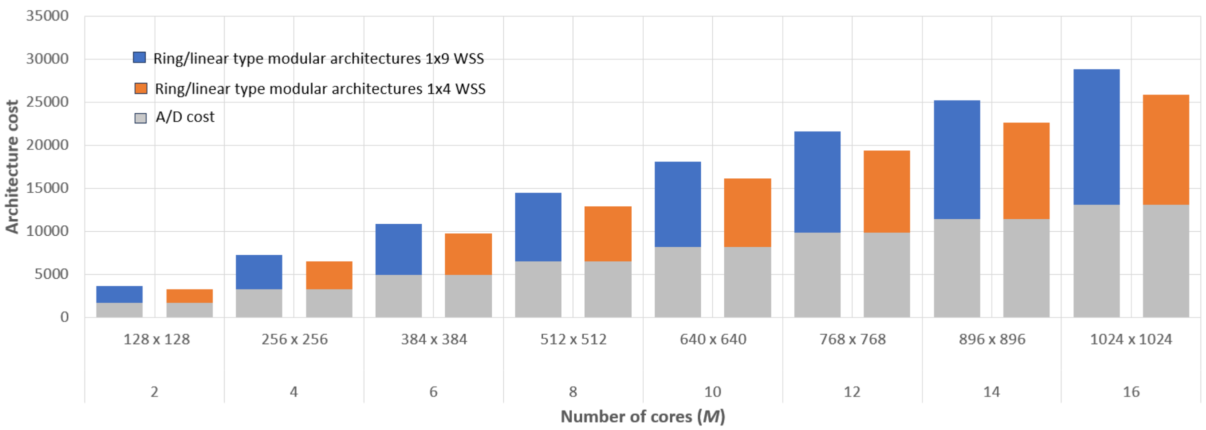

Figure 3.22 - Cost of the Ring Type and Linear Type modular architectures as a function of the ROADM dimension considering D=64 assuming a single MxN WSS in the A/D structure and an A/D ratio of 20% and two different WSS dimensions inside the subsystems

In summary, it is possible to conclude that modular architectures constructed by interconnecting multiple ROADM subsystems with cost-effective low-degree WSSs offer a promising approach to reducing the number and size requirements of WSSs in large-scale ROADMs noting that each architecture can be arranged in ring or linear configurations. Considering the comparison between architectures with the same switching capacity for architectures with a large number of directions, conventional core-wise switching architectures are more expensive than modular architectures due to the increased size and cost of WSSs. However, the cost advantage of modular architectures diminishes when considering the additional costs of input and output stages WSSs. For a small number of directions, the number of WSSs required for ring/linear modular architectures and conventional architectures is not significantly different. The modular architectures generally offer better cost advantages as the number of directions increases, as the core-wise switching architectures, particularly those with lane changes, become substantially more expensive due to the need for larger WSSs. However, for a scenario with a bank of WSSs, the modular architectures lose a large part of their cost advantage compared to a single WSS scenario. The fractional-space wavelength architecture remains a cost-effective alternative under these conditions, demonstrating lower relative costs compared to core-wise switching architectures without lane changes. Finally, while the use of smaller WSS dimensions (e.g., 1×4) increases the number of required subsystems and components, it results in a more cost-effective solution. The 1×4 WSSs, despite necessitating a greater number of components, prove to be less expensive overall compared to the 1×9 WSSs. These analysis highlights the importance of considering both the size and cost of WSS components when designing and scaling ROADM architectures.

3.3.2. Ring/linear type modular architectures with $D_S \times D_S$ WSS modules

In the following, we are going to use $D_S \times D_S$ WSSs as subsystems modules (see Figure 3.16 b)), instead of R&S architectures, with the goal of reducing the architectures cost [21].

Figure 3.23 shows a comparison between the total cost of using as subsystem modules, a $D_S \times D_S$ R&S architecture with D_S $1 \times D_S$ WSSs and D_S $D_S \times 1$ WSSs and a $D_S \times D_S$ WSS with D_S=4 as subsystems modules as a function of the ROADM dimension. The cost assigned to the 4×4 WSS is α=6. This cost is calculated in a proportional way having in mind the 9×18 WSS cost, shown in Table 3.2.

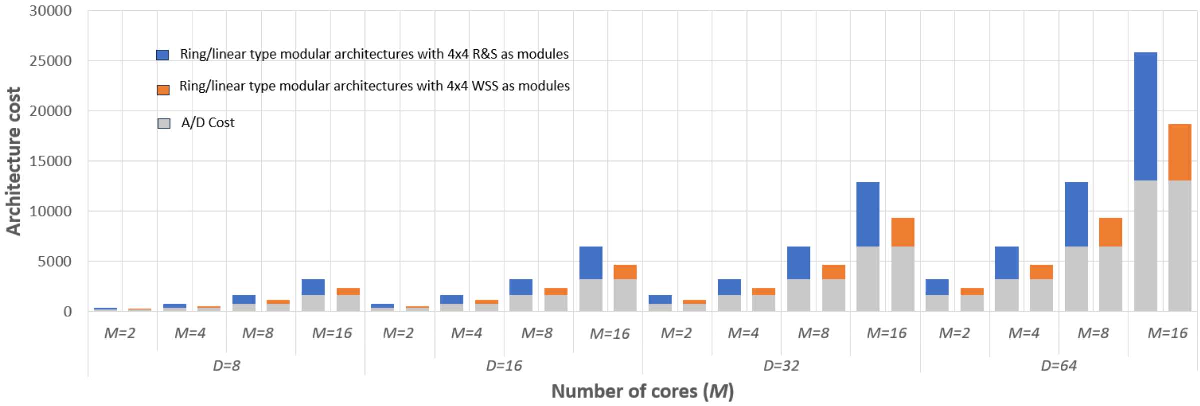

Figure 3.23 - Cost of the modular architecture using a 4×4 R&S architecture and a 4×4 WSS as subsystems modules as a function of the ROADM dimension considering D=8 , D=16, D=32 and D=64 assuming a single WSS in the A/D structure, and an A/D ratio of 20%

From Figure 3.23, in general, the cost of the R&S architecture using 1×4 WSS is higher than the cost of using 4×4 WSSs as modules for larger values of *M* and *D*. When *M* is small, the costs between the two architectures are comparable, with a slight advantage for the architecture using 4×4 WSS as modules. As *M* increases, especially for *D*=64, the cost difference between the two architectures becomes more significant, with the 4×4 R&S architecture being more expensive. It is also important to note that the express cost of the architecture using 4×4 WSSs as subsystems modules is less than half (about 2.27 times less) the express structure cost of the 4×4 R&S architecture and is independent of the ROADM dimension. The additional cost of the A/D becomes a significant part of the node total cost for higher values of *D*, however, it is important to note that the cost of the A/D structure is the same for both architectures.

Figures 3.24 and 3.25 show the cost of the modular architectures using 4×4 WSSs as subsystem modules and the cost of the core-wise switching architecture with lane changes represented as a function of the ROADM dimension, considering in the A/D structure a single and a bank of WSSs in parallel, respectively, with an A/D ratio of 20%. The value at the top of each bar shows the architecture express structure cost, and the value below each grey column represents the cost of the A/D structure.

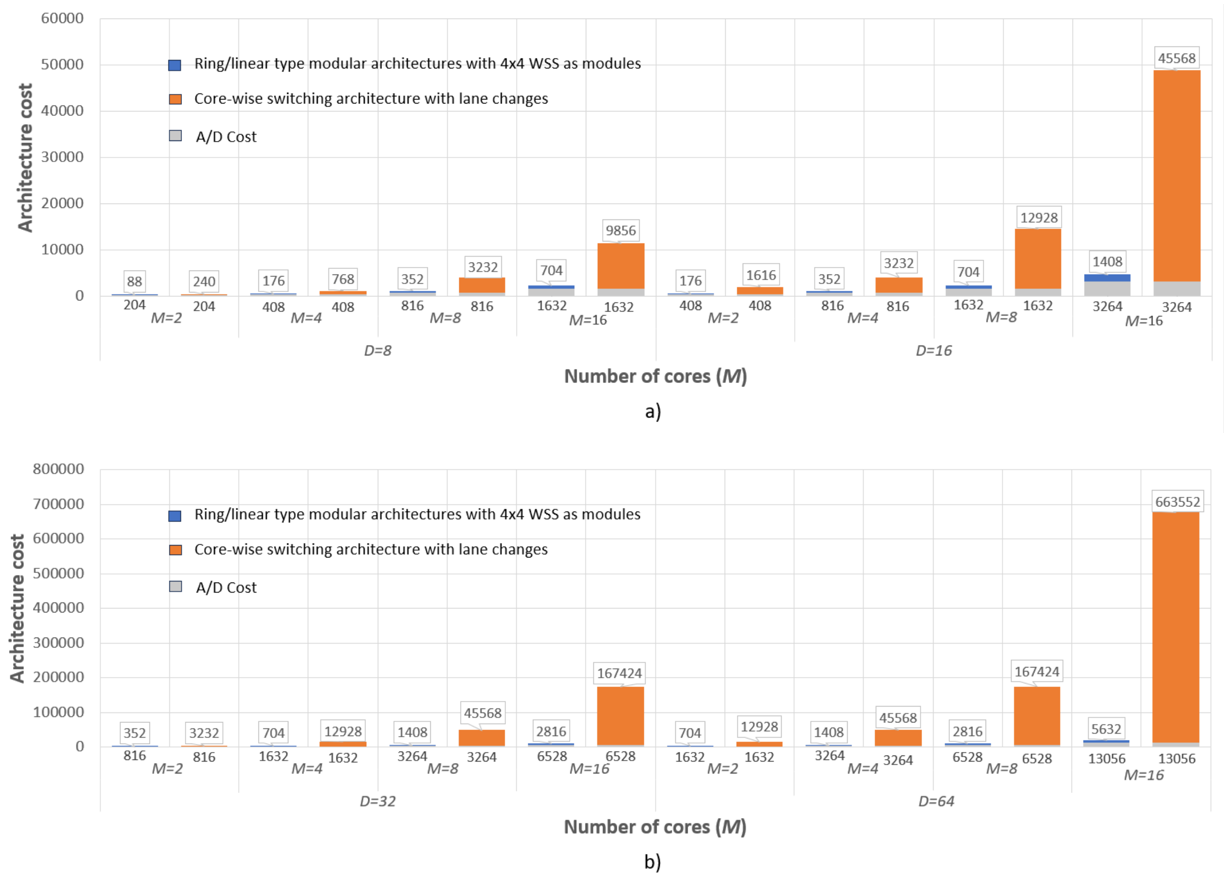

Figure 3.24 - Cost of the core-wise switching ROADM and both modular architectures as a function of the ROADM dimension considering a) D=8 and D=16 and b) D=32 and D=64 assuming a single WSS in the A/D structure, 4x4 WSSs in the subsystems and an A/D ratio of 20%

From Figure 3.24, it is possible to conclude that for a greater number of directions and the same A/D structure, the core-wise switching architecture with lane changes is much more expensive than the modular architectures. Although both have the same switching capacity, the total relative cost of the architectures is significantly cheaper for a scenario using 4×4 WSSs compared to Figure 3.22 using 4×4 R&S as modules, for a single WSS in the A/D structure. For a 16×16 ROADM dimension, in Figure 3.22, we have a total cost of 6464 for the modular architecture using 4x4 R&S as module, while in Figure 3.24, we have a total cost of 292 using 4×4 WSSs as modules.

In Figure 3.25, it is shown the cost of the modular architectures using 4×4 WSS and the core-wise switching architecture with lane changes, represented as a function of the ROADM dimension, from *D*=8 to *D*=64, (the number of cores, *M*, is varied between 2 and 16 for each direction) considering in the A/D structure, a bank of WSSs with an A/D ratio of 20%.

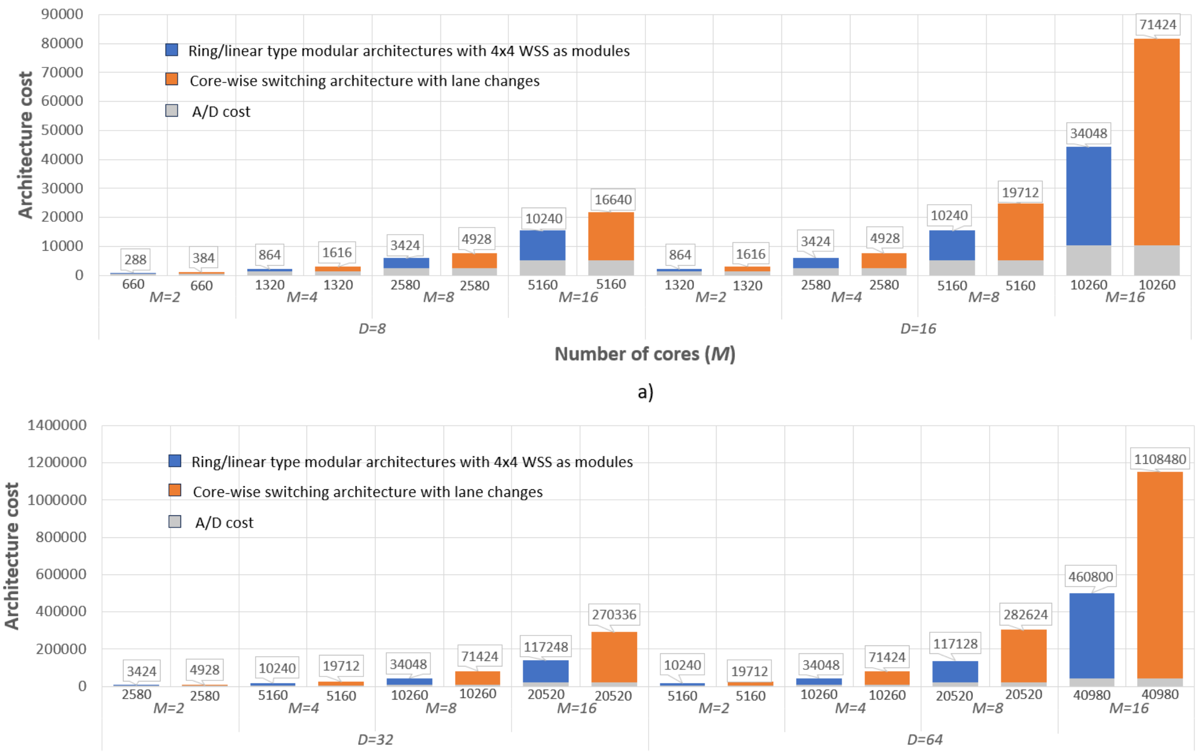

b)

Figure 3.25 - Cost of the core-wise switching ROADM and both modular architectures as a function of the ROADM dimension considering a) D=8 and D=16 and b) D=32 and D=64 assuming a bank of WSSs in parallel in the A/D structure, WSSs 4x4 in the subsystems and an A/D ratio of 20%

From Figure 3.25, it is possible to conclude that the cost associated with the modular architectures is lower for all the ROADM dimension scenarios considered, due to the fact that 4×4 WSSs are considered in each subsystem. Although the cost is much lower when using for example a 8 4×4 WSSs with a cost of 48 instead of a R&S architecture with 32 1×4 and 32 4×1 WSSs in the subsystems with a cost of 160 (assuming *D*=8 and *M*=2), the total relative cost between the two architectures in both cases is very similar. This is due to the fact that the node's input and output WSSs have several outputs/inputs for the A/D due to the bank of WSSs in parallel considered which leads to a higher total cost. Comparing Figure 3.24 with Figure 3.25, it can be seen that the total cost is much higher in the scenario with a bank of WSSs. For example, for modular architectures assuming a ROADM dimension of 1024×1024, the cost increases by around 10 times compared to the scenario with a single WSS.

In Figure 3.26, the relative cost between the A/D structure and the express structure costs for the scenario in Figure 3.25 (Full CDC with a bank of WSSs) as a function of *M* and *D* is represented, considering the modular architectures with Full CDC in the A/D structure, the core-wise switching architectures and the fractional-space wavelength architecture with *B*=3. The relative cost is defined as the ratio between the A/D structure cost and the express structure cost.

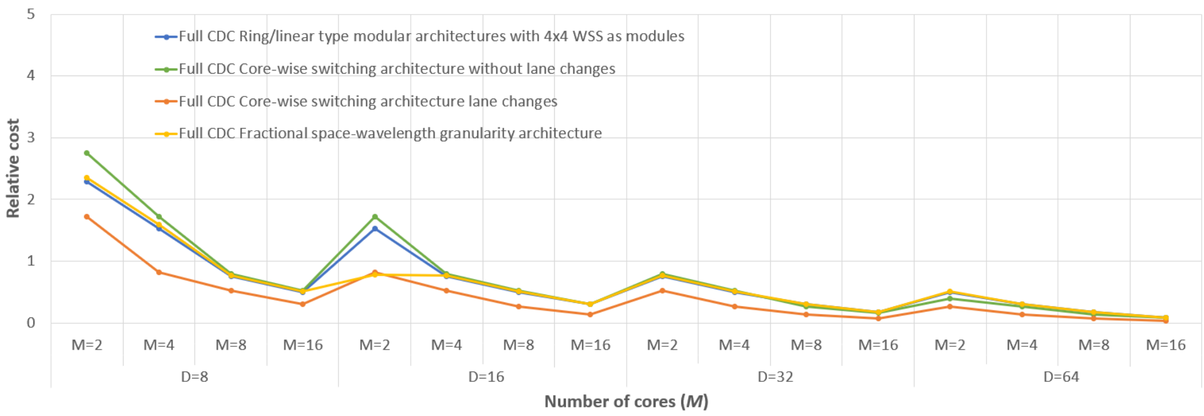

Figure 3.26 - Relative cost between the A/D structure and the express structure for the modulars architecture, core-wise architectures and fractional-space wavelength granularity architecture as a function of the ROADM dimension, assuming Full CDC in the A/D structure (bank of WSSs) and an A/D ratio of 20%

From Figure 3.26, it is possible to conclude that the core-wise switching architecture with lane changes (orange line), has the lowest relative cost in particular for smaller ROADM dimensions, but has the ROADM dimension increases the relative cost of all the architectures analysed in Figure 3.26 tend to zero, since the cost of the express structure is much higher than the cost of the A/D structure, due to the increasing number of inputs and outputs required in the node's input and output WSSs.

3.4. Strategies for using WSSs with smaller dimensions in the A/D structure

Since the main goal of this dissertation is to study solutions for reducing the cost of large SDM ROADM architectures, in addition to using a bank of WSSs in parallel to reduce the WSSs size in the A/D structure, there are other possible solutions that could reduce the cost of the node architecture by reducing the size of the WSSs in the A/D structure, such as the A/D structures presented in Figure 2.8 b) corresponding to a CDC per spatial channel solution and c) corresponding to a CDC per direction solution. Nevertheless, these strategies reduce the switching capacity of the node in comparison with the Full CDC A/D structure (shown in Figure 2.8 a)).

3.4.1. CDC per direction

In order to reduce the WSSs dimension in the A/D structure, the A/D structure considered can be CDC per direction or CDC per spatial channel instead of Full CDC [7]. These strategies have less switching capacity than the A/D structure with the bank of WSSs in parallel, but require WSSs with smaller dimension, and potentially lowering the node cost.

An example of these A/D structures is represented in Figure 3.27, considering *D*=4 and *M*=2. For this case, an 8×8 ROADM scenario, with *D*=4 and *M*=2, as indicated in Table 3.13, a drop structure with 1 WSS 8×128 (Full CDC with a single WSSs) or 6 WSSs 16×24 (Full CDC with a bank of WSSs) is considered, as represented in Figure 3.27 a) and b), respectively. Note that the input and output WSSs in the architectures using Full CDC with a single WSS have one output to the express structure and one to the drop structure, whereas using Full CDC with a bank of WSSs have one output to the express structure and six to the drop structure. In Figure 3.27 c), the drop structure has 4 WSSs 2×32 (CDC per direction) and in Figure 3.27 d), the drop structure has 2 WSS 4×64 (CDC per spatial channel). The input and output WSSs of both architectures using CDC per direction and CDC per spatial channel have one output to the express structure and one to the drop structure.

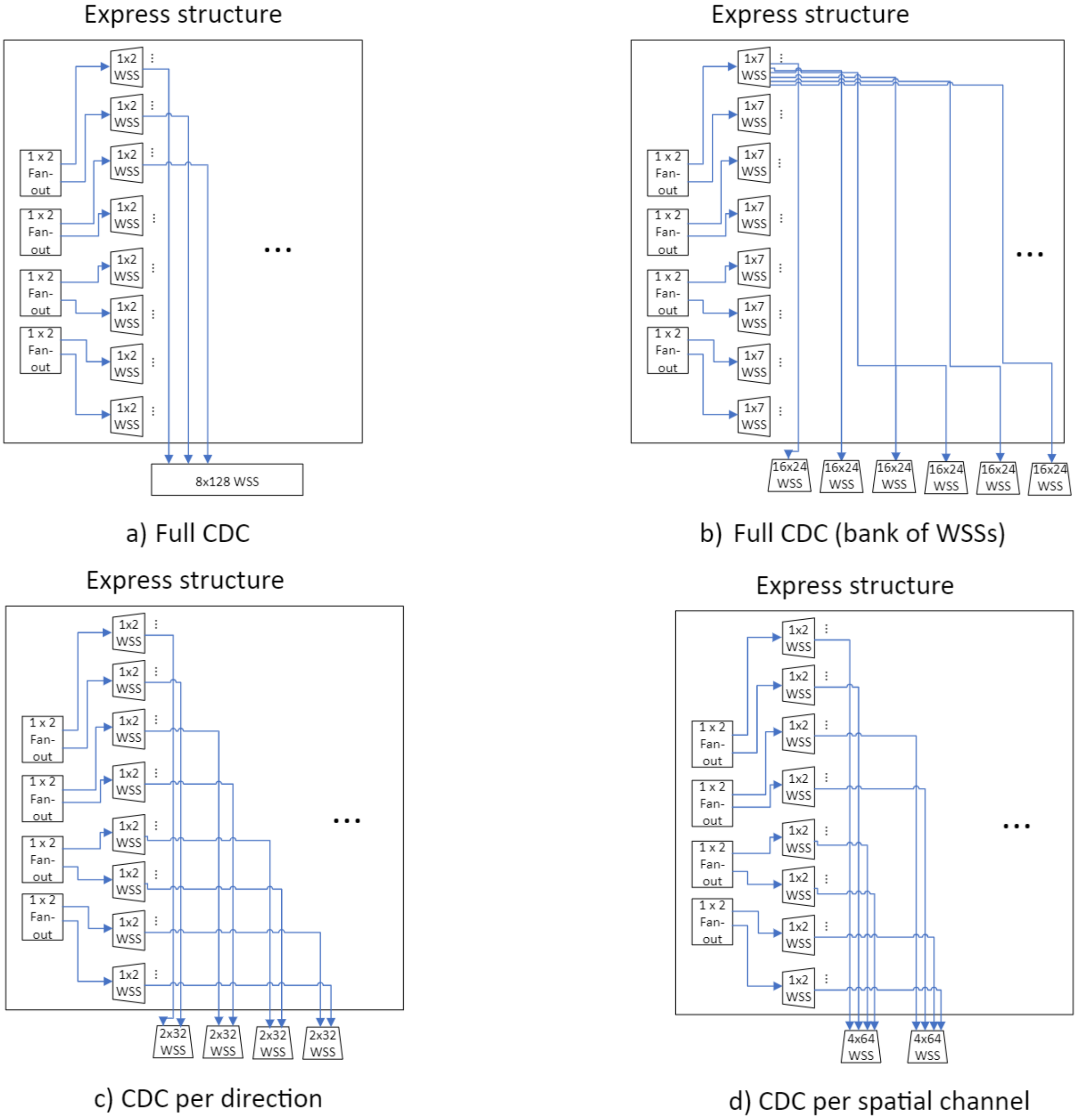

Figure 3.27 - Different drop structures considering a) Full CDC with a single WSS b) Full CDC with a bank of WSSs in parallel, c) CDC per direction and d) CDC per spatial channel assuming an 8x8 (D=4 and M=2) ROADM and an A/D ratio of 20%

Table 3.13 shows the number of WSSs and its dimension for three different A/D strategies, Full CDC (single WSS), Full CDC (bank of WSSs in parallel) and CDC per direction, for several ROADM dimensions, from 8×8 to 64×64, assuming an A/D ratio of 20%. For the 16×16 ROADM scenario where *D*=4 and *M*=4, an A/D structure with Full CDC (single WSS) has a 16×256 WSS, with Full CDC (bank of WSSs in parallel), the A/D structure has 11 WSSs 16×24, and the CDC per direction strategy requires 4 WSSs 4×64. The cost of the latter A/D structure is 204, considering a cost of 51 per 4×64 WSS, calculated by having in mind the port count and cost of the 16×24 WSS presented in Table 3.2. Although the CDC per direction strategy requires a greater number of components in the A/D structure compared to the Full CDC with a single WSS in the A/D (4 WSS 4×64 vs 1 WSS 16×256), the dimension of the WSSs required in the express structure for both strategies is the same, as shown in Figure 3.27.

It is possible to conclude that, although a Full CDC architecture with a single WSS in the A/D structure has the same port count that the CDC per direction strategy, the CDC per direction architecture has less switching capacity due to the impossibility of extracting or adding all the signals from any direction. It is also important to emphasize that a Full CDC architecture with a bank of WSSs in the A/D structure has a larger port count and therefore, is the most expensive architecture.

Table 3.13 - Number and dimension of the WSSs for the three different A/D structure strategies for various ROADM dimensions with D=4.

ROADM Dimension	A/D components		
	Full CDC		CDC per direction
	Single WSS	Bank of WSSs in parallel	Bank of WSSs
8x8 (*D*=4; *M*=2)	1 WSS 8x128 + 1 WSS 128x8	6 WSS 16x24 + 6 WSS 24x16	4 WSS 2x32 + 4 WSS 32x2
16x16 (*D*=4; *M*=4)	1 WSS 16x256 + 1 WSS 256x16	11 WSS 16x24 + 11 WSS 24x16	4 WSS 4x64+ 4 WSS 64x4
24x24 (*D*=4; *M*=6)	1 WSS 24x384 + 1 WSS 384x24	16 WSS 16x24 + 16 WSS 24x16	4 WSS 6x96+ 4 WSS 96x6
32x32 (*D*=4; *M*=8)	1 WSS 32x512 + 1 WSS 512x32	22 WSS 16x24 + 22 WSS 24x16	4 WSS 8x128 + 4 WSS 128x8
40x40 (*D*=4; *M*=10)	1 WSS 40x640 + 1 WSS 640x40	27 WSS 16x24 + 27 WSS 24x16	4 WSS 10x160 + 4 WSS 160x10
48x48 (*D*=4; *M*=12)	1 WSS 48x768 + 1 WSS 768x48	32 WSS 16x24 + 32 WSS 24x16	4 WSS 12x192 + 4 WSS 192x12
56x56 (*D*=4; *M*=14)	1 WSS 56x896 + 1 WSS 896x56	38 WSS 16x24 + 38 WSS 24x16	4 WSS 14x224 + 4 WSS 224x14
64x64 (*D*=4; *M*=16)	1 WSS 64x1024 + 1 WSS 1024x64	43 WSS 16x24 + 43 WSS 24x16	4 WSS 16x256 + 4 WSS 256x16

In Figure 3.28, the cost of the modular architectures considering the A/D structure with CDC per direction and Full CDC and the core-wise switching architectures with CDC per direction in the A/D structure (with and without lane changes) is represented as a function of the ROADM dimension considering an A/D ratio of 20%. For the modular architecture, a 4×4 WSS is considered in each subsystem noting that the express structure is the same considering the Full CDC (single WSS) and CDC per direction strategy. It is important to note that, the Full CDC strategy used in the modular architectures is compared to the core-wise switching with lane changes, whereas the CDC per direction used in the modular architectures is compared to the core-wise switching without lane changes.

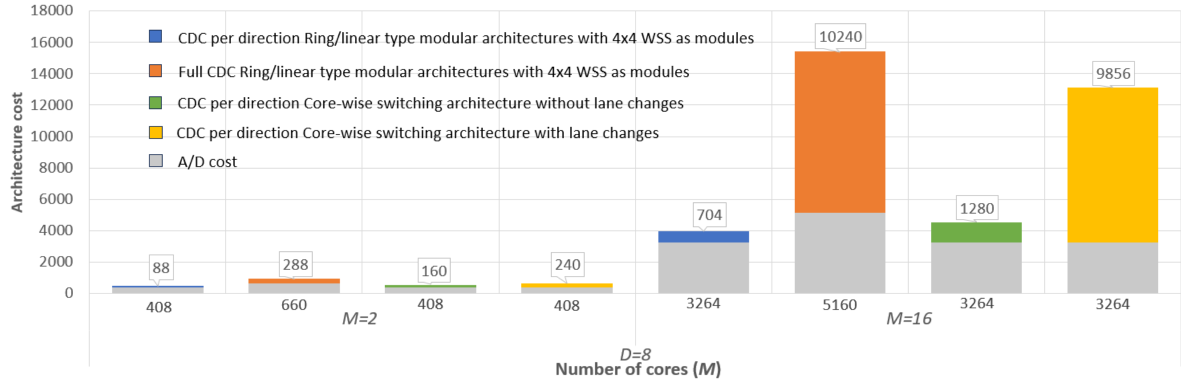

a)

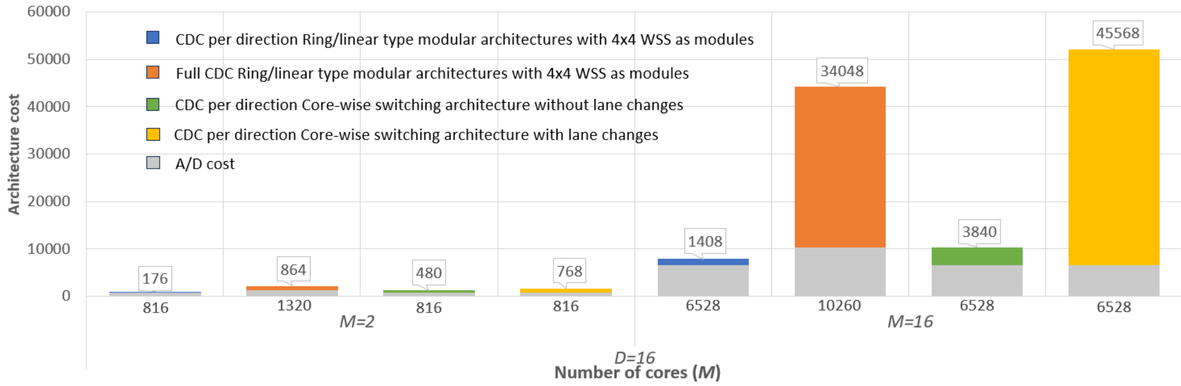

b)

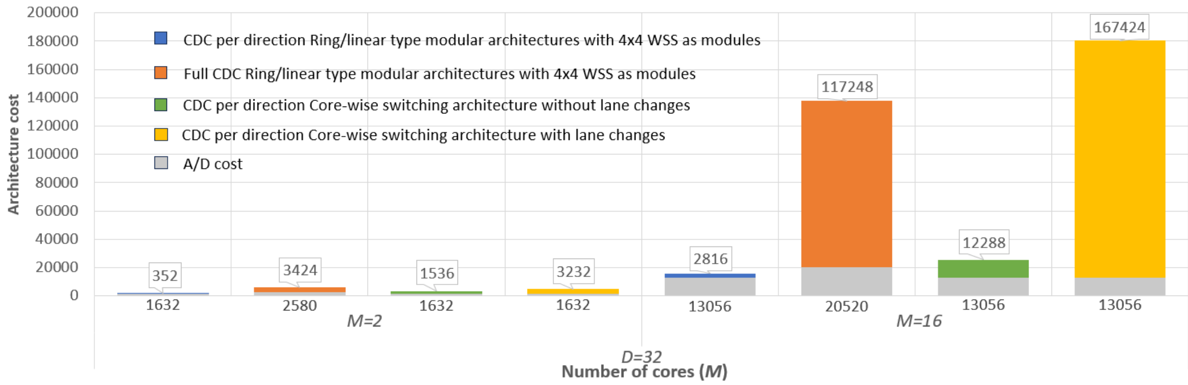

c)

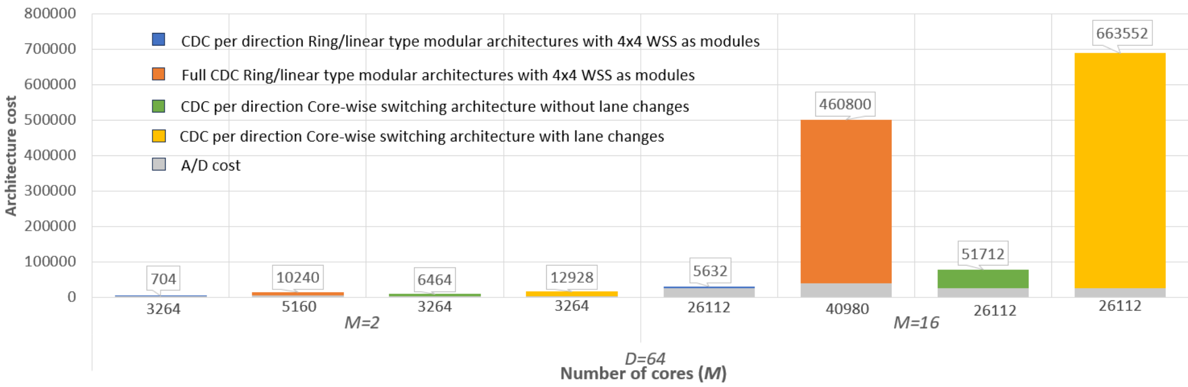

d)

Figure 3.28 - Cost of the core-wise switching and modular architectures as a function of the ROADM dimension considering a) D=8 ,b) D=16, c) D=32 and d) D=64 assuming CDC per direction and Full CDC (bank of WSSs) in the A/D structure for modular architectures, assuming WSSs 4x4 in the subsystems, and only CDC per direction for the core-wise switching architecture for an A/D ratio of 20%

From Figure 3.28, it is possible to conclude that: 1) as expected the cost of the modular architecture with Full CDC is much higher than the cost of the modular architecture with CDC per direction (almost 4 times for *D*=8 and almost 16 times for *D*=64), although the Full CDC has a much higher switching capacity; 2) the cost of the core-wise architecture with lane changes with CDC per direction is much higher than the cost of the modular architecture with CDC per direction (around 3 times for *D*=8 and almost 22 times for *D*=64); 3) the cost of the core-wise architecture without lane changes with CDC per direction is still a bit higher than the cost of the modular architecture with CDC per direction despite this last architecture have a higher switching capability (around 1.14 times for *D*=8 and 2.5 times for *D*=64); 4) the cost differences just referred are mostly related to the express structure cost, since the A/D structure cost is practically the same for the studied architectures.

In Figure 3.29, the relative cost between the cost of the A/D structure and the cost of the express structure for the scenario in Figure 3.27 (CDC per direction) as a function of *M* and *D* is represented considering the modular architectures with CDC per direction in the A/D structure, the core-wise switching architectures and the fractional-space wavelength architecture.

From Figure 3.29, it is possible to conclude that the core-wise switching architectures have the lowest relative cost, mainly the architecture with lane changes (orange line), because the express structure cost is much higher than the A/D structure cost. It is also possible to conclude that the ring/linear type modular architectures with 4×4 WSS as modules (blue line) and fractional space-wavelength granularity architecture (yellow line) have higher relative costs, since the express structure is between 4 and 5 times less expensive than the A/D structure cost. It is also important to note that the relative costs of the modular architecture and the fractional space-wavelength granularity architecture are practically constant for all ROADM dimensions considered, because the cost of the express structure and the cost of the A/D structure increase at the same rate, with the ROADM dimension increase. For the 16×16 ROADM, we have a cost of 88 for the express structure and 408 for the A/D structure while, for the 32×32 ROADM, we have a cost of 176 for the express structure and 816 for the A/D structure, revealing that the cost of both structures doubles as the ROADM dimension increases.

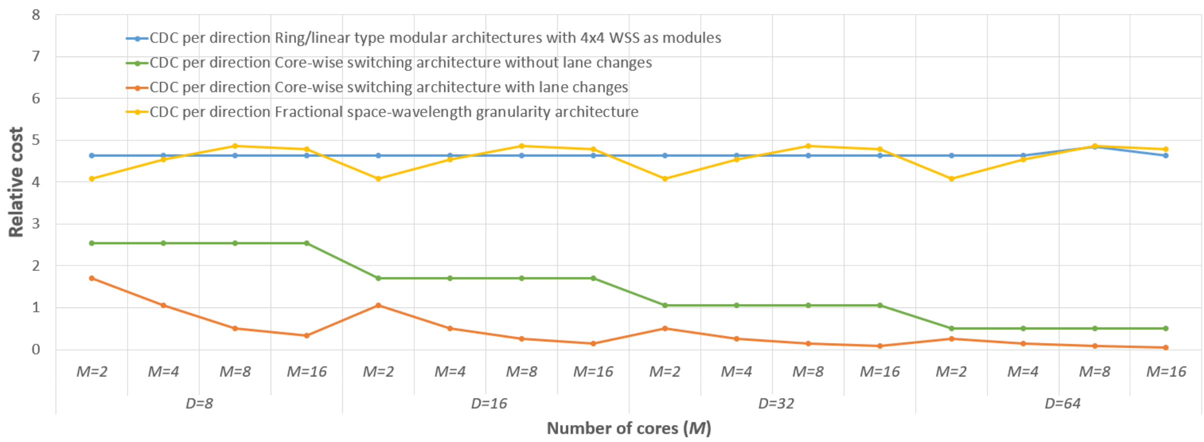

Figure 3.29 - Relative cost between the A/D structure and the express structure for the modular architecture, core-wise switching architectures and fractional space wavelength granularity architecture as a function of the ROADM dimension, assuming CDC per direction in the A/D structure (bank of WSSs) and an A/D ratio of 20%

Comparing Figure 3.29 with Figure 3.26, it is possible to conclude that the core-wise switching architecture with lane changes (orange line), continues to have the lowest relative cost due to the huge cost of its express structure, independently of being Full CDC or CDC per direction. It also can be concluded that, in Figure 3.29, the relative cost tends to zero only for the core-wise architectures, while in Figure 3.26, with CDC per direction, for all architectures, the relative cost tends to zero as the ROADM dimension increases due to the use of the Full CDC strategy in the A/D structure. In this case, the increase of the ROADM dimension leads to a significant in increase of the size of the input/output WSSs of the express structure and, therefore, the cost of the express structure becomes much higher than the cost of the A/D structure as the ROADM dimension increases.

3.4.2. CDC per spatial channel

The CDC per spatial channel strategy allows the use of fewer WSSs than the CDC per direction, although their dimensions are larger, as can be seen in Figure 3.27 for the scenario with D=4 and M=2. Note that if D and M are equal, both strategies lead to the same WSS dimensions, as for the 16×16 ROADM shown in Table 3.14. In Appendix B (Figure B.1), a cost comparison between modular architectures considering different A/D structures, Full CDC, CDC per direction and CDC per spatial channel, can be found using 4×4 WSSs and assuming an A/D ratio of 20%.

Table 3.14 shows the number of components and their dimension for the two different A/D strategies, CDC per direction and CDC per spatial channel, considering ROADM dimensions, from 8×8 to 64×64, assuming an A/D ratio of 20%. For the 8×8 ROADM scenario, where *D*=4 and *M*=2, a drop structure with 4 WSSs 2×32 WSSs must be considered in the CDC per direction solution with a total drop cost of 102, whereas the CDC per spatial channel solution requires 2 WSSs 4×64, leading also to the same cost. So, it is possible to note that, although the CDC per direction strategy requires a greater number of components in the drop structure compared to the CDC per spatial channel (4 WSSs 2×32 vs 2 WSSs 4×64), the dimension of the WSSs required in the drop structure by the CDC per spatial channel strategy is the double, which means that the architecture cost is the same. Hence, the results shown in Figure 3.28 correspond to both CDC per direction and CDC per spatial channel strategies.

Table 3.14 - Number and dimension of the components for the CDC per direction and CDC per spatial channel strategies at the A/D structure for a given ROADM dimension considering D=4 and assuming a bank of WSSs in parallel

ROADM Dimension	A/D components	
	CDC per direction	CDC per spatial channel
8x8 (*D*=4; *M*=2)	4 WSS 2x32 + 4 WSS 32x2	2 WSS 4x64 + 2 WSS 64x4
16x16 (*D*=4; *M*=4)	4 WSS 4x64+ 4 WSS 64x4	4 WSS 4x64+ 4 WSS 64x4
24x24 (*D*=4; *M*=6)	4 WSS 6x96+ 4 WSS 96x6	6 WSS 4x64+ 6 WSS 64x4
32x32 (*D*=4; *M*=8)	4 WSS 8x128 + 4 WSS 128x8	8 WSS 4x64 + 8 WSS 64x4
40x40 (*D*=4; *M*=10)	4 WSS 10x160 + 4 WSS 160x10	10 WSS 4x64 + 10 WSS 4x64
48x48 (*D*=4; *M*=12)	4 WSS 12x192 + 4 WSS 192x12	12 WSS 4x64 + 12 WSS 64x4
56x56 (*D*=4; *M*=14)	4 WSS 14x224 + 4 WSS 224x14	14 WSS 4x64 + 14 WSS 64x4
64x64 (*D*=4; *M*=16)	4 WSS 16x256 + 4 WSS 256x16	16 WSS 4x64 + 16 WSS 64x4

3.5. SDM architectures based on SPOC technology

The spatial and planar optical circuit (SPOC) technology has been developed with the aim to address the challenge related to the increased number of input/output ports in optical nodes, enabling the integration of multiple WSSs and filters into a single module by combining waveguide and free-space optics into a single system. Therefore, the SPOC technology enables compact devices and reduces the physical space required for network equipment. This integration helps overcoming the challenges faced by the large number of input/output ports in SDM systems [22].

In traditional SDM-based OXC nodes, the R&S architecture is typically used, requiring multiple high-port-count WSSs and many complex interconnections with a high number of fibres, as shown in

Figure 3.30 a) for a 6×6 WSS. This configuration takes up a lot of space as the number of SDM channels grows [1,22,23]. By adopting SPOC technology, the architecture eliminates the need for full mesh interconnections, by integrating multiple WSSs into a single module through a compact design, allowing for straight optical wiring and leads to a significant decrease in the physical space. Additionally, the SPOC technology minimizes the overlap between different WSSs, which can reduce the PLIs, namely, in this case, the crosstalk (XT) levels and improve signal quality [22]. Figure 3.30 b) represents a 6×6 WSS based on the SPOC technology that uses 2-f and 4-f optical systems [22]. It can be noted that the number of WSSs is the same in both solutions, so the cost should be similar.

In summary, SPOC technology enhances the scalability of SDM-based OXC nodes by integrating multiple WSSs into a compact module, reducing space requirements, and mitigating crosstalk. This makes it a promising solution for future high-capacity optical networks.

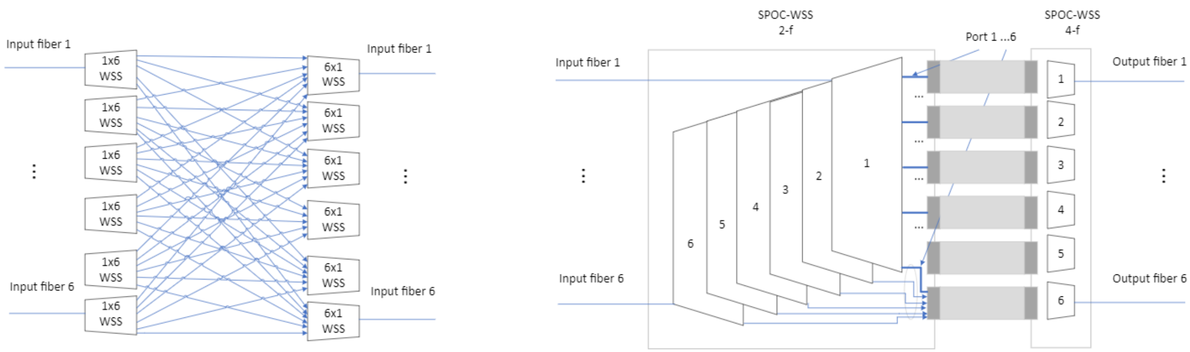

Figure 3.30 - Large-scale wavelength switching for SDM network nodes with (a) conventional 6x6 WSS and b) 6x6 WSS with subsystems using 2-f/4-f integrated SPOC systems as modular modules.

3.6. Node switching capacity overview

Switching capacity refers to the total number of possible connection states that a SDM-ROADM node can handle in an optical network including the routing of wavelengths for each spatial channel and the ability to add or drop channels in a R&S architecture. It is important to highlight that the description presented in this section is focused on the performance of a single SDM ROADM node rather than the performance of interconnected SDM ROADMs within an optical network.

The node maximum switching capacity, which is the product of the permutations across all directions and spatial channels combined, is $(D!)^{M_{Total}}$, where M_{Total} represents the total number of spatial configurations across all wavelengths and spatial channels ($M_{Total} = M \times N_W$) [24]. Each permutation represents a unique routing configuration for wavelengths between D directions. For example, for M=1, N_W=1 and D=4 (i.e. 4 directions labelled West (W), South (S), North (N), and East (E)) and corresponding number of A/D assignments, we would have 4!=24 possible permutations as shown in Table 3.15.

In Table 3.15, the WSNE initial permutation is considered fixed, and all the 4 directions are being added or dropped. This is indicated in the row Drop/Route as DDDD and on the A/D row, that tells the number of A/Ds as 4. Permutations may have no drops (where all input directions of the wavelength channel are routed) or up to D drops. The other permutations in Table 3.15 are always referring to the initial permutation WSNE, so if a direction remains unchanged in the other permutations that direction is either added or dropped (D, drop), whereas if a direction changes, it means that direction is set to be routed (R, routing). For example, in the second permutation WSEN, directions W and S remain unchanged and directions E and N change relatively to the initial permutation WSNE, where North is being routed to East and East to North, so there are 2 A/D (DDRR).

Table 3.15 - All 24 permutations of WSNE nodal directions (D=4), for a single spatial channel and single wavelength node and corresponding number of A/D and routing assignments. Only 10 of the permutations with bidirectional traffic constraints (no circular routing), remain valid (white entries)

Directions	**W S N E**	**W S** E N	**W** N S **E**	**W** N E S	**W** E S N	**W** E **N** S	S W **N E**	S W E N
Drop/Route	**DDDD**	**DD**RR	**D**RR**D**	**D**RRR	**D**RRR	**D**R**D**R	RR**DD**	RRRR
A/D	4	2	2	1	1	2	2	0
Directions	S N W **E**	S N E W	S E W N	S E **N** W	N W S **E**	N W E S	N **S** W **E**	N **S** E W
Drop/Route	RRR**D**	RRRR	RRRR	RR**D**R	RRR**D**	RRRR	R**D**R**D**	R**D**RR
A/D	1	0	0	1	1	0	2	1
Directions	N E W S	N E S W	E W S N	E W **N** S	E **S** W N	E **S N** W	E N W S	E N S W
Drop/Route	RRRR	RRRR	RRRR	RR**D**R	R**D**RR	R**DD**R	RRRR	RRRR
A/D	0	0	0	1	1	2	0	0

Now, we consider some realistic traffic constraints from real optical networks, such as, (1) all wavelength routing on spatial channels is bidirectional ensuring that connections between two nodes follow the same path in both directions, meaning circular routing of spatial channels is prohibited (e.g., assigning routes like 'East' → 'West' → 'North' → 'East' is not allowed), and (2) spatial channels in one or more nodal directions can remain idle, denoting the potential for unused wavelengths on any spatial channel or in any direction.

When considering bidirectional traffic constraints, cases of circular routing (shown as grey entries in Table 3.15) are excluded, resulting in 10 (out of 4!= 24) distinct permutation options, shown in white entries in Table 3.15. For example, in permutation WESN, position of W is unchanged ('West' direction is dropped) and position S, N, and E are circularly changed with respect to WSNE, i.e. 'South' is routed to 'East', 'North' is routed to 'South', 'East' is routed to 'North'. Such case is not a valid permutation for bidirectional traffic, because it corresponds to circular routing. In permutation WNSE, position of W and E are unchanged ('West'and 'East' directions are dropped) and 'South' is routed to 'North' and 'North' is routed to 'South' with respect to WSNE. Such case is a valid permutation for bidirectional traffic, because this connection follows the same path in both directions, as is also valid the permutation ENSW, where ‘West’ is routed to ‘East’, ‘East’ is routed to ‘West’, ‘North’ is routed to ‘South’ and ‘South’ is routed to ‘North’.

When there are idle states in $L \in \{0, 1, 2, . . ., D\}$ directions, meaning that traffic is limited to $D - L$ directions, the number of distinct permutation options is 65 for D=4, as indicated in Table 3.16. The first 24 permutations match those shown in Table 3.15. Additionally, there are 24 permutations with one idle channel, 12 with two idle channels, 4 with three idle channels, and 1 with four idle channels.

An idle state in a specific direction is denoted by 'U', representing an unused direction. For instance, in the permutation UNSE, the drop/route state is URRD, where 'U' indicates an idle state in the 'West' direction, 'D' represents a drop in the 'East' direction, and the exchange between 'N' and 'S' (relative to WSNE) representing a valid permutation for bidirectional traffic and idle channel. In the permutation UESN, the drop/route state is URRR, so W remains unused and position S, N and E are circularly changed with respect to WSNE, i.e. ‘South’ is routed to ‘East’, ‘North’ is routed to ‘South’, ‘East’ is routed to ‘North’. So, this permutation is not valid for bidirectional traffic and idle channel. To account for all switching states, including idle channels and bidirectional routing constraints among nodal directions, permutations that result in circular routing (grey entries) are excluded, leaving 43 valid distinct permutation options, highlighted in white in Table 3.16.

To calculate the switching capacity of SDM-ROADM nodes, initially we calculate the capacity of SDM-ROADM nodes without applying any network node constraints from the optical network. Afterwards, we introduce these constraints, such as bidirectional traffic and idle channels, to assess their effect on the capacity of the SDM-ROADM nodes. To assess the performance of ROADM nodes in terms of switching capacity under different possible scenarios, we define two metrics:

$$\eta = \frac{R}{R_{total}} \tag{3.11}$$

$$\eta[\rho] = \frac{R}{R[\rho]} \tag{3.12}$$

where R represents the switching capacity of a SDM-ROADM node with specific features (such as bidirectional traffic and idle channels), while R_{total} refers to the switching capacity of an unconstrained SDM-ROADM node (when all possible routing and A/D states are supported) and $R[\rho]$ denotes the switching capacity of a CDC SDM-ROADM for a given number ρ of A/D transceivers. The first metric, η, identifies the relative routing capacity of the SDM-ROADM, ranging between 0 and 1. A higher value of η means that the SDM-ROADM node has better routing or A/D capabilities, which leads to a lower chance of channels being blocked. The second metric, $\eta[\rho]$, reflects the relative routing capacity of an SDM-ROADM node with specific features and a limited number of A/D transceivers compared to an unconstrained node.

Table 3.16 - All 65 permutations of WSNE nodal directions (D=4), for a single spatial channel and single wavelength and corresponding number of A/D and routing assignments. Only 43 of the permutations with bidirectional traffic constraints (no circular routing) and allowing idle states, remain valid (white entries)

Directions	**W S N E**	**W S** E N	**W** N S **E**	**W** N E S	**W** E S N	**W** E **N** S	S W **N E**	S W E N	S N W **E**
Drop/Route	**DDDD**	**DD**RR	**D**RR**D**	**D**RRR	**D**RRR	**D**R**D**R	RR**DD**	RRRR	RRR**D**
A/D	4	20	2	1	1	2	2	0	1
Directions	S N E W	S E W N	S E **N** W	N W S **E**	N W E S	N **S** W **E**	N **S** E W	N E W S	N E S W
Drop/Route	RRRR	RRRR	RR**D**R	RRR**D**	RRRR	R**D**R**D**	R**D**RR	RRRR	RRRR
A/D	0	0	1	1	0	2	1	0	0
Directions	E W S N	E W **N** S	E **S** W N	E **S N** W	E N W S	E N S W	U S N E	U **S** E N	U N S **E**
Drop/Route	RRRR	RR**D**R	R**D**RR	R**DD**R	RRRR	RRRR	UDDD	U**D**RR	URR**D**
A/D	0	1	1	2	0	0	3	1	1
Directions	U N E S	U E S N	**U** E **N** S	W U N E	**W** U E N	N U W **E**	N U E W	E U N W	E U **N** W
Drop/Route	URRR	URRR	UR**D**R	DUDD	**D**URR	RUR**D**	RURR	RURR	RU**D**R
A/D	0	0	1	3	1	1	0	0	1
Directions	W S **U** E	S W U **E**	S E U W	E **S** U W	**W** E U S	E W U S	**W S N** U	**W** N S U	S W **N** U
Drop/Route	DDUD	RRU**D**	RRUR	R**D**UR	**D**RUR	RRUR	**DDD**U	**D**RRU	RR**D**U
A/D	3	1	0	1	1	0	3	1	1
Directions	S N W U	N W S U	N **S** W U	U U **N E**	U U E N	U **S** U **E**	U E **U** S	U **S N** U	U N S U
Drop/Route	RRRU	RRRU	R**D**RU	UU**DD**	UURR	U**D**U**D**	UR**U**R	U**DD**U	URRU
A/D	0	0	1	2	0	2	0	2	0
Directions	**W** U U **E**	E U U W	**W** U **N** U	N U W U	**W S** U U	S W U U	U U U **E**	U U **N** U	U **S** U U
Drop/Route	**D**UU**D**	RUUR	DUDU	RURU	**DD**UU	RRUU	UUU**D**	UU**D**U	U**D**UU
A/D	2	0	2	0	2	0	1	1	1
Directions	**W** U U U	U U U U							
Drop/Route	**D**UUU	UUUU							
A/D	1	0							

Next, we will consider all possible switching states for the Full CDC SDM-ROADM architecture shown in Figure 3.27 a), taking into account all permutations of N_W wavelengths across *M* spatial channels. To compute the switching capacity of the Full CDC SDM-ROADM, we have consider that the total number of adds/drops, *Q*, from *D* directions with *M* spatial channels for a single wavelength is between 0 and $D \times M$.

The SDM-ROADM node A/D scenario can be expressed as an integer partition problem, where each partition represents the number of A/Ds for a specific number of spatial channel [24]. So, the partition size is limited by D, the number of partitions is limited by M and the sum of the elements in each partition is equal to Q - the number of A/Ds. For the scenario presented in Figure 3.27 with D=4 and M=2 and considering Q=4 (noting that $0 \leq Q \leq 8$) the potential integer partitions are: {4}, {3, 1}, {2, 2}. The possible partitions for each of the Q values from 0 to 8 are shown in Table 3.17.

Table 3.17 - All possible permutations for *Q* from 0 to 8 considering *M*=2 and *D*=4

Q	Partitions
0	{0,0}
1	{1}
2	{2},{1,1}
3	{3},{2,1}
4	{4},{3,1},{2,2}
5	{4,1},{3,2}
6	{4,2},{3,3}
7	{4,3}
8	{4,4}

For a better understanding, in the case of Q=4 the partition {3, 1} means that three A/Ds occur on one spatial channel from 3 directions and one A/D occurs on another spatial channel from a single direction. Here you can choose which channel will have three A/Ds and which will have one A/D, whether channel 1 or channel 2, so there are 2 ways to do this. Partition {4} means that a specific spatial channel has four A/Ds (one from each direction), whereas the other spatial channel does not have any A/Ds. Partition {2, 2} means that the four A/Ds are distributed evenly between two spatial channels, with two A/Ds in each. The total number of permutations of four adds/drops, Q= 4, is computed by accounting for all possible spatial channel selections from a finite subset of M:

$$Y_{Q=4} = C(M,1) \times X_{D=4} \times (X_{D=0})^{M-1} + C(M,1) \times X_{D=3} \times C(M-1,1) \times X_{D=1} \times (X_{D=0})^{M-2} + C(M,2) \times (X_{D=2})^2 \times (X_{D=0})^{M-2} \tag{3.13}$$

where the term $C(M,n) = \binom{M}{n}$ defines the number of n-combinations from a set of M elements. The first term of eq. (3.13) corresponds to partition {4}, the second term corresponds to partition {3,1} , and the last term corresponds to partition {2,2}. The variable $X_{D=P}$ represents the number of possible permutations with P A/Ds operations for a single spatial channel per wavelength and can be extracted from Tables 3.15 and 3.16, respectively, for the scenarios without and with idle channels. For example, for $X_{D=1}$ with full traffic, there are 8 valid permutations out of 24 and, for bidirectional routing, there are no valid configurations out of 10. In the idle traffic scenario without bidirectional routing, there are 24 valid configurations out of 65, whereas with idle traffic and bidirectional routing, the number is reduced to 16 out of 43 possible configurations. Note also that $X_{D=0}$ corresponds to zero A/Ds, which means that all channels are routed and to calculate $Y_{Q=0}$ we only consider the term $(X_{D=0})^2$. Table 3.18 shows the number of permutations associated with each $X_{D=P}$ depending on the scenario considered.

Table 3.18 - Number of permutations associated with each $X_{D=P}$ depending on the traffic scenario considered where $0 \leq P \leq 4$

Traffic scenarios	Number of permutations				
	$X_{D=0}$	$X_{D=1}$	$X_{D=2}$	$X_{D=3}$	$X_{D=4}$
Full Traffic	9	8	6	0	1
Bidirectional traffic	3	0	6	0	1
Idle channel	24	24	12	4	1
Idle channel and Bidirectional traffic	10	16	12	4	1

According to this reasoning, the value of eq. (3.13) representing $Y_{Q=4}$ is 54 for full traffic, 42 for bidirectional traffic, 384 for idle channel and 292 for idle channel and bidirectional traffic as shown in Table 3.19 that shows the possible number of permutations for four different scenarios considering D=4, M=2 and P values from 0 to 8. It can be noted that the total number of permutations for the full traffic case is given by $(4!)^2$. Each value of $Y_{Q=4}$ is obtained in a similar way as described in eq. (3.13).

Table 3.19- All possible number of permutations per wavelength Y_Q (Q=0…8), for M= 2 and D= 4 for full traffic and traffic constraints

Traffic constraints	0	1	2	3	4	5	6	7	8	Total
Full Traffic	81	144	172	96	54	16	12	0	1	576
Bidirectional traffic	9	0	36	0	42	0	12	0	1	100
Idle channel	576	1152	1152	768	384	144	40	8	1	4225
Idle channel and Bidirectional traffic	100	320	496	464	292	128	40	8	1	1849

Table 3.19 shows that the scenario with bidirectional traffic allows the lowest number of permutations, while the scenario with idle channels allows the highest number. If we consider Q=8, all scenarios allow the same number of permutations, because only the {4,4} partition is considered and the value of $X_{D=4}$ is 1 for all scenarios (see Table 3.17). It should also be noted that for Q=7, both full traffic and bidirectional traffic scenarios do not allow any permutations, while the idle channel and idle channel and bidirectional traffic scenarios both allow 8 permutations.

Now considering the CDC per direction scenario, we are limited to one A/D per direction, so the partitions can only be {0,0}, {0,1}, {1,0} and {1,1} as shown in Table 3.20 for *M*=2 and *D*=4. Since *M*=2 the maximum A/Ds per direction is 2, so 0≤*Q*≤2.

Table 3.20 - All possible permutations for *Q* from 0 to 2 considering *M*=2 and *D*=4 for CDC per direction

Q	Partitions
0	{0,0}
1	{1,0}
2	{1,0},{1,0},{1,0},{0,1}

Table 3.21 shows the number of permutations associated with each $X_{D=P}$ depending on the scenario considered for a CDC per direction strategy. For example, if we choose the West (W) direction for $X_{D=1}$, we can only choose cases where the West direction is dropped and the other directions are routed.

Table 3.21 - Number of permutations associated with each $X_{D=P}$ depending on the traffic scenario considered for CDC per direction where 0 ≤ *P* ≤ 4

Traffic scenarios	Number of permutations	
	$X_{D=0}$	$X_{D=1}$
Full Traffic	9	2
Bidirectional traffic	3	0
Idle channel	24	6
Idle channel and Bidirectional traffic	10	4

Table 3.22 shows the possible number of permutations for the four different traffic scenarios considering *D*=4, *M*=2 and *P* values from 0 to 2 for CDC per direction.

Table 3.22 shows that the scenario with bidirectional traffic continues to allow the lowest number of permutations, while the scenario with idle channels allows the highest number as in Table 3.19. It can also be seen that for the $X_{D=0}$, the number of permutations are the same in Tables 3.19 and 3.22 for all the scenarios considered, since the values of $X_{D=0}$ do not change between strategies. Overall, it is possible to conclude that the CDC per direction scenario has a lower number of permutations compared to the Full CDC scenario, thus revealing a lower switching capacity.

Table 3.22 - All possible number of permutations per wavelength Y_Q (Q=0…2), for M= 2 among D= 4 for full traffic and traffic constraints considering CDC per direction scenario

Traffic constraints	0	1	2	Total
Full Traffic	81	36	144	261
Bidirectional traffic	9	0	0	9
Idle channel	576	288	1152	2016
Idle channel and Bidirectional traffic	100	80	320	500

3.7. Conclusions

In this chapter, we have analysed the cost of two architectures for SDM nodes, the fractional space-wavelength and the modular architectures, and compared it with the conventional core wise switching architecture cost. We have also analysed two A/D structures, the CDC per direction and CDC per spatial channel, which require fewer WSSs than the Full CDC A/D structure. Finally, a brief description of the SPOC architecture and an overview of the node switching capacity is done.

We have analysed and concluded that a value of *B*=3 for the fractional space-wavelength architecture offers a good trade-off between cost and switching capacity when compared to the core-wise switching architecture without lane changes. Nevertheless, the fractional space-wavelength architecture employing a single WSS in the A/D structure shows limited cost advantages and lacks the switching capacity compared to the core-wise switching architecture without lane changes. The scenario worsens with a bank of WSSs in the A/D structure since this architecture is always more expensive than the core-wise switching architecture without lane changes, which means the short cost advantage seen with a single WSS in the A/D disappears.

Furthermore, we have concluded that the modular architectures build by interconnecting multiple ROADM subsystems with cost-effective low-degree WSSs offer a promising approach to reducing the number and size requirements of WSSs in large-scale ROADMs. The core-wise switching architecture with lane changes is more expensive than modular architectures due to the increased size and cost of the input/output WSSs. The modular architectures generally offer better cost advantages as the number of directions increases, as the core-wise switching architectures, particularly those with lane changes, become substantially more expensive due to the need for larger WSSs. However, for a scenario with a bank of WSSs, the modular architectures lose a large part of their cost advantage compared to a single WSS scenario. It is also possible to conclude that in general, the cost of the modular architectures with $D_S \times D_S$ R&S modules is higher than the cost of using modular architectures with $D_S \times D_S$ WSS modules for larger values of *M* and *D*.

It can also be concluded that, when comparing different A/D structures, it is more beneficial to use either CDC per direction or CDC per spatial channel, instead of Full CDC. We have concluded that the cost of the modular architecture with Full CDC is much higher than the cost of the modular architecture with CDC per direction (almost 16 times for *D*=64). Also, it was concluded that the cost of the core-wise architecture with lane changes with CDC per direction is much higher than the cost of the modular architecture with CDC per direction, which shows the advantage in using this A/D strategy.

The chapter ends by describing the SPOC technology and giving a brief overview of the node switching capacity where is possible to conclude that only for *Q* values lower than two, the CDC per direction scenario has a lower number of permutations compared to the Full CDC scenario, thus revealing a lower switching capacity for a lower number of A/Ds.

CHAPTER 4

Conclusions and future work

4.1. Final conclusions

In this dissertation, we have studied and analysed two architectures for SDM-ROADM nodes that have the potential to be more cost effective than the traditional core-wise switching architecture. We have evaluated the cost of the fractional space and wavelength architecture, as well as the cost of modular architecture considering several A/D structures.

In Chapter 2, an analysis of SDM-based ROADM architectures is conducted, analysing four different switching by granularity: space, space-wavelength, wavelength, and fractional space-full wavelength, each with specific benefits, practical applications and limitations. Spatial granularity switching provides the most cost-effective solution, but with a reduced flexibility. In space-wavelength granularity, switching across wavelength channels and spatial channels offers the finest switching granularity, ideal for metro networks, but with added implementation complexity (i.e. WSSs with greater dimensions). Wavelength granularity routes all spatial channels per wavelength, simplifying hardware, but limiting spatial flexibility. The fractional space-full wavelength granularity architecture enables routing with spatial groups, giving a compromise solution in terms of cost and flexibility between spatial granularity and spatial-wavelength granularity solutions.

Chapter 3 has provided a comprehensive analysis of cost implications across two SDM node architectures—fractional space-wavelength and modular—and compared these to the traditional core-wise switching architecture. We have concluded that in a practical scenario, where the A/D structure uses a bank of WSSs, the fractional space-wavelength architecture is always more expensive than the core-wise switching architecture without lane changes and has also less switching flexibility. Nevertheless, we have concluded that modular architectures, in particular with $D_S \times D_S$ WSSs modules, offer a promising approach to reduce the cost in SDM ROADMs, since they are more cost effective than the core-wise switching architecture with lane changes, in particular as the number of directions increases, and they have the same switching flexibility. We have also evaluated two different A/D structures, CDC per direction and CDC per spatial channel, both requiring fewer WSSs than the Full CDC structure. It was possible to achieve a cost reduction of about 50% for a 16×16 ROADM comparing modular architectures with CDC per direction structure with $D_S \times D_S$ WSSs with the core-wise switching architecture with lane changes with Full CDC structure. Additionally, an overview of the node switching capacity was presented where it was possible to conclude that the CDC per direction strategy offers a more practical and scalable configuration for deployment, because it reduces the complexity and hardware requirements compared to the Full CDC, however, it has a lower switching capacity, while the Full CDC has full switching capacity but with an increase in cost when the complexity increases.

4.2. Future work

In this section, some suggestions for future work are presented:

- Study the network cost of several topologies considering fractional and modular node architectures.
- Study the cost effectiveness of other A/D structures, like CD per direction and CD per spatial channel.
- Study the node switching capacity for the two node architectures analysed in this work (fractional and modular architectures), following the procedure given in [24].
- Calculate the cost savings provided by the SPOC technology in comparison with standard SDM and modular ROADM architectures.

References

[1] D. Marom and D. Neilson, "Optical Switching in Future Fiber-Optic Networks Utilizing Spectral and Spatial Degrees of Freedom," Proceedings of the IEEE, vol. 110, no. 11, pp. 1704-1721, November 2022. Available: https://doi.org/10.1109/JPROC.2022.3207576.

[2] P. Winzer, "The Future of Communications is Massively Parallel," Journal of Optical Communications and Networking, vol. 15, no. 10, pp. 783-787, October 2023. Available: https://doi.org/10.1364/JOCN.496992.

[3] M. Cantono, R. Schmogrow, M. Newland, V. Vusirikala, and T. Hofmeister, “Opportunities and challenges of C+L transmission systems,” Journal of Lightwave Technology, vol. 38, no. 5, pp. 1050–1060, March 2020. Available: https://doi.org/10.1109/JLT.2019.2959272.

[4] E. Mateo, "Multicore-Fiber Submarine Systems," Journal of Optical Communications and Networking, vol. 16, no. 11, pp. H1-H8, Nov. 2024. Available: https://doi.org/10.1364/JOCN.532163.

[5] T. Kuno, Y. Mori, S. Subramaniam, M. Jinno, and H. Hasegawa, "Design and evaluation of a reconfigurable optical add-drop multiplexer with flexible wave-band routing in SDM networks," Journal of Optical Communications and Networking, vol. 14, no. 4, pp. 248-255, April 2022. Available: https://doi.org/10.1364/JOCN.450504

[6] H. Hasegawa, S. Subramaniam, and K.-I. Sato, "Criteria for Selecting Subsystem Configuration in Creating Large-Scale OXCs," IEEE/OSA Journal of Optical Communications and Networking, vol. 7, no. 10, pp. 1009-1017, Oct. 2015. Available: https://doi.org/10.1364/JOCN.7.001009.

[7] A. Anchal and D. Marom "Practical SDM-ROADM designs for uncoupled spatial channels and their switching capacity," 2019 Optical Fiber Communications Conference and Exhibition (OFC), pp. 1-3, San Diego, USA, March 2019. Available: https://doi.org/10.1109/OFC.2019.8696486.

[8] D. Marom, P. Colbourne, A. D’Errico, N. Fontaine, Y. Ikuma, R. Proietti, L. Zong, J. Moscoso, and I. Tomkos, "Survey of photonic switching architectures and technologies in support of spatially and spectrally flexible optical networking," Journal of Optical Communications and Networking, vol. 9, no. 1, pp. 1-26, January 2017. Available: http://dx.doi.org/10.1364/JOCN.9.000001

[9] D. Marom and M. Blau, "Switching solutions for WDM-SDM optical networks," IEEE Communications Magazine, vol. 53, no. 2, pp. 60-67, February 2015. Available: https://doi.org/10.1109/MCOM.2015.7045397.

[10] B. Quigley and M. Cantono, "Delivering multi-core fiber technology in subsea cables," SubTel Forum, August 14, 2023. Available: https://subtelforum.com/delivering-multi-core-fiber-technology-in-subsea-cables/.

[11] NEC Press Release, "NEC Successfully Demonstrates First Trans-oceanic Transmission Over 19-core Optical Fiber," NEC Press Release, October 4, 2021. Available: https://www.nec.com/en/press/202110/global_20211004_01.html.

[12] Infinera Corporation, "The Seven Vectors of ROADM Evolution," White Paper, November 2021. Available: https://www.infinera.com/wp-content/uploads/The-Seven-Vectors-of-ROADM-Evolution-0302-WP-RevA-1121.pdf.

[13] T. Kuno, Y. Mori, S. Subramaniam, M. Jinno, H.Hasegawa, "A Programmable ROADM System for SDM/WDM Networks," Applied Sciences, vol. 11, no. 9, May 2021. Available: https://doi.org/10.3390/app11094195.

[14] M. Silva, L. Cancela, and J. Rebola, "Cost, power consumption and performance analysis in SDM ROADM architectures for uncoupled spatial channels," in Proceedings of the 13th IEEE/IET International Symposium on Communication Systems, Networks and Digital Signal Processing (CSNDSP), Porto, Portugal, pp. 857-862, July 2022. Available: https://doi.org/10.1109/CSNDSP54353.2022.9907949.

[15] Y. Mori, K. Yamashita, and M. Jinno, "Feasibility Demonstration of Integrated Fractional Joint Switching WSS Applicable for Few-Mode Multicore Fiber," in Proceedings of the 2018 Photonics in Switching and Computing (PSC), pp. 2018–2020, 2018. Available: https://doi.org/10.1109/PS.2018.8751404.

[16] M. Ganbold, T. Yasuda, Y. Mori, H. Hasegawa, and K. Sato, "Assessment of optical cross-connect architectures for the creation of next generation optical networks," in 2018 23rd OptoElectronics and Communications Conference (OECC) and 2018 International Conference on Photonics in Switching and Computing (PSC), pp. 1-3, 2018. Available: https://doi.org/10.1109/OECC.2018.8729881.

[17] M. Nakagawa, T. Seki, and T. Miyamura, "Techno-Economic Potential of Wavelength-Selective Band-Switchable OXC in S+C+L Band Optical Networks," in Optical Fiber Communication Conference (OFC) 2022, Optica Publishing Group, paper W2A.24, March 2022.

[18] H. Hasegawa, S. Subramaniam, and K. Sato, "Node Architecture and Design of Flexible Waveband Routing Optical Networks," IEEE/OSA Journal of Optical Communications and Networking, vol. 8, no. 10, pp. 734–744, Oct. 2016. Available: https://doi.org/10.1364/JOCN.8.000734.

[19] D. Sequeira, L. Cancela and J. Rebola, "Impact of physical layer impairments on multi-degree CDC ROADM-based optical networks," at International Conference on Optical Network Design and Modeling (ONDM), Dublin, Ireland, pp. 94-99, 2018. Available: https://doi.org/10.23919/ONDM.2018.8396113.

[20] H. Hasegawa, Y. Iwai, and K. Sato, "OXC Hardware Scale Reduction Attained by Using Interconnected Subsystem Architecture," IEEE/OSA Journal of Optical Communications and Networking, vol. 7, no. 10, pp. 900-910, Oct. 2015. Available: https://doi.org/10.1364/NFOEC.2013.NW1J.2.

[21] M. Niwa, Y. Mori, H. Hasegawa, and K. Sato, "Tipping Point for the Future Scalable OXC: What Size MxM WSS Is Needed?," IEEE/OSA Journal of Optical Communications and Networking, vol. 9, no. 1, pp. A18–A25, Jan. 2017. Available: https://doi.org/10.1364/JOCN.9.000A18.

[22] K. Seno, N. Nemoto, K. Yamaguchi, M. Nakajima, K. Suzuki, Y. Miyamoto, et al., "Wavelength Selective Devices for SDM Applications Based on SPOC Platform," Journal of Lightwave Technology, vol. 40, no. 6, pp. 1583-1592, March 15, 2022. Available: https://doi.org/10.1364/JOCN.9.000001.

[23] Y. Ikuma, K. Suzuki, O. Moriwaki, T. Watanabe, M. Itoh, T. Takahashi, et al., "8 x 8 Wavelength Cross Connect with Add/Drop Ports Integrated in Spatial and Planar Optical Circuit," in Proceedings of the European Conference on Optical Communication (ECOC), Valencia, Spain, Sep. 27, 2015. Available: https://doi.org/10.1109/ECOC.2015.7341950.

[24] A. Anchal and D. Marom, "Impact of Joint and Independent Switching Paradigms on Switching Capacity of Contention/-less SDM-ROADM Designs," Journal of Lightwave Technology, vol. 42, no. 9, pp. 3081-3092, May 2024. Available: https://doi.org/10.1109/JLT.2024.3352739.

Appendices

APPENDIX A.

Ring and linear type ROADM-subsystems modular architectures using different WSSs dimensions inside the subsystems

In Figure A.1, a ring and linear ROADM-subsystems modular architectures are represented considering an 8×8 ROADM dimension and D=4 e M=2, using 1×9 WSSs and assuming a single $M \times N$ WSS in the A/D structure and an A/D ratio of 20%.

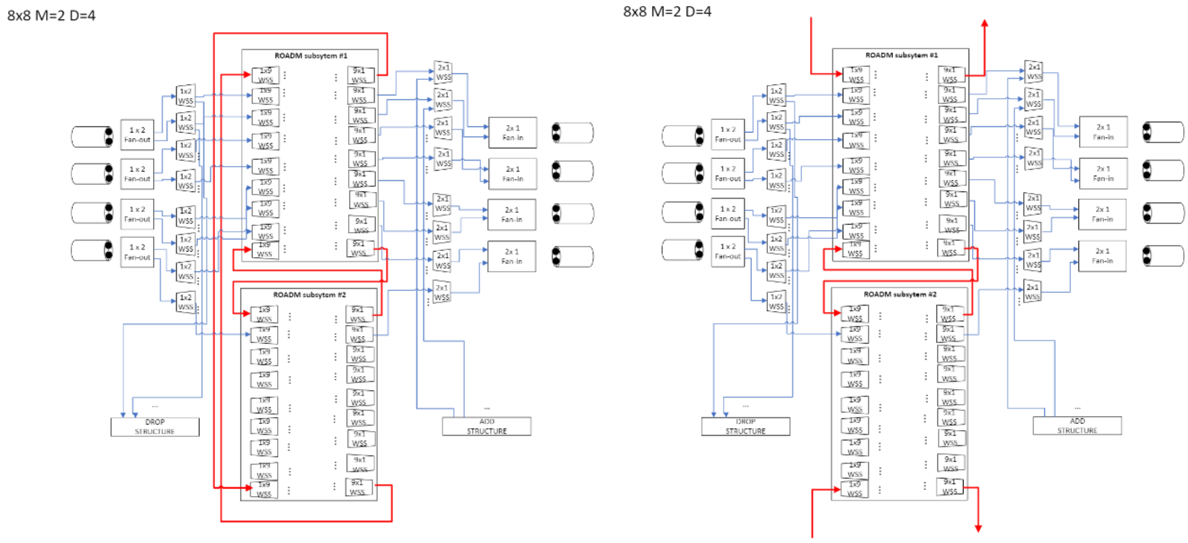

Figure A.1 - 8x8 R&S interconnected Ring and Linear modular architecture ROADM with 2 modules using 1x9 WSS considering D=4, M=2 and assuming a single MxN WSS in the A/D structure and an A/D ratio of 20%

In Figure A.2, a ring ROADM-subsystems modular architecture is represented considering an 8×8 ROADM dimension and D=4 e M=2, but this time using 1×4 WSSs and assuming a single $M \times N$ WSS in the A/D structure and an A/D ratio of 20%.

8x8 M=2 D=4

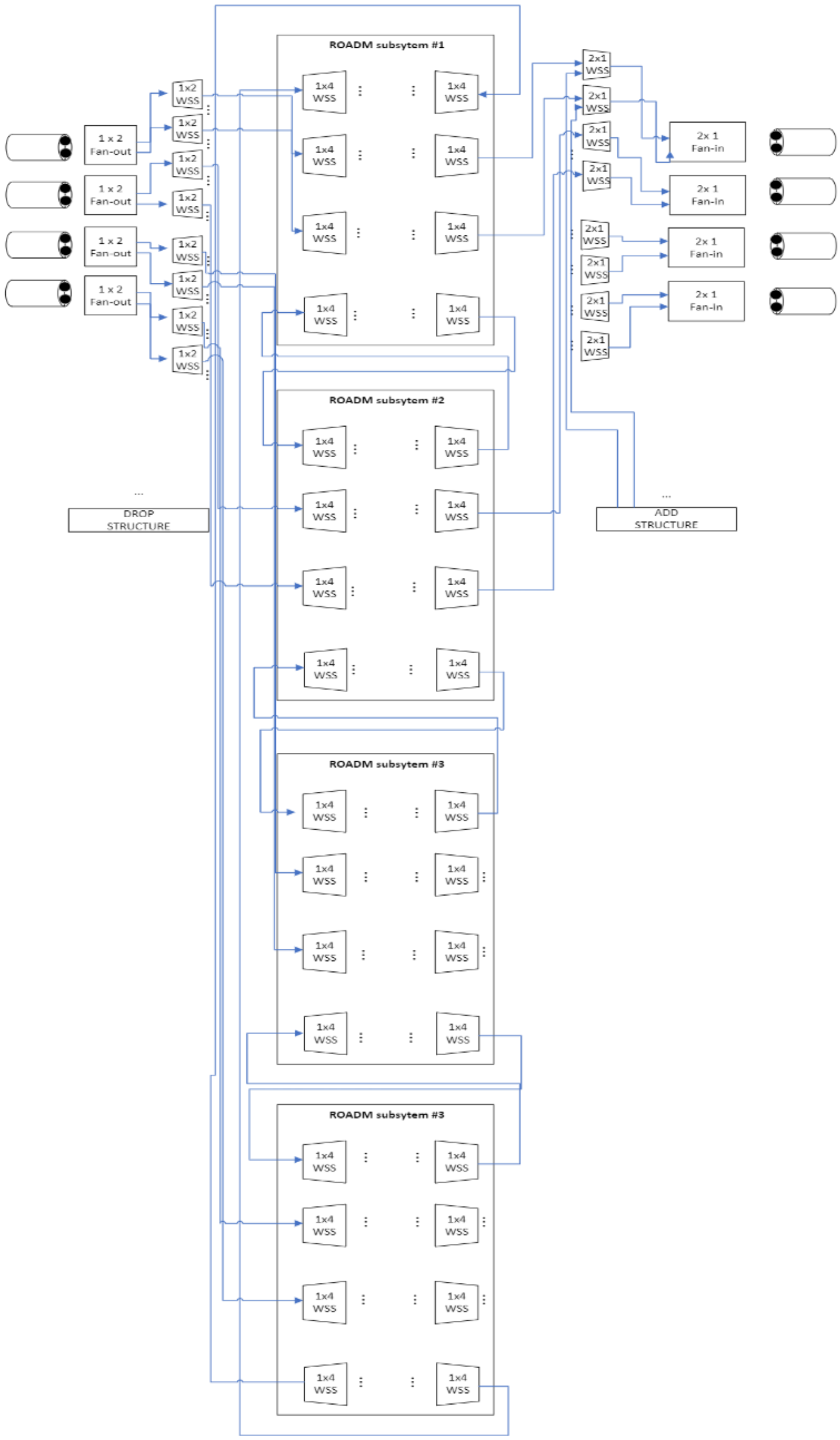

Figure A.2 - 8x8 R&S interconnected ring modular architecture ROADM with 4 modules using 1x4 WSS considering D=4, M=2 and assuming a single MxN WSS in the A/D structure and an A/D ratio of 20%

APPENDIX B.

Cost comparison of the modular architectures using different A/D structures

In Figure B.1, the modular architectures are represented considering different A/D structures (Full CDC, CDC per direction and CDC per spatial channel) for different ROADM dimensions, using 4×4 WSS in the subsystem and assuming an A/D ratio of 20%.

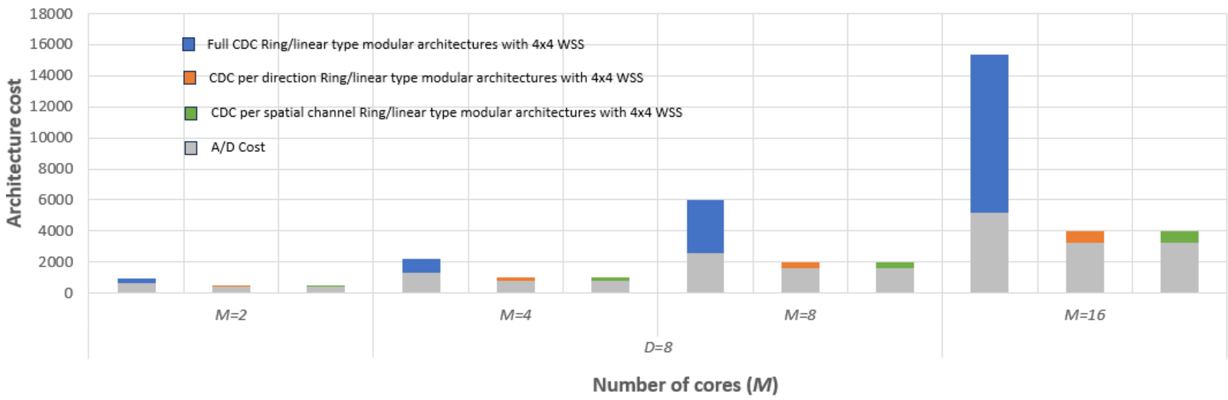

a)

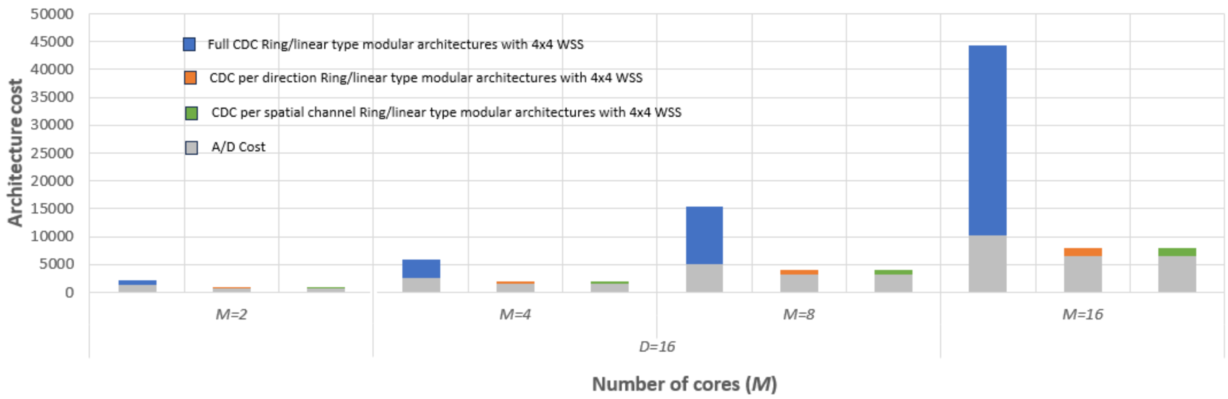

b)

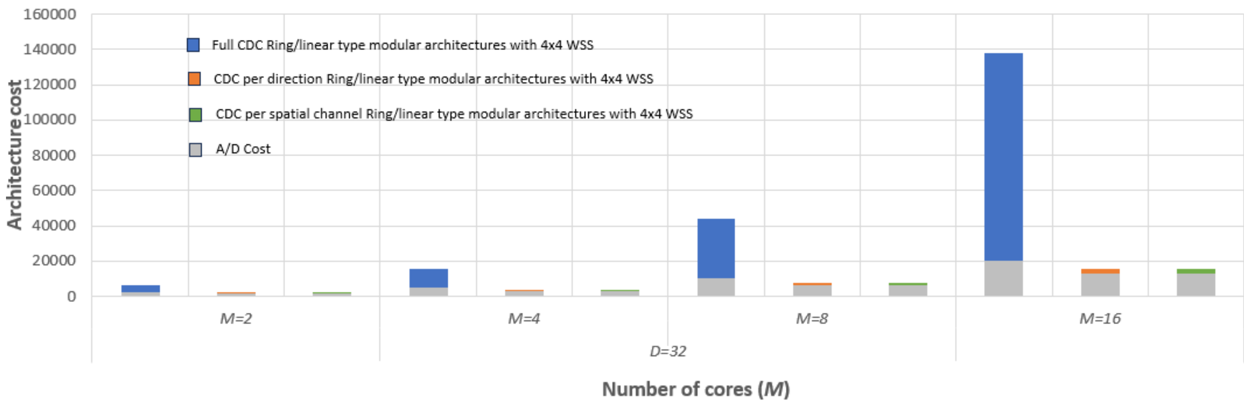

c)

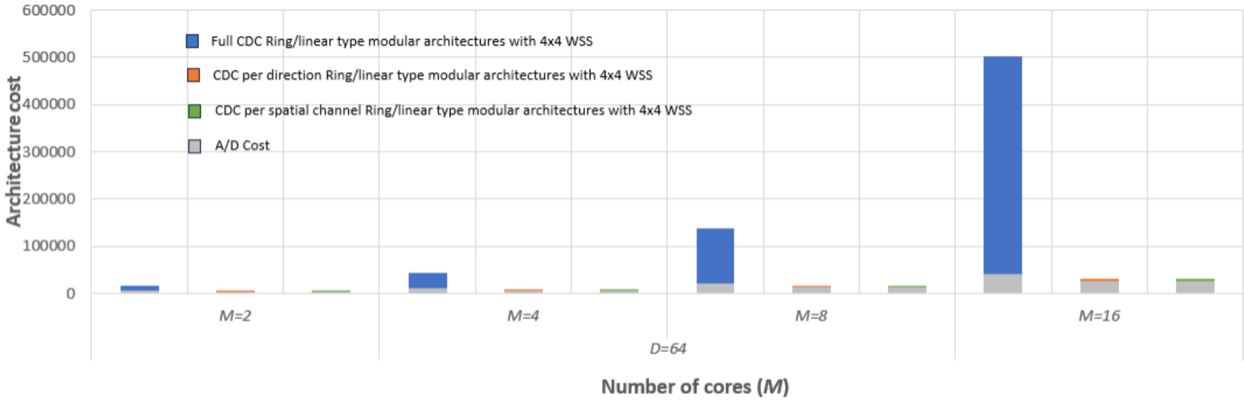

d)

Figure B.1 - Cost of the modular architectures as a function of the ROADM dimension considering a) D=8 ,b) D=16, c) D=32 and d) D=64 assuming Full CDC (bank of WSSs), CDC per direction and CDC per spatial channel in the A/D structure, 4x4 WSS in the subsystem and an A/D ratio of 20%